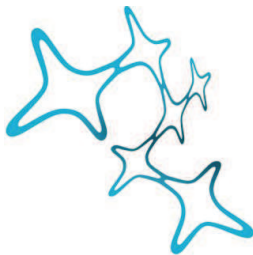


Cellular and molecular function of Uhrf1 in neural stem cells

“Dissertation der Graduate School of Systemic Neurosciences der Ludwig-Maximilians-Universität München”



Graduate School of
Systemic Neurosciences
LMU Munich



Prepared in the group of Professor Dr. Magdalena Götz at the Institute for Stem Cell Research, Helmholtz Zentrum München

Vidya Ramesh

Submitted on 2nd March 2017

First supervisor: Professor Dr. Magdalena Götz, Institute for Stem Cell Research,
Helmholtz Zentrum München and Biomedical Center Munich, Germany

Second reviewer: Professor Dr. Peter Becker, Biomedical Center Munich, Germany

Third reviewer: Professor Dr. Wolfgang Enard, Biomedical Center Munich, Germany

External reviewer: Professor Dr. Stephan Beck, University College London, UK

Date of defense: 25th July 2017

Acknowledgements

This PhD would not have been possible without the support and friendship of many people in my professional and personal life.

I would like to first thank my supervisor Dr. Magdalena Götz for her wonderful support over these years of my PhD. Her guidance, knowledge and new unique ideas towards this work has been extremely valuable. Her enthusiasm and motivation for science has been a great influence for me. I am also glad that we had the opportunity to get to know each other and have a warm rapport.

I would like to thank Efil Bayam for all her help with this project and the opportunity to work on it.

I would also like to thank Dr. Gunnar Schotta and Dr. Filippo Cernilogar who were both excellent collaborators. Their ideas and help towards this project has been invaluable. I am extremely glad we had the chance to meet and have great discussions.

I would like to also particularly thank Dr. Jovica Ninkovic and Dr. Stefan Stricker for a lot of interesting and useful scientific discussions about epigenetics. I would also like to thank Jovica for his valuable suggestions during my thesis committee meetings. Thank you to my other thesis committee members, Dr. Peter Becker and Dr. Francois Guillemot. I really value your great suggestions and support during these years. To my graduate school – the Graduate School of Systemic Neurosciences, I thank you for your excellent assistance during the PhD and helping me attend many outstanding conferences. I would also like to thank the people involved in the GSN for always being so kind and helpful.

I also thank Dr. Markus Riemenschneider and Dr. Markus Schulze for their great collaboration and help towards this project.

A big thank you to all the fantastic people in the Götz lab. I have really loved working in this environment and will always treasure all the emotional and scientific support from all of you! In particular, I would like to acknowledge the embryo group, which taught me so many scientific skills and a great foundation for neuroscience. I would also like to thank our wonderful technicians in the lab – Andrea, Sarah, Angelika and Sabine for their help in running our lab smoothly. I thank Andrea Steiner for so patiently and kindly helping me with cell culture experiments.

I would also like to thank my students – Isabel, Daniela and Linnea for their great help towards the Uhrf1 project.

Acknowledgements

The time in my lab and these years in Munich were especially wonderful because of the great people I have met and known.

I would like to thank Joana, Emily, Tessa and Francesca for their amazing support and affection through all these years. Thank you to Elsa, Judith, Sven, Pia, Silvia, Ruth and Rossella for your awesome friendship. I really enjoyed all the time we spent together and it has been a pleasure to know you all.

I would also like to thank other people in the lab for always being so friendly, supportive and fun to hang out with – Miriam, Tjasa, Chris, Maxi, Valentin, Filippo, Adam, Giacomo, Sergio, Ronny, Gregor, Anita, Christina, Alessandro, Rosario, Kalina, Tamara and German.

Big thanks to my amazing ‘flowers’ –Noelia, Patricia and Roberta for their awesome friendship and support through all my ‘neuroscience years’.

A very special thanks to Yamini and Katerina for always, always being there for me.

I am really very grateful to my parents, my brother and grandparents for always supporting me to pursue my dreams.

Table of Contents

1. Abstract	1
2. Introduction	3
2.1 Epigenetic regulators of stem cells and NSCs	3
2.1.1 Histone marks and their role in neurogenesis.....	5
2.1.2 DNA modifications	6
2.1.3 Role of Dnmts and Tets in ESCs, early development and NSCs.....	10
2.1.4 Uhrf1 and Uhrf2.....	11
2.2 Endogenous retroviral elements	13
2.3 Embryonic neurogenesis	15
2.3.1 Development of the embryonic forebrain	15
2.3.1 Overview of embryonic neurogenesis.....	16
2.3.2 Cell types in the embryonic neocortex	17
2.3.3 Cortical layering and postnatal terminal neuron differentiation	19
2.4 Adult neurogenesis	22
2.4.1 Adult neurogenic niches and cell types	22
2.4.2 Gliogenesis	24
3. Aims of my thesis	26
4. Results	27
4.1 Uhrf1 expression from embryonic to adult stages	27
4.2 Characterisation of the Uhrf1 cKO cellular phenotype	29
4.2.1 Comparable neuronal and glial cells at embryonic stages	29
4.2.2 Cortical layering appeared normal in the cKO	33
4.2.3 Cell death peaks in the postnatal Uhrf1 cKO	34

4.3 Transcriptional profiling of Uhrf1 cKO	37
4.3.1 Activation of cellular stress genes at E16 and P5 Uhrf1 cKO	37
4.3.2 Specific endogeneous retroviral elements are activated in Uhrf1 cKO	47
4.4 Alterations in methylation and chromatin marks in Uhrf1 cKO	55
4.4.1 Loss of DNA methylation in Uhrf1 cKO	55
4.4.2 Loss of 5mC in specific genes and transposable elements	57
4.4.3 Gain of 5hmC in Uhrf1 cKO on IAP elements	61
4.4.4 Assessing changes in histone marks in the cKO	65
4.5 Manipulation of Tet enzymes to rescue IAP activation	66
4.5.1 In vivo knockdown of Tet enzymes by in utero electroporation of the cKO cortex	66
4.5.2 Generating an in vitro system to investigate the relationship between Tet enzymes and IAP activation	71
4.6 Investigating changes in the proteasome of cKO cortices and controls	76
4.7 Generating neural stem cells from Uhrf1 KO ES cells	81
4.8 Conditional knockout of Uhrf1 in adult neurogenic niches	82
4.8.1 Loss of Uhrf1 in the adult subependymal zone and dentate gyrus – further characterization of the cellular phenotype.....	82
4.8.2 Differences in IAP activation in the adult cKO of the SEZ and dentate gyrus	87
5. Discussion	
5.1 Expression of Uhrf1 in the developing cerebral cortex	91
5.2 Cellular function of Uhrf1 in the embryonic cerebral cortex	91
5.3 Transcriptional control of Uhrf1 in the embryonic cortex	94
5.4 Molecular mechanism of Uhrf1 in the developing neocortex	99
5.5 Uhrf1 function in adult neurogenesis	103
5.6 Conclusions and prospects	104

6. Methods

6.1 Materials

6.1.1 Chemicals	107
6.1.2 Tissue culture reagents	109
6.1.3 Standard solutions and buffers	110
6.1.4 Cell culture media.....	112
6.1.5 Kits	113
6.1.6 Antibodies	114
6.1.6.1 Primary antibodies.....	114
6.1.6.2 Secondary antibodies	115
6.1.7 Primers.....	115
6.1.7.1 Genotyping primers	115
6.1.7.2 Real time PCR primers	116
6.1.7.3 Bisulfite sequencing primers	117
6.1.7.4 Bisulfite sequencing primers	117
6.1.8 Constructs.....	118

6.2 Methods

6.2.1 In vivo methods	118
6.2.1.1 Mouse lines	118
6.2.1.2 Perfusion and anesthesia	119
6.2.1.3 In utero electroporation.....	119
6.2.1.4 Tamoxifen induction.....	120
6.2.2 Methods in cell biology	120

6.2.2.1 Tissue dissection	120
6.2.2.2 Tissue sectioning.....	120
6.2.2.3 Immunostaining	121
6.2.2.4 Fluorescence activated cell sorting	121
6.2.3 Methods in molecular biology	122
6.2.3.1 Extraction of DNA from mouse tail	122
6.2.3.2 Plasmid DNA extraction.....	122
6.2.3.3 RNA extraction for cDNA synthesis and qRT-PCR	122
6.2.3.4 RNAseq at E16 - VZ	123
6.2.3.5 RNAseq at E16 full cortex and P5 cortex	123
6.2.3.6 Oxidative reduced representation bisulfite sequencing	123
6.2.3.7 Oxidative bisulfite sequencing	123
6.2.3.8 Hydroxy methylated DNA immunoprecipitation.....	124
6.2.3.9 Determining concentration and quality of nucleic acids.....	124
6.2.3.10 Genotyping PCR.....	125
6.2.3.11 Bacterial transformation.....	125
6.2.3.12 Bacterial cultures	126
6.2.3.13 Gel electrophoresis	128
6.2.3.14 Western blotting and mass spectrometry	128
6.2.3.15 Methylation digests	129
6.2.4 Data analysis.....	129
6.2.4.1 Bioinformatic analysis	129
6.2.4.2 Analysis of immunostainings and qRT-PCR	131
7. Abbreviations	132

8. References	137
9. Curriculum vitae	155
10. List of publications	157
11. Affidavit	158
12. List of contributions	159

Table of Contents

1. Abstract

Central Nervous System (CNS) injuries and neurodegenerative diseases can lead to a critical loss of neurons and other nerve cells, which often in mammals cannot be regenerated by the organism itself. To recover the neural damage, great efforts are being undertaken in the field of neuronal reprogramming and other modes of repair. In order to execute neural repair, a thorough understanding of the underlying molecular mechanisms of neurogenesis is required. Although great strides have been made in uncovering key transcription factors and other modulators of neurogenesis, the emerging field of neuroepigenetics is still in its infancy.

Many studies have individually highlighted the importance of novel and key players of embryonic and adult neurogenesis. However, less is known about similarities and differences between the molecular mechanisms underlying neurogenesis at these two stages. To shed light on these processes, we decided to employ a candidate approach, focusing on a factor which is expressed highly in both embryonic and adult neural stem cells and progenitors and downregulated in differentiated cells. Our rationale was that such a factor could play a key role in instructing neurogenesis and allow a comparison of embryonic and adult neurogenesis.

To identify new factors playing roles in neurogenesis, we mined data from transcriptional profiling carried out by our lab previously. Our lab designed protocols to isolate embryonic progenitors from the developing cerebral cortex (Pinto et al. 2008) and adult neural stem cells (NSCs) and their progeny from the subependymal zone (SEZ) (Beckervordersandforth et al. 2010; Fischer et al. 2011). From these data, we screened for epigenetic regulators of neurogenesis and identified *Uhrf1* (Ubiquitin-like with PHD and RING Finger Domain 1). *Uhrf1* is a multi-domain protein, described to play a role in DNA methylation, histone methylation and ubiquitination. Previous data from our lab indicated that *Uhrf1* is highly expressed in the embryonic cortex by progenitors and adult neural stem cells in development and adulthood and played an important role in neurogenesis (Bayam. 2014).

We observed that loss of *Uhrf1* in the developing cortex primarily resulted in impaired terminal neuronal differentiation, culminating in severe postnatal death. Surprisingly, we did not observe significant changes in cell fate, progenitor proliferation or initial neuronal differentiation. Analysis of transcriptional changes largely mirrored the cellular phenotypes observed. Additionally, we could identify transcriptional programs related to cellular stress to be activated in the cortical conditional knockout (cKO) of *Uhrf1*. The most striking effects we observed were in the activation

of specific retroviral elements (type of transposable element) known as IAPs in the cKO, which are normally silenced in control animals. We determined a loss of DNA methylation of several loci, including several groups of transposable elements. Interestingly, we could detect a selective increase of 5-hydroxy methyl cytosine (5hmC, a mark associated with transcriptional activation) on Intracisternal A-Particles (IAPs), as opposed to other elements. We could perform molecular rescue experiments to elucidate interplay between Uhrf1 and Tet enzymes in the regulation of IAP elements, in cortical neural stem cells.

To examine the role of *Uhrf1* in adult neurogenesis we used the *Glastcre*^{ERT2} mice (Mori et al. 2006) and CAG reporter mice (Nakamura et al. 2006) to inducibly delete Uhrf1 in adult neural stem cells and all their progeny. As opposed to the role of Uhrf1 in embryonic neurogenesis, we observed strong changes in progenitor proliferation in the adult cKO of Uhrf1 in the SEZ. Moreover, in contrast to embryonic stages, we could not detect significantly altered cell death in the adult cKO. Analysis of the molecular role of Uhrf1 in this niches, uncovered a surprising difference in IAP regulation between the SEZ and dentate gyrus. Although we detected upregulation of IAP structural proteins in the SEZ cKO, this was not the case in the dentate gyrus cKO. However, the dentate gyrus adult neurogenesis was severely impaired, with much reduced proliferation and neuroblasts. Thus, the cellular and molecular function of *Uhrf1* is clearly different in adult neurogenesis compared to development.

The data from my thesis allowed us to draw several key conclusions regarding the molecular role of Uhrf1. Firstly, we observed specificity in regulation of retroviral elements by Uhrf1 in the embryonic cortex and adult SEZ. Secondly, we uncovered a role for factors expressed in early neural stem cells (in this case, *Uhrf1*) to exert long-term effects on their progeny. Altogether, our data implicate an important unique function for *Uhrf1* in neurogenesis and further research can indicate its relevance in the fields of reprogramming and repair.

2. Introduction

2.1 Epigenetic regulators of neurogenesis

Epigenetics is the study of changes that occur in the DNA of a cell which affects gene expression without modifying the original genetic code. The changes affect two classes of molecules – either histones or DNA. The histones or DNA undergo certain modifications by methylation, acetylation or other chemical modifications. Such modifications can either positively affect transcription, thus termed 'activating', or negatively affect transcription, termed 'repressive'. Epigenetic marks occur on chromatin which is composed of nucleosomes (complex of histones and DNA) (Figure 2-1). Chromatin conformation can vary from being tightly packaged (as observed in heterochromatin) or as an open conformation (often occurring in euchromatin). Open chromatin is accessible for transcription factors and is thus considered to be more transcriptionally active than the closed conformation.

Epigenetics has been described to play important roles in cellular processes such as proliferation and differentiation, in several cell types in tissues. One such region is the embryonic and adult brain, wherein residing stem cells generate neurons, a process known as neurogenesis.

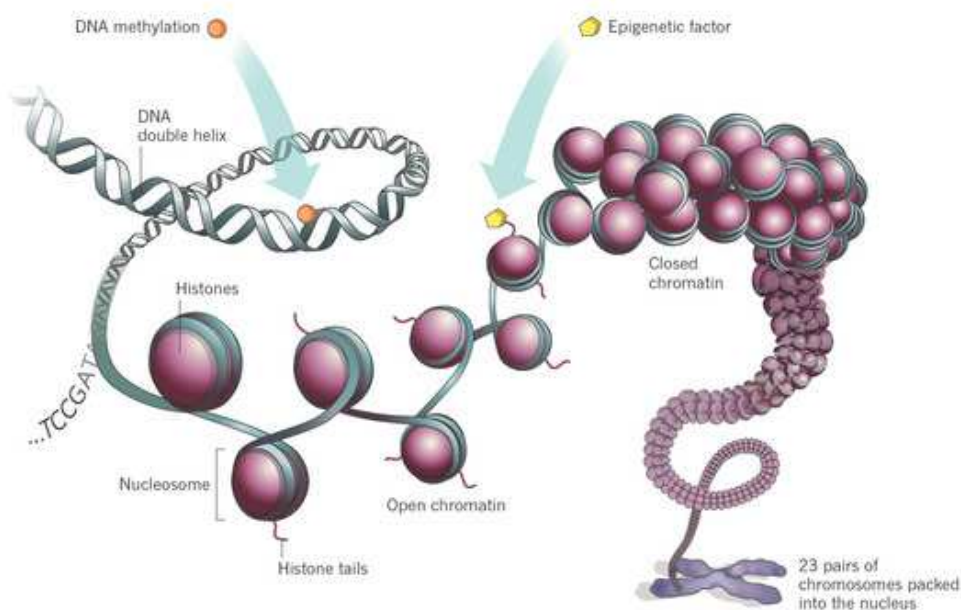


Fig. 2-1 Chromatin conformation showing epigenetic modifications

Adapted by permission from Macmillan Publishers Ltd: Nature (Marx 2012) copyright (2012). License no. 4050260546065.

Chromosomes are packaged in cells in the form of chromatin which comprise of nucleosomes containing histones and DNA. Chromatin can be both open and closed and modified by epigenetic modifications such as DNA methylation and modified histone tails.

Most of the studies in neurogenesis have focused on the role of signaling pathways, transcription factors and cytoplasmic/membrane related proteins. For example, the transcription factors Pax6, Arx and Lhx2 have been shown to be control NSC proliferation and differentiation (Manuel et al. 2015). Moreover, the bHLH family of transcription factors such as Ngn2 and Ascl1 have been described to act as important regulators of neurogenesis (Schuurmans and Guillemot 2002; Wilkinson et al. 2013). Certain signaling pathways acting upstream of the transcription factors have also been described to control stem cell renewal and proliferation, such as Notch, FGF and Wnt signaling (Martynoga et al. 2012). However, there has been a recent burst of publications illuminating the importance of chromatin and epigenetic factors in both embryonic and adult neurogenesis.

Chromatin remodelers such as the SWI-SNF complex have been described to control neuronal differentiation in the embryonic cerebral cortex, as well as cell fate in an adult neurogenic niche, SEZ (Matsumoto et al. 2006; Ninkovic et al. 2013). Epigenetic regulators such as those controlling histone methylation and DNA methylation can also regulate neurogenesis. Components of the polycomb repressor complex, which are involved in setting the H3K27me3 mark, such as *Ezh2* or *Ring1b* have been described to regulate cerebral cortical neurogenesis (Fasano et al. 2007; Hirabayashi et al. 2009; Pereira et al. 2010). Moreover, ESET and Kap1, both involved in setting the H3K9me3 mark, have also been implicated in cerebral cortical neuron differentiation (Tan et al. 2012; Fasching et al. 2015). Besides histone methylation, components of the DNA methylation machinery can impact neuronal survival. The DNA methyltransferases, *Dnmt1*, *Dnmt3a* and *Dnmt3b* have been described to ensure appropriate cortical neuron numbers and neuronal maturation (Hutnick et al. 2009; Feng et al. 2010). Recent data have also implicated the role of

non-coding elements such as non-coding RNA and micro RNA in regulation of neurogenesis (Iyengar et al. 2014).

2.1.1 Histone marks and their role in neurogenesis

The main histone marks which are 'activating' in terms of transcription are acetylation of H3K27 in enhancers (Creighton et al. 2010) and H3K9 in promoters (Koch et al. 2007) and methylation of H3K4 in promoters (Benevolenskaya 2007; Koch et al. 2007) (Figure 2-2). In contrast, trimethylation of H3K9 and H3K27 in genes (Barski et al. 2007) are considered largely repressive marks. These modifications are carried out by specific enzymes which can acetylate histones (eg. p300), deacetylate histones (eg. HDAC1) and methylate histones (eg. Setdb1).

Two of the repressive histone marks which have been widely studied in neurogenesis are H3K9me3 and H3K27me3. H3K9me3 is set by a complex of ESET or Setdb1 which acts a histone methyl transferase and Trim28 or Kap1 which acts a co-factor (Schultz et al. 2002). Both Setdb1 and Kap1 are expressed by embryonic NSCs in the cerebral cortex (Tan et al. 2012; Fasching et al. 2015). Conditional deletion of Setdb1 in the embryonic cortex resulted in defects in neuronal differentiation and proliferation (Tan et al. 2012), suggesting an important role for histone methylation in neurogenesis. Moreover, conditional deletion of both Setdb1 and Kap1 resulted in activation of transposable elements (Tan et al. 2012; Fasching et al. 2015).

H3K27me3 is regulated by the polycomb repressive complex PRC1 and PRC2 (Cao et al. 2002; Cao and Zhang 2004; Leeb et al. 2010; Simon and Kingston 2013). Loss of certain components of the polycomb machinery led to defects in neurogenesis. Conditional deletion of *Bmi-1* in adult NSCs, both in vitro and in vivo, affects their maintenance (Molofsky et al. 2003). However, acute deletion of *Bmi-1* in embryonic neural stem cells does not affect progenitor proliferation (Fasano et al. 2007). These data highlight an importance difference between NSCs during development and adult and between in vitro/in vivo experiments. Conditional deletion of *Ezh2* and *Ring1b* in cortical NSCs leads to a prolongation of the usual period of neurogenesis in this region (Hirabayashi et al. 2009). However, early deletion of *Ezh2* prior to neurogenesis disturbs the balance between proliferation and differentiation in the cerebral cortex (Pereira et al. 2010).

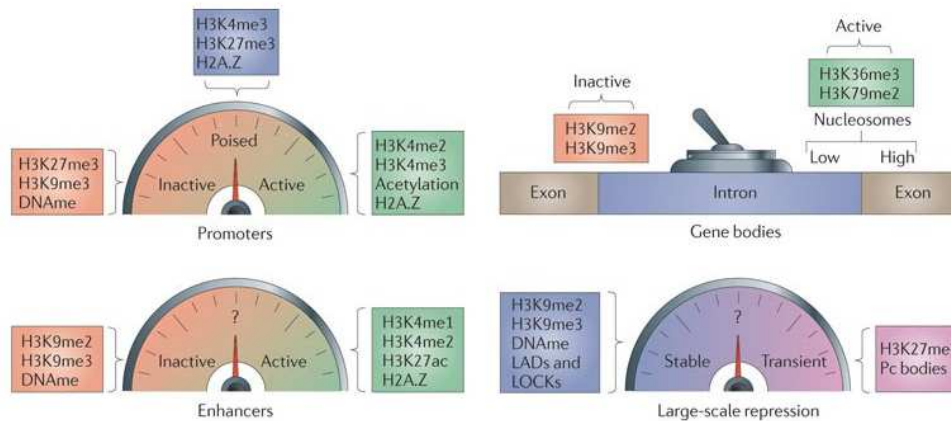


Fig. 2-2. Activated and repressed gene promoters and gene bodies by histone modifications. Adapted by permission from Macmillan Publishers Ltd: Nature (Zhou et al. 2011) copyright (2011). License no. 4050271026920

A. Active promoters often contain H3K4me3 and repressed promoters contain high levels of H3K9me3 and H3K29me3.

B. Genes bodies vary in different histone marks depending on active and inactive regions. In particular, exons of active genes often contain high levels of H3K36me3.

2.1.2 DNA modifications

The other key group of epigenetic modifications are DNA modifications. The main type of DNA modification identified and studied till date is that of DNA methylation. DNA methylation involves the addition of a methyl group to the fifth carbon atom of the cytosine residue which lies adjacent to a guanine residue. This mode of methylation is an active process which is carried out by a group of enzymes termed DNA methyl transferases (Dnmts). There are 5 known Dnmts – *Dnmt1*, *Dnmt3a*, *Dnmt3b*, *Dnmt3c* and *Dnmt3L*. *Dnmt3a* and *Dnmt3b* act as de novo methyltransferases which initially adds the methyl group to unmethylated cytosine on both strands of DNA (Bird 1999). *Dnmt3L* lacks the catalytic domain of other Dnmts but is important for establishing imprinting control regions in gametes (Bourc'his et al. 2001; Bourc'his and Bestor 2004). Recently, a new Dnmt member, *Dnmt3c*, has been described in male germ cells to arise from a duplication of

Dnmt3b (Barau et al. 2016). On the other hand, Dnmt1 is a maintenance methyl transferase which adds the methyl group to the newly synthesized DNA strand wherein the other older strand is already methylated (Bird 1999). Studies have indicated another molecule, Uhrf1 (Ubiquitin-like with PHD and RING finger domains) to play a crucial role in DNA methylation. Uhrf1 binds hemimethylated DNA (Arita et al. 2008) as well as Dnmt enzymes (Meilinger et al. 2009; Berkyurek et al. 2014), thus maintaining DNA methylation. Another member of the Uhrf family, Uhrf2, which has similar domains to Uhrf1 (Bronner et al. 2007) has also been implicated in DNA methylation as it can bind hemimethylated DNA (Pichler et al. 2011).

DNA can be either actively or passively demethylated. Until recently, the only form of demethylation was considered passive wherein lack of maintenance of DNA methylation in dividing cells causes the daughter cells to lose the 5mC mark. However, recent evidence has shown the presence of enzymes capable of converting the 5mC mark to 5-hydroxy methyl cytosine (5hmC) (Tahiliani et al. 2009; Ito et al. 2010) (Figure 2-3). These enzymes are termed as Ten-Eleven-Translocation (Tet) enzymes. The Tet family of enzymes has 3 members till date – Tet1, Tet2 and Tet3. The Tet enzymes function by oxidizing 5mC to 5hmC as an initial intermediate (Ito et al. 2011). The 5hmC mark can be further oxidized to 5-carboxyl cytosine (5CaC) and 5-formyl cytosine (5fC) (Ito et al. 2011) (Figure 2-3). The 5fC and 5caC mark can be reverted to an unmodified cytosine by Base Exchange Repair (BER) (He et al. 2011; Maiti and Drohat 2011). Interestingly, a recent study has elucidated that Uhrf1 can bind the 5hmC mark with equal affinity at 5mC (Frauer et al. 2011).

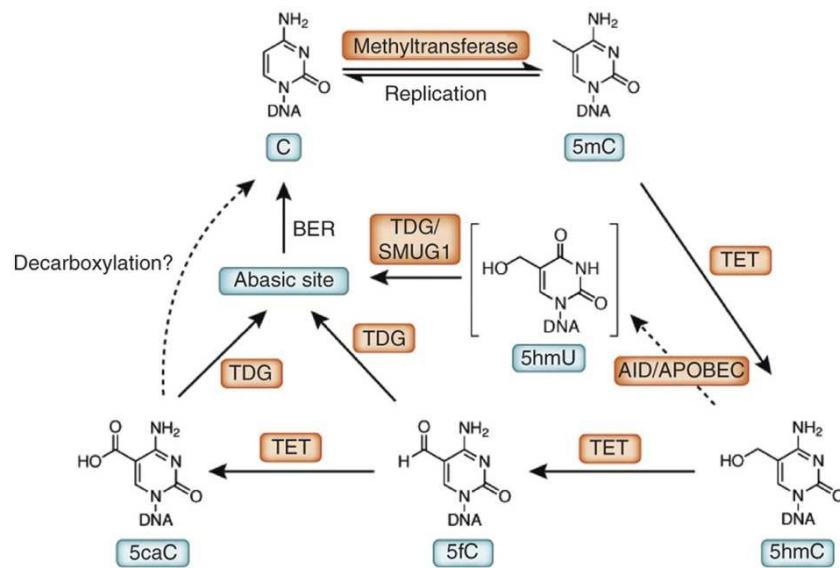


Fig. 2-3. Epigenetic modifications of cytosine residue in DNA. Reprinted by permission from Macmillan Publishers Ltd: Nature biotechnology (Song et al. 2012) copyright (2012). License no. 4056700245047

Cytosine can be modified from C to 5mC by methyltransferases such as Dnmt enzymes. 5mC can be converted to 5hmC, 5fC and 5caC by the Tet enzymes. The oxidation products of 5fC and 5caC can be removed by TDG to generate an abasic site which is converted to a cytosine by BER (Base Exchange Repair). 5hmC can be converted to 5hmU by AID/APOBEC and 5caC can be converted to C by decarboxylation. The solid arrows indicate pathways which have been validated whereas the dotted arrows need yet to be confirmed.

DNA methylation is a largely repressive mark wherein stretches of CpGs, identified as CpG islands, are methylated and subsequently the corresponding genes are transcriptionally silent (Deaton and Bird 2011). Methylated CpGs can be recognized by Methylated DNA binding domain proteins (MBDs) such as MecP2 (Fraga et al. 2003). Of the 28 million CpGs in the human genome, about 60-80% are methylated (Smith and Meissner 2013), including CpG islands and other regions. DNA methylation is extremely widespread and can occur both in promoters and gene bodies as well as in non-coding regions of the genome. Most methylated genes and elements in

the genome are static across development and into adulthood and across somatic tissues. From the 60-80% of CpG methylation (among all CpGs) only about 10% occurs at CpG islands which are mainly at the transcription start sites of either housekeeping genes or developmentally regulated genes (Deaton and Bird 2011). Mechanisms by which DNA methylation prevents transcriptional activation have been studied widely and are largely attributed to the activity of CpG binding proteins and histone deacetylases and histone methylases. There are some hypotheses that DNA methylation in promoters can prevent access for transcription factors due to the binding of MBDs (Bird 1992). This additional layer of epigenetic complexity allows certain genes to be expressed in specific tissues and not others.

Compared to 5mC, the other DNA marks are much lower in abundance in the genome. Whole genome mapping of the mouse genome revealed the 5hmC is present in about 0.1% of all cytosine in mouse embryonic stem cells (ESC) (Yu et al. 2012). However, the highest abundance of 5hmC has been described to be in the mouse brain, about 0.4-0.7% of all cytosines (Szulwach et al. 2011; Song et al. 2011). In comparison, 5caC and 5fC are extremely rare with only about 20ppm (parts per million) of all cytosines and 3 ppm of all cytosines respectively in mouse ESCs (Ito et al. 2011). Studies are still early in understanding the stability of these new DNA marks and their functions. However, there is indication that the 5hmC mark can correlate with transcriptional activation (Wu et al. 2011).

There are two instances during development wherein the global static nature of DNA methylation is drastically erased. These are during early pre-implantation development and in the germ line. During early pre-implantation development, the hypermethylated sperm undergoes rapid loss of 5mC (Santos et al. 2002). Interestingly, although majority of the genome is demethylated, certain transposable elements called Intracisternal A-Particles (IAP) are kept methylated (Lane et al. 2003)

The other instance wherein DNA methylation is massively erased is in primordial germ cells at about embryonic day E10-11. Genome-wide studies indicate that also in these cells, although methylation is almost completely erased, on IAPs and some other retroviral elements, methylation remains intact (Hackett and Surani 2013).

2.1.3 Role of Dnmts and Tets in ESCs, early development and NSCs

To understand the importance of epigenetic regulators in stem cells and neurogenesis, most studies have employed loss-of-function studies. Both *Dnmt1* and *Uhrf1* are highly expressed by mouse ESCs (Bostick et al. 2007; Sharif et al. 2007). *Dnmt3a* is predominantly expressed in oocytes and early preimplantation embryos where it establishes DNA methylation at imprinting control regions in gametes (Kaneda et al. 2004; Kato et al. 2007). *Dnmt3b* is strongly expressed at the blastocyst stage (Watanabe et al. 2002).

Complete knockout of *Dnmt1* enzyme is embryonically lethal due to a massive loss of methylation (Li et al. 1992). Interestingly, loss of *Uhrf1* causes a similar phenotype (Sharif et al. 2007). Deletion of *Dnmt3b* also causes embryonic lethality (Okano et al. 1999). However, knockout of *Dnmt3a* is partially viable (Okano et al. 1999). *Dnmt3L* knockout mice are also partially viable (Bourc'his et al. 2001; Bourc'his and Bestor 2004)

In contrast to the Dnmts and *Uhrf1*, the Tet enzymes are more dispensable in terms of embryonic lethality. *Tet1* single knockout and *Tet1/Tet2* double knockouts are viable with a slight developmental delay (Dawlaty et al. 2011; Dawlaty et al. 2013). Triple knockout of *Tet1/Tet2/Tet3* led to a significant loss of 5hmC and defects in ESC differentiation (Dawlaty et al. 2014).

Conditional knockout of *Dnmt* enzymes have been generated and studied in neurogenic niches. *Dnmt1* is expressed by cortical radial glia, adult neurons and adult neural stem cells (Hutnick et al. 2009; Feng et al. 2010; Noguchi et al. 2015). Deletion of *Dnmt1* in the dorsal telencephalon at early embryonic stages resulted in severe neuronal death with an activation of the retroviral elements, IAPs (Fan et al. 2001; Hutnick et al. 2009). Interestingly, deletion of *Dnmt1* in hippocampal neurons did not affect their numbers but synaptic plasticity was affected (Feng et al. 2010). Loss of *Dnmt1* in aNSCs of the hippocampus affected the production of new neurons (Noguchi et al. 2015).

Dnmt3a is expressed by NSCs derived from ESCs and loss of function studies indicated defects in both proliferation and differentiation (Wu et al. 2010). *Dnmt3b* function in NSCs was studied by using *Dnmt3b* knockout ESCs and differentiating them into early neuroepithelial stages. In this study, *Dnmt3b* was found to be important for early neuroepithelial specification (Martins-Taylor et al. 2012). A comprehensive study of *Dnmt3a* expression and function was performed in postnatal neural stem cells (Wu et al. 2010). *Dnmt3a* was found to be highly expressed by postnatal NSCs of the SEZ and dentate gyrus and conditional deletion led to defects in neurogenesis. Moreover,

Dnmt3a was found to occupy and methylate intergenic regions and gene bodies of several neurogenic genes (Wu et al. 2010).

Besides Dnmts, many studies have investigated the role of proteins binding methylated DNA (MBDs) in the neurogenic niches. *MBD1* knockout mice showed impaired neurogenesis in the adult (Zhao et al. 2003; Li et al. 2008). Another heavily studied protein is MeCP2 which is implicated in Rett's syndrome. *MeCP2* is most expressed in neurons and *MeCP2* knockout mice exhibit defects in neuronal maturation but not in their numbers (Smrt et al. 2007).

As 5hmC is most abundant in the brain, many studies have investigated the role of 5hmC and Tet proteins in neurogenesis. In the embryonic cortex, 5hmC is abundant in neurons and accumulates in gene bodies of neuronal genes (Hahn et al. 2013). *Tet1* has very low expression in the embryonic cortex, with *Tet2* and *Tet3* being highly expressed by progenitors and neurons (Hahn et al. 2013). Acute knockdown of *Tet2* and *Tet3* in cortical radial glia resulted in accumulation of cell clusters in the cortex, suggesting aberrant neuronal migration (Hahn et al. 2013). *Tet1* knockout mice exhibited impaired hippocampal neurogenesis with some genes being hypermethylated

In summary, loss of function studies of Dnmt and Tet protein suggest that these proteins play key cell-type and niche specific roles in regulating transcription and cell fate.

2.1.4 Uhrf1 and Uhrf2

Besides Dnmts and Tet enzymes, another protein has been described to play a key role in maintaining DNA methylation, Uhrf1. Uhrf1 is a multi-functional protein with several domains. As mentioned previously, Uhrf1 can bind hemi-methylated DNA with its SRA domain. Uhrf1 possesses a RING finger domain, linked to histone and protein ubiquitination and turnover (Citterio et al. 2004; Liu et al. 2013; Nishiyama et al. 2013; Qin et al. 2015). Furthermore, Uhrf1 has also been described to establish and reorganize heterochromatin (Papait et al. 2008; De Vos et al. 2014). Uhrf1 also possesses a tandem tudor domain (TTD) which can bind the H3K9me3 mark (Karagianni et al. 2008). Besides Dnmts, Uhrf1 can also interact with histone modifying enzymes such as HDAC1, Tip60 and G9a (Unoki et al. 2004; Achour et al. 2009; Kim et al. 2009) (Figure 2-4). These data suggest Uhrf1 to be an important link between DNA and histone methylation. Indeed, deletion of the RING finger domain which binds methylated histones, can lead to defects in DNA methylation in mouse ESCs (Nishiyama et al. 2013).

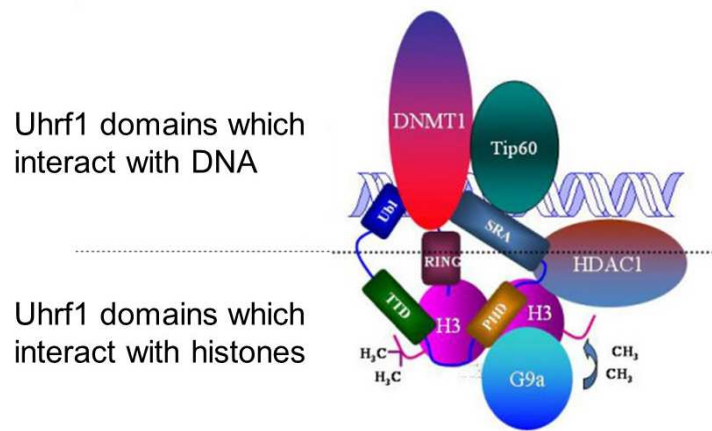


Fig.2-4 The different domains of Uhrf1 and its interaction partners. Modified from (Alhosin et al. 2011) (Open Access article distributed under the terms of the Creative Commons Attribution License)

Schematic of the domains of Uhrf1 – SRA interacting with DNA and Dnmt1, RING, TTD and PHD domain which binds histones. Uhrf1 can interact with the proteins HDAC1, G9a and Tip60.

Besides ESCs, *Uhrf1* is expressed in skin stem cells during proliferation and downregulated upon differentiation (Sharif et al. 2007; Sen et al. 2010). It has also been described to play a crucial role in regulatory T cell differentiation, whereby loss of Uhrf1 in these cells led to defects in proliferation and differentiation (Obata et al. 2014). Many studies have implicated a role for Uhrf1 in cancer formation and progression (Hervouet et al. 2010; Tien et al. 2011; Babbio et al. 2012; Pacaud et al. 2014). Moreover, Uhrf1 has been shown to negatively regulate the Pml protein in human endothelial cells (Guan et al. 2013). Uhrf1 has been recently been shown to be important in maintaining the balance between self-renewal and differentiation of hematopoietic stem cells by regulating DNA methylation of key stem cell genes (Zhao et al. 2016).

Uhrf2 is also expressed by mouse ESCs (Pichler et al. 2011). However, in contrast to *Uhrf1*, *Uhrf2* is expressed highly during ESC differentiation (Pichler et al. 2011). Thus, *Uhrf1* and *Uhrf2* seem

to exhibit contrasting modes of expression. Genetic knockouts of *Uhrf2* has not been studied yet and thus its exact function is largely unknown.

Although many studies have examined the role of Dnmts and Tet enzymes in neurogenesis, the function of Uhrf1 has not been examined in NSCs.

2.2 Transposable elements

One group of genomic loci wherein DNA methylation has been described to play a key role in regulating their epigenomic landscape and transcription, is that of ERVs. ERVs form a class of transposable elements (TEs) which are sequences of DNA that can jump around the genome. However, ERVs form a part of the retrotransposon family which can multiply prior to transposition (Sharif et al. 2013). Nearly half of the genome is comprised of TEs and ERVs are about 5% of the mouse and human genome (Kassiotis 2014) (Figure 2-5). Other types of retrotransposons are more abundant such as LINE-1 elements (19% of genome) and SINE elements (8% of genome) (Kassiotis 2014). ERVs have arisen from germline integration of retroviruses which have infected mammals through evolution (Dewannieux and Heidmann 2013). These ERVs largely resemble retroviruses, comprising of gag, pro, pol and env genes flanked by long-terminal repeats or LTRs. The LTR region often act as promoters. There are many different types of ERVs in both the mouse and human genome. The mouse genome has a specific ERV known as IAP (Figure 2-5) which is present as about 1000 copies in the genome (Barbot et al. 2002). The IAP elements themselves comprise of several subtypes, largely based on their structure, as some of them are heavily truncated (Sharif et al 2013).

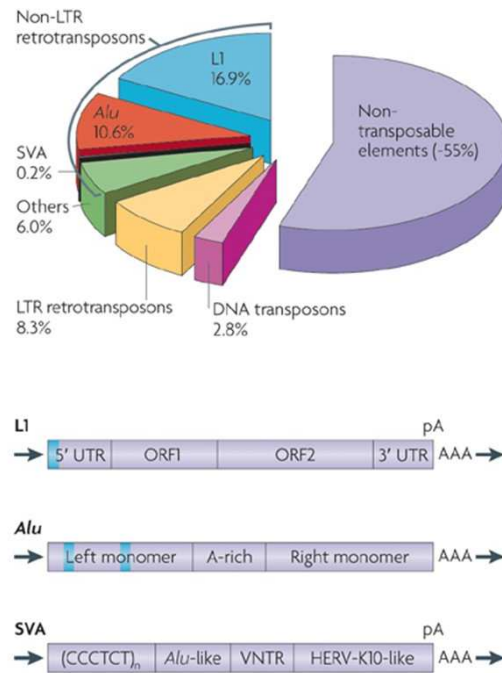


Fig. 2-5 Transposable elements in the genome. Reprinted by permission from Macmillan Publishers Ltd: Nature Reviews Genetics (Cordaux and Batzer 2009) copyright (2009). License no. 4056710870507

Schematic showing the percentage of different types of transposable elements in the genome. The sequence of LINE-1 elements with its open reading frames (orf) and the sequences of ERVs is depicted. Note that IAP elements form a part of ERVs which contain *gag*, *pro*, *pol* and *env* genes with flanked LTRs.

During development, in preimplantation blastocysts and in primordial germ cells, there is a genome-wide erasure of 5mC which occurs (Messerschmidt et al. 2014). During this time, many regions in the genome have been shown to resist the loss of 5mC, such as the IAP subclass of ERVs (Guibert et al. 2012; Hackett and Surani 2013). However, interestingly, loss of 5mC in somatic cells at later stages of development, does indeed cause IAP activation. Therefore,

depending on the cell-type and developmental time, IAP transcription can be under the control of levels of DNA methylation.

The impact of retrotransposons on mammalian cells has been described to be both beneficial and harmful. Studies have suggested that LINE-1 elements can contribute to the evolution of complex brains and the generation of neuronal diversity (Muotri et al. 2005; Singer et al. 2010) . However, there are also multiple reports which have linked overexpression of retrotransposons to cell death, genome instability, stress response and cancer (Morrish et al. 2002; Belgnaoui et al. 2006; Sinibaldi-Vallebona et al. 2006; Pasquarella et al. 2016).

Regulation of retrotransposons in neural development is still in its infancy and data from the LINE-1 studies suggest that it may be of importance in this niche.

2.3 Embryonic forebrain

2.3.1 Development of the embryonic forebrain

Neurogenesis is a dynamic process which requires tight transcriptional control in a spatial and temporal manner. The main events occurring during neurogenesis are neural stem and progenitor proliferation and neuronal differentiation and maturation. Each of these steps are regulated by several key coding genes and non-coding elements in the genome.

Neurogenesis is widespread during embryonic development, occurring in several regions of the brain. In the embryonic cerebral cortex, neurogenesis commences at about E10. Prior to this stages, the developing cortex is derived from the neural tube. The neural tube is initially divided into the prosencephalon (which forms the telencephalon or anterior embryonic forebrain and diencephalon or posterior forebrain), the mesencephalon (midbrain), the rhombencephalon or hindbrain (develops into pons, cerebellum and medulla oblongata) and the spinal cord.

At about E8.5, the telencephalic primordium is specified by the induction of the transcription factor Foxg1 (Tao and Lai 1992; Shimamura and Rubenstein 1997). Following this, the telencephalon is subdivided into two specific domains - the ventral and dorsal telencephalon. The specific domains of the telencephalon are established by signaling gradients which control the expression of specific transcription factors in each domain. The ventral telencephalon is further subdivided into the neocortex which lies in the anterior lateral region and the posterior medial region which

develops in the hippocampus, cortical hem and the choroid plexus. The ventral telencephalon is also divided into the medial region termed the medial ganglionic eminence (MGE) and the posterior lateral regions are termed lateral ganglionic eminence (LGE) and caudal ganglionic eminence (CGE).

The telencephalon is composed of the lateral ventricles which are lined by germinal zones. The ventricle itself is composed of cerebral-spinal fluid produced by the choroid plexus (a network of ependymal cells).

2.3.2 Overview of embryonic neurogenesis

At about E9-E10, the process of neurogenesis commences in the telencephalon. Neurogenesis is the process by which neurons are generated from neural stem and progenitor cells. The main difference between the dorsal and ventral region of the telencephalon lies in the type of neurons they produce. The dorsal telencephalon primarily produces glutamatergic neurons whereas the ventral telencephalon generates mainly GABAergic neurons. Neurons generated in the neocortex migrate radially and remain in the neocortical domain. However, neurons generated in the ganglionic eminences can migrate tangentially to different regions (Figure 2-6A). The LGE derived neurons migrate primarily to the olfactory bulb and amygdala. The MGE and CGE derived neurons migrate tangentially to the neocortex and integrate into the existing neuronal network (Marin and Rubenstein 2001) (Figure 2-6A). The different regions of the telencephalon and their molecular markers are depicted in Figure 2-6B. These molecular markers are specific transcription factors which instruct certain cell fates in a spatial and temporal manner. The sharp border between the dorsal and ventral telencephalon is primarily setup by the transcription factors Pax6 and Gsx2 (Figure 2-6B). In fact, in Pax6 knockout embryos, the ventral part of the neocortex become specified as the dorsal LGE and in the Gsh2 knockout embryos, the dorsal LGE is specified into the ventral cortex (Corbin et al. 2000; Stoykova et al. 2000; Toresson et al. 2000; Yun et al. 2001). In the mouse telencephalon, neurogenesis occurs until about E18 with the process peaking at E14. Following neurogenesis, the generation of glia, a process known as gliogenesis, occurs from the end of development and into postnatal stages.

Much of our understanding of neurogenesis in the telencephalon is derived from studies in the neocortex, with the ganglionic eminence exhibiting some differing and some common features (Pilz et al. 2013).

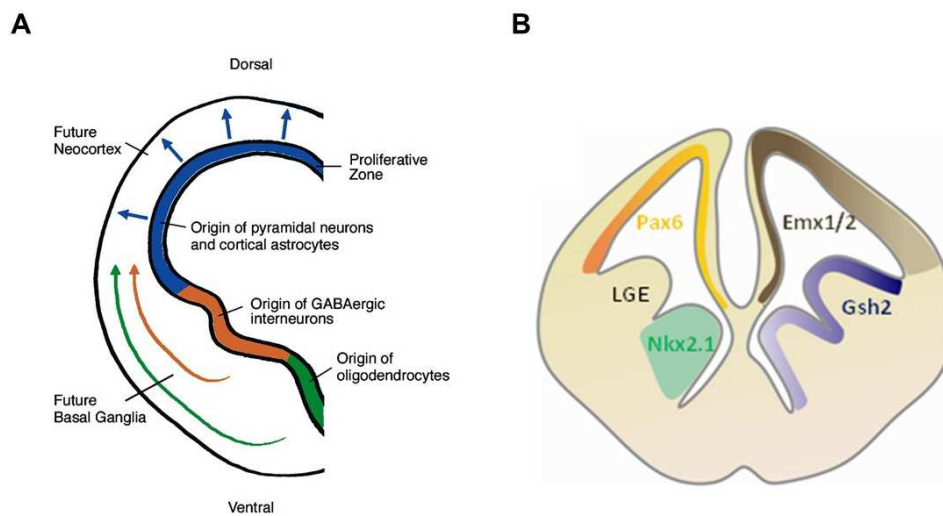


Fig.2-6 Regions of the telencephalon

Adapted by permission from Macmillan Publishers Ltd: Neuron (Ross et al. 2003) copyright (2003). License no. 4050741125950. (A) and (Nat et al. 2013) (open access under CC BY 3.0 license) (B)

A. Coronal section of the telencephalon depicting the dorsal and ventral regions and their respective types of neurons.

B. Coronal section of the telencephalon depicting the specific transcription factors in each domain. *Emx1/2* and *Pax6* are dorsally expressed. *Nkx2.1* is specific to the MGE and *Gsh2* is in the LGE and MGE.

2.3.3 Cell types in the embryonic neocortex

The neuroepithelium of the telencephalon at the onset of neurogenesis is composed of neuroepithelial cells termed radial glia. These cells act as neural stem cells - capable of self-renewal and multipotency, generating both neurons and glia. Radial glia are situated in the ventricular zone (VZ) and maintain contact to the inner ventricular surface and the outer pial surface via apical and basal process. However, their cell body is stationed in the ventricular zone, which is the region adjacent to the ventricle (Figure 2-7). At early neurogenic stages, until about

E11, the radial glia mainly undergo symmetric self-renewal cell divisions in order to expand their pool (Gotz and Huttner 2005). Following this time, they start generating a population of transit-amplifying progenitors termed basal or intermediate progenitors via asymmetric divisions (Haubensak et al. 2004; Noctor et al. 2004; Noctor et al. 2007). These basal progenitors do not exhibit apical-basal polarity and are multipolar in nature. In addition to apically located radial glia, another type of cell termed as subapical progenitors has been recently reported (Pilz et al. 2013). Moreover, another type of progenitor has been identified termed as basal radial glia (Reillo et al. 2011; Wang et al. 2011; Florio and Huttner 2014) which are cells harboring radial glia features but with only a basal process in contact with the pial surface (Figure 2-7). Moreover, they are situated more basally outside the ventricular zone.

Generation of basal progenitors leads to the appearance of an additional zone in the neocortex (Figure 2-7) termed as the subventricular zone (SVZ) wherein most of these progenitors reside. Basal progenitors mainly undergo symmetric divisions to either self-renew or generate neurons (Haubensak et al. 2004; Miyata et al. 2004; Noctor et al. 2004; Noctor et al. 2007). Radial glia and basal progenitors can be differentiated by the expression of certain transcription factors. Radial glia express *Pax6* whereas basal progenitors express *Tbr2*. Basal progenitors can also self-renew and undergo terminal divisions to generate neurons at different periods of neurogenesis. These neurons migrate through the intermediate zone (IZ) and form the developing cortical plate (CP).

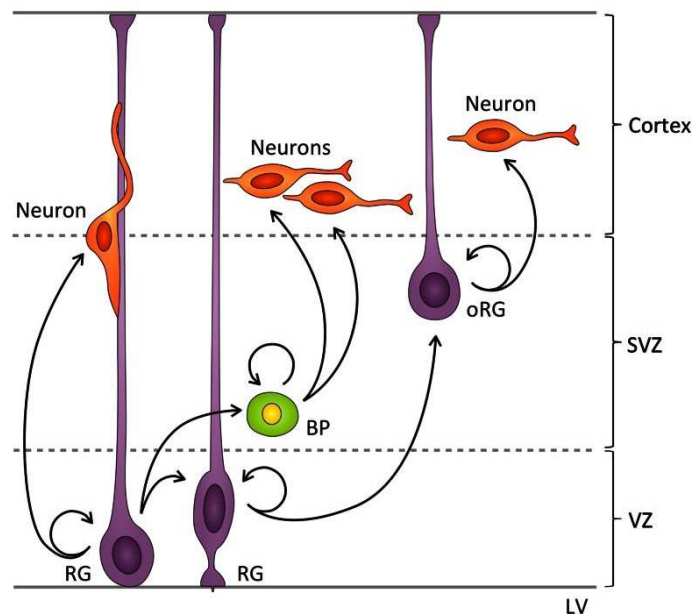


Fig.2-7 Cell types in the embryonic cortex. Modified from (Gomez-Lopez et al. 2014) (Open Access article distributed under the terms of the Creative Commons Attribution License)

At early neuroepithelial stages, the neuroepithelial cells divide to generate radial glia (purple cells with process). The radial glia divide both symmetrically to self-renew and asymmetrically to generate basal progenitors and neurons. Radial glia can generate neurons both by direct neurogenesis (first purple radial glia generating neurons, depicted in orange), as well as by indirect neurogenesis (via basal progenitors depicted in green). Neurons migrate into the cortical plate and reside per their birthdate and layer. The mammalian cortex also contains basal or outer radial glia (purple cells with only basal process) and subapical radial glia (not shown).

LV – lateral ventricle; VZ – ventricular zone; SVZ – subventricular zone; RG – radial glia; BP – basal progenitor; oRG – outer radial glia

2.3.4 Cortical layering and postnatal terminal neuron differentiation

Newly generated neurons in the neocortex migrate radially to form the 6-layered cortex in an inside-out manner wherein the early born neurons are situated close to the ventricle and the late born neurons are close to the pial surface (Figure 2-8). The first-born neurons, termed Cajal-Retzius cells, which comprise of layer I of the cortex, are generated at E11. Layer VI neurons are

generated following these neurons at about E13-E14 and express the transcription factor Tbr1. Following Layer VI, layer V neurons are produced which are mainly labelled by Ctip2. Layer IV neurons are labelled by Rorb/Satb2, layer II/III neurons by Cux1.

During the first few weeks of postnatal development, the neurons in the cerebral cortex undergo terminal neuronal differentiation. Most of the neurons born in the cerebral cortex are projection neurons. However, it is important to note here that GABAergic neurons migrate into the cortex from the GE. Projection neurons can either form connections with neurons of the contralateral hemisphere via the callosum (cortico-cortico projection neurons) or anterior commissure (Greig et al. 2013) or form corticofugal projections which project away from the cortex. The corticofugal connections are either thalamocortical (to the thalamus) or other subcerebral projections (Greig et al. 2013).

Once the projection neurons in the embryonic cortex migrate to the correct layer, they initiate axon and dendritic growth. These processes are essential to further build synapses which enable specific connections between neurons. In early postnatal stages, between P1 to P8, there is additional axon growth and guidance (Lewis et al. 2013). From P8 to P21 axon branching and synapse formation occurs (Lewis et al. 2013). Defects in any of these processes can lead to neurodevelopmental disorders such as autism spectrum disorders, epilepsy and mental retardation (Zoghbi and Bear 2012).

Another important process which occurs in postnatal neurons is the downregulation of cell cycle proteins. Postmitotic neurons still express members of the Retinoblastoma family of proteins, E2F transcription factors, Cyclin-dependent kinases and inhibitors after terminal neuron differentiation (Yoshikawa 2000). It has been hypothesized that these cell cycle proteins are relevant for neuron survival and maintenance of differentiation (Cicero and Herrup 2005; Liu et al. 2005; Kurita et al. 2006; Nguyen et al. 2006; Hasegawa and Yoshikawa 2008). Regulation of these cell-cycle proteins seems critical as misregulation could lead to neuronal death in adult neurons (Herrup and Yang 2007).

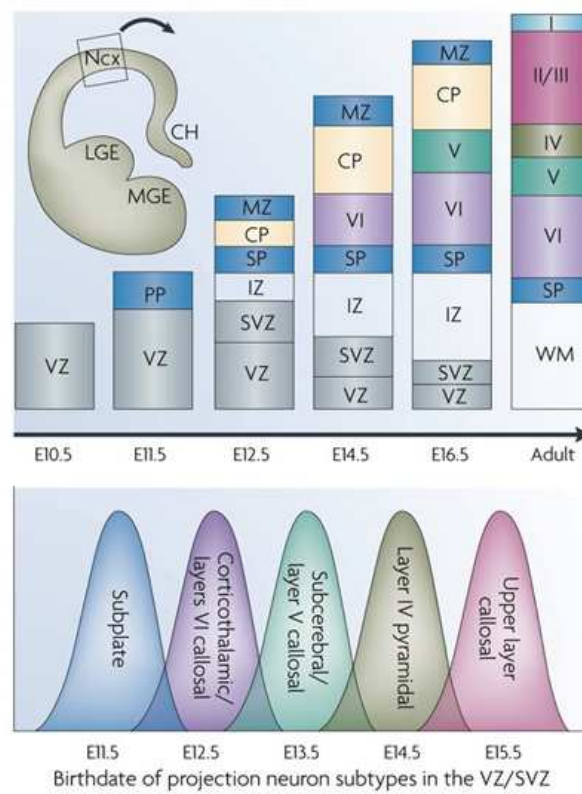


Figure 2-8 Chronological generation of different types of cortical neurons in an inside-out manner. Adapted by permission from Macmillan Publishers Ltd: Nature reviews neuroscience (Molyneaux et al. 2007) copyright (2007). License no. 4052120920271.

The early born neurons form the preplate which later splits into the superficial marginal zone and deep subplate. The different layers of the cortical plate are formed between these two layers during the main period of neurogenesis from E12-E16.

2.4 Adult neurogenesis and gliogenesis

2.4.1 Adult neurogenic niches and cell types

In the postnatal and adult brain, neurogenesis occurs only in certain specific niches, namely the subependymal zone (SEZ) of the lateral ventricle and the dentate gyrus (DG) of the hippocampus (Kriegstein and Alvarez-Buylla 2009) (Figure 2-9A). The early evidence for these niches were from first from neurosphere experiments showing the ability of aNSCs to self-renew and be multipotent (Reynolds and Weiss 1992). Following this, transplantation experiments were performed wherein SEZ cells were grafted either homotypically (i.e. SEZ from one mouse into SEZ of another mouse) (Lois and Alvarez-Buylla 1994) or heterotypically (SEZ of one mouse into other regions of the brain of another mouse) into the striatum wherein neurogenesis does not occur (Herrera et al. 1999). In the homotypic situation, the grafted cells could integrate and differentiate, but not in the heterotypic condition

The source of adult neural stem cells was previously shown to be radial glia (Merkle et al. 2004). Moreover, recent studies have indicated that LGE progenitors could be ancestors of adult neural stem cells (Furutachi et al. 2013). Adult neural stem cells (aNSCs) exhibit many radial glial features, sharing common molecular markers. Adult neural stem cells in the SEZ are relatively quiescent but can divide to generate actively proliferating transit-amplifying progenitors (TAP) (Doetsch et al. 1999). These TAPs generate immature neuroblasts which migrate tangentially to the olfactory bulb from the SEZ and differentiate into interneurons (Lois and Alvarez-Buylla 1994; Belluzzi et al. 2003; Carleton et al. 2003), which integrate into existing circuitry (Figure 2-9B).

In the dentate gyrus, aNSCs also possess radial glial properties (Seri et al. 2001; Fukuda et al. 2003; Garcia et al. 2004). These aNSCs generate intermediate progenitor cells which in turn give rise to neurons which migrate radially and reside in the hippocampus (Seri et al. 2004) (Figure 2-9C). Neurons in the dentate gyrus are glutamatergic projection neurons and play important roles in learning and memory.

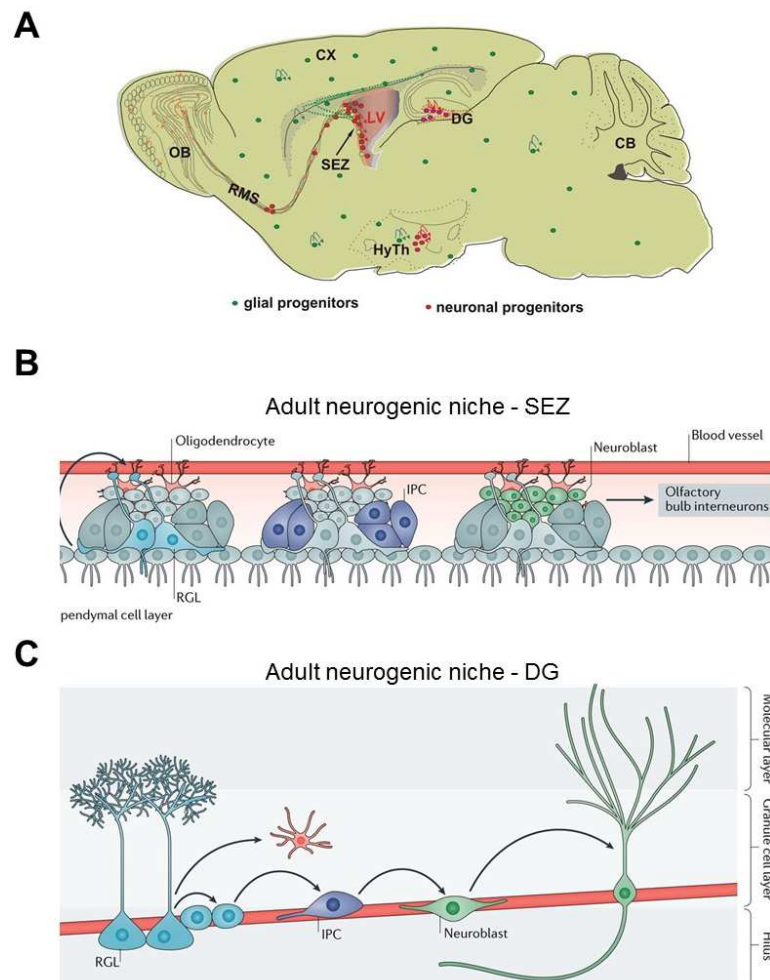


Fig.2-9. Adult neurogenic niches.

Adapted by permission, (Ninkovic and Gotz 2013) License no. 4050750571282 (A) and adapted by permission from Macmillan Publishers Ltd: Nature reviews neuroscience (Yao et al. 2016) copyright (2016). License no. 4050750893071 (B,C)

A. Scheme showing transverse section of the adult brain. The regions in red indicate the neurogenic niches in the SEZ and DG of the hippocampus. The scheme shows the restriction of neurogenesis to these regions as compared the widespread gliogenesis (green dots are cells) occurring throughout the parenchyma.

B. Scheme showing the cell types and the process of neurogenesis in the SEZ. Radial glia like NSCs get activated (blue cells, left group of cells) and generate IPCs or TAPs (purple cells, middle group of cells) which in turn generate neuroblasts (green cells, right panel). The neuroblasts migrate along the rostral migratory stream to the olfactory bulb.

C. Scheme of the cell types and the process of neurogenesis in the SGZ. Radial glia like NSCs get activated (blue cells) and generate IPCs or TAPs (purple cells) which in turn generate neuroblasts (green cells). The neuroblasts mature into neurons which migrate radially and remain in the hippocampus. The NSCs also generate parenchymal astrocytes (in red).

2.4.2 Gliogenesis

As mentioned earlier, neurogenesis subsides towards the end of embryonic development, allowing gliogenesis to commence. Glia are mainly generated either by precursor cells or by terminal differentiation of radial glia into differentiated glia. There are two main types of glial cells – astrocytes and oligodendrocytes. Astrocytes are mainly generated from radial glia, possibly as a direct conversion (Noctor et al. 2008; Kriegstein and Alvarez-Buylla 2009) (Figure 2-10A). Astrocytes can range from about 20-40% of all glia and perform several functions from providing biochemical support to endothelial cells of the blood-brain barrier, acting as a source of nutrients and other extracellular factors to neurons and playing roles in brain injury and repair. Most astrocytes have a characteristic morphology of short, highly branched tertiary processes.

The other type of glia, namely oligodendrocytes, are born at early embryonic stages as well as later stages. Oligodendrocytes provide trophic support to neurons (Bradl et al. 2010). Furthermore, they produce myelin sheaths which are important for nerve impulses and reducing ion leakage. There are three known waves of oligodendrocyte production in the forebrain. The first wave occurs at E16 wherein progenitors in the MGE generate a wave of oligodendrocytes which migrate towards the cortex (Pringle and Richardson 1993; Spassky et al. 1998; Tekki-Kessarlis et al. 2001). Following this wave, another group of oligodendrocytes appear from the LGE (Kessarlis et al. 2006). Finally, at E18, a third wave of oligodendrocytes are locally born from cortical progenitors (Kessarlis et al. 2006) (Figure 2-10B). It is interesting to note that at postnatal stages, most of the early born oligodendrocytes disappear and only the late born oligodendrocytes remain in the cerebral cortex (Kessarlis et al. 2006).

Some studies have indicated that a subpopulation of OPCs are also generated postnatally (Levison and Goldman 1993; Nait-Oumesmar et al. 1999; Menn et al. 2006; Aguirre et al. 2007).

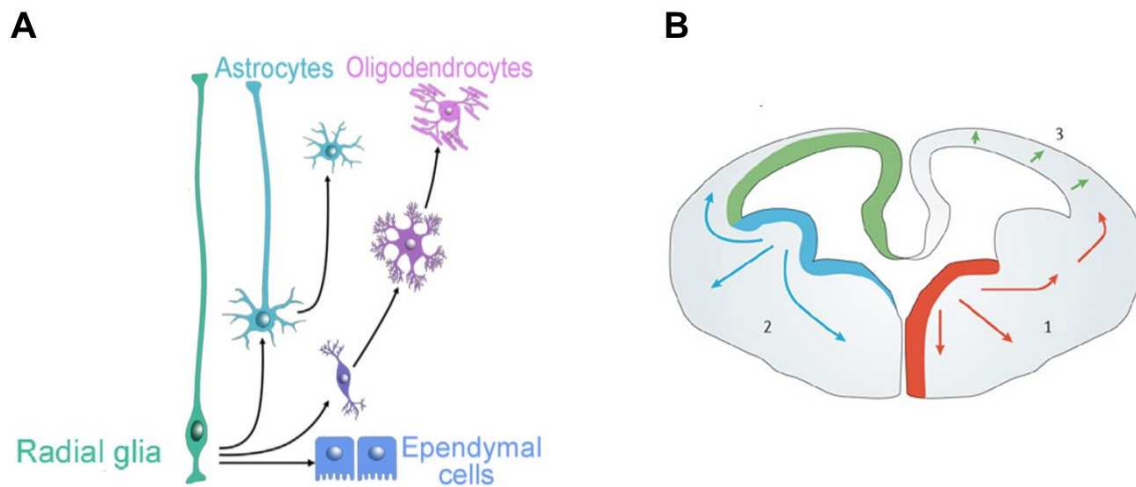


Fig.2-10. Gliogenesis in the embryonic forebrain

Reprinted with permission from Elsevier (Barry et al. 2014) License no. 4050751151722 (A) and adapted by permission from Macmillan Publishers Ltd: Nature reviews neuroscience (Richardson et al. 2006) copyright (2006) License no. 4057890885482 (B).

A. Schematic showing the generation of astrocytes and oligodendrocytes from embryonic radial glia and adult neural stem cells, from radial glia at the end of neurogenesis.

B. Schematic of a coronal section of the embryonic brain indicating the modes of OPC generation. OPC1 (Red arrows, 1) indicates the first wave at E16 from the MGE. OPC2 (blue arrows, 2) is the second wave following the first wave from the LGE and MGE and the third wave (green arrows, 3) occurs around E18 from cortical radial glia.

3. Aims of my thesis

Conditional deletion of Uhrf1 in the dorsal telencephalon (using Emx1-Cre) (Cappello et al. 2006; Iwasato et al. 2000) led to decreased cerebral cortical thickness in 1-month old mice (Bayam. 2014). Moreover, loss of Uhrf1 in adult neurogenic niches led to defects in neuronal differentiation (Bayam. 2014). These data have implicated an important role for Uhrf1 in regulating appropriate cerebral cortex neurons numbers and adult neurogenesis. Defects in progenitor proliferation were not observed at embryonic stages (analysed by pH3 and Pax6). However, an increase in cell death was observed with TUNEL mid embryonic stages. In contrast, conditional deletion of Uhrf1 in the adult SEZ and dentate gyrus (using GlastCre ERT2; Uhrf1 flox; CAG) (Mori et al. 2006) resulted in a decrease in transit-amplifying progenitors (TAPs) and neuroblasts, indicating differing roles for Uhrf1 in embryonic and adult neurogenesis.

Based on these findings, the main of my project was in unravelling the molecular mechanism of Uhrf1 in neural stem cells. Additionally, we made some preliminary attempts to test if these mechanisms could act during adulthood as well. In particular, we first studied the cellular phenotypes observed during conditional loss of Uhrf1 in neural stem cells of the developing cerebral cortex. Following this, we dissected the molecular role of Uhrf1 in these cells, analyzing transcriptional and epigenetic processes. Finally, we examined some of the phenotypes observed in the conditional knockout of Uhrf1 in adult neurogenic niches, with emphasis on its molecular function.

4. Results

4.1 *Uhrf1* expression from embryonic to adult stages

To characterize *Uhrf1* expression, we performed *Uhrf1* qRT-PCR in E14 NSCs (isolated by FACS with Prominin 1 antibody), E14 neurons (isolated by FACS by PSA-NCAM antibody), adult subependymal zone and adult grey and white cortical matter (Figure 4-1A). Indeed, we could observe about 40-fold higher *Uhrf1* mRNA in E14 NSCs as compared to neurons. Moreover, *Uhrf1* mRNA was barely detectable in adult cortical grey matter (Figure 4-1A). We also performed *Uhrf1* immunostainings at postnatal day 5 (P5). We observed only few cells in the cortex to express *Uhrf1* (Figure 4-1B). These cells did not colocalize with NeuN, a neuronal marker (Figure 4-1C), however, some did co-label with Ki67, indicating some of the *Uhrf1*+ve cells are proliferating (Figure 4-1D). Thus, our data in conjunction with the previous study, shows that *Uhrf1* is primarily expressed in NSCs and progenitors and is largely absent in neurons of the embryo and adult cerebral cortex.

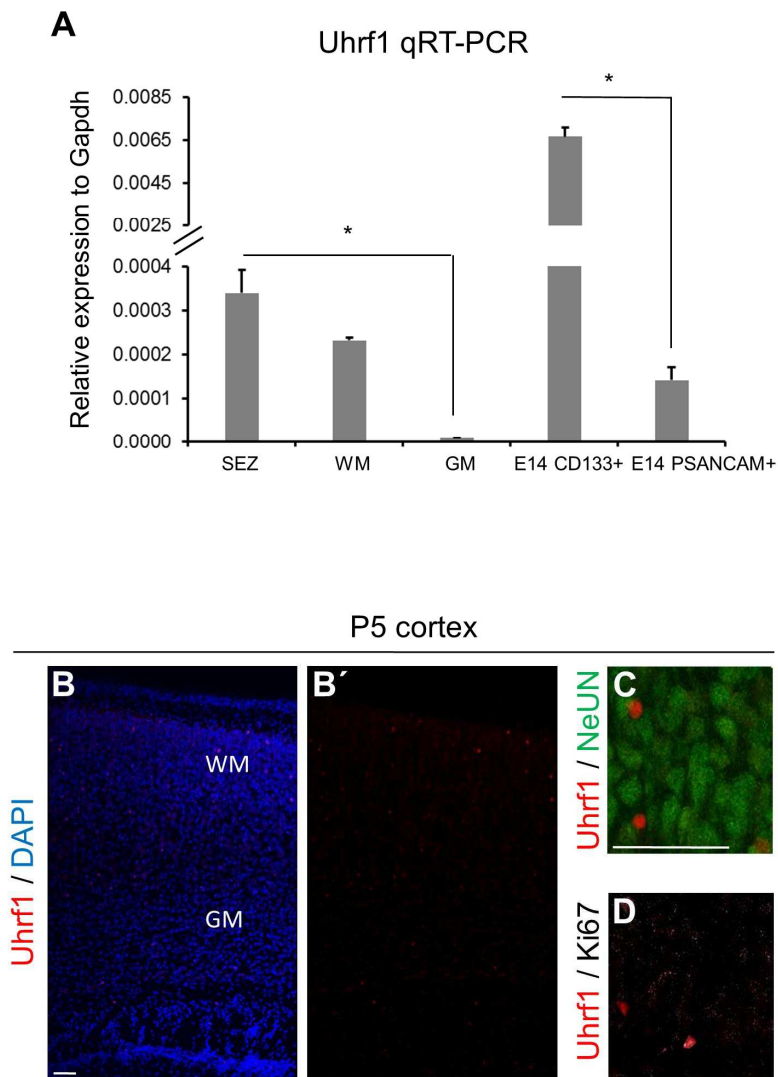


Fig.4-1 Uhrf1 expression in embryonic and adult neurogenic niches

A. qRT-PCR for *Uhrf1* showing high expression in NSCs and almost absence in neurons. E14 cortical tissue was dissociated to isolate NSCs by Prominin 1 and neurons by PSA-NCAM by FACS. Grey and white matter and SEZ tissue was isolated from 2-month old mice. qRT-PCR was performed for *Uhrf1* in the above populations using *Gapdh* as the housekeeping gene. * indicates significance with p-values 0.009 and 0.00005 respectively. Error bars indicate standard error of mean. n=3.

B-D. Confocal images of coronal sections of P5 cerebral cortex immunostained for *Uhrf1* (B), *Uhrf1* and NeuN (C) and *Uhrf1* and Ki67 (D) showing the absence of *Uhrf1* in neurons. Scale bar = 50 μ m.

4.2 Characterization of Uhrf1 cKO cellular phenotype

4.2.1 Comparable numbers of neurons and glia at E16

A conditional knockout of Uhrf1 was generated specifically in the developing cerebral cortex using the Emx1-Cre mouse line (Iwasato et al. 2000; Ramesh et al. 2016) which recombines specifically in the dorsal telencephalon, deleting Uhrf1 in this region. *Emx1^{cre+/-} Uhrf1^{fl/fl}* mice (hereby referred to as cKO) is compared to *Emx1^{cre+/-} Uhrf1^{fl/-}* mice (hereby referred to as controls). We performed Uhrf1 immunostaining at E12 and could observe a loss of Uhrf1 protein in the cKO (Figure 4-2A,B), specifically in the dorsal telencephalon and not in the LGE where *Uhrf1* was not deleted (Figure 4-2B). We further investigated the cellular phenotype by assessing proliferation of progenitors and numbers of neurons at embryonic stages. We assessed proliferation with Ki67 immunostaining at E16 in cKO cortices and controls. We could not observe a significant difference in the cKO compared to the control (Figure 4-2C,D). However, we did detect an increase in non-apical Ki67 positive cells in the cKO. We performed Tuj1 (to label all neurons) and Tbr1 (label neurons in the cortical plate) immunostaining at E16 and did not detect any evidence of premature differentiation (Figure 4-2E-H). Moreover, the numbers of Tbr1+ve neurons were unchanged (Figure 4-2I).

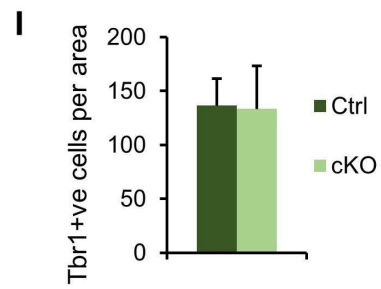
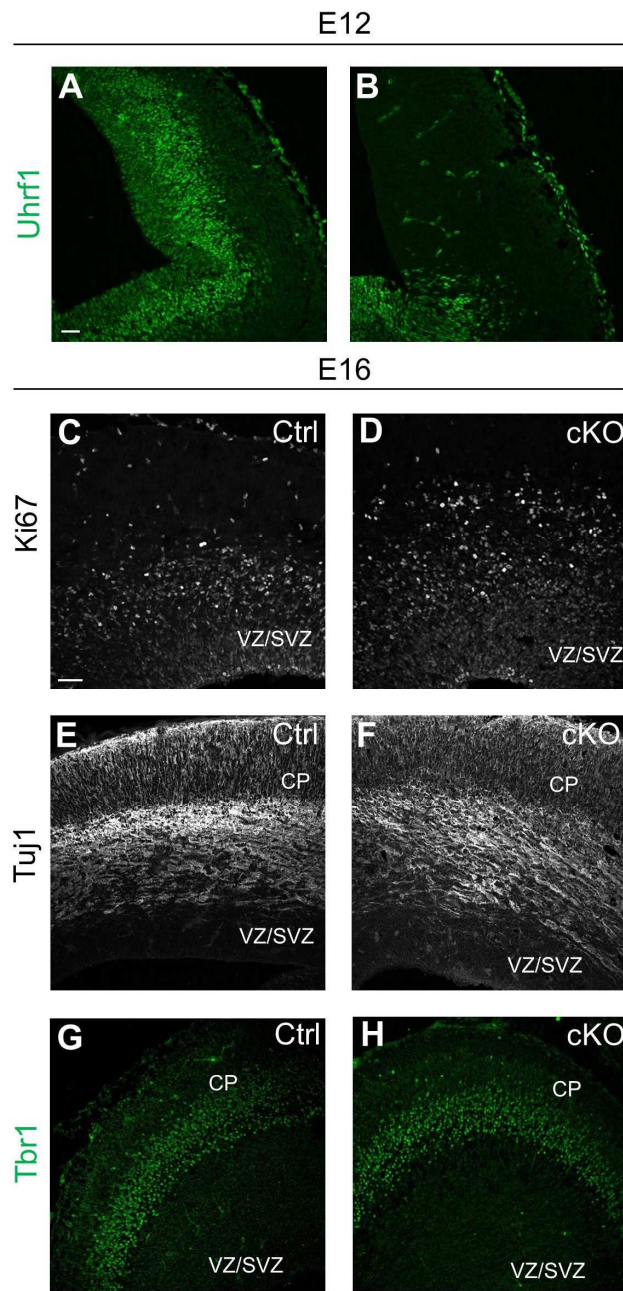


Fig. 4-2 Comparable proliferation and neuron numbers at E16 in the cKO

A-B. Confocal images of coronal sections at E12 of cerebral cortex of controls (A) and cKO (B) immunostained for Uhrf1 (A,B). Note the loss of Uhrf1 in cKO in the cerebral cortex wherein it was deleted as opposed to the LGE where Cre recombination did not occur (B).

C-H. Confocal images of coronal sections of the cerebral cortex at E16 of controls (C,E,G) and cKO (D,F,H) immunostained for Ki67 (C,D), Tuj1 (E,F) and Tbr1 (G,H).

I. Quantifications of Tbr1+ve cells per area of sections from (G) and (H). Error bars indicate standard error of mean. N=4.

Scale bar = 50µm. Abbreviations: CP – cortical plate; VZ – ventricular zone; SVZ – subventricular zone

It has been previously reported that cell death can lead to activation of glial cells (Robel et al. 2011). Thus, we investigated if glial cells were altered in the *Uhrf1* cKO compared to controls. We performed immunostaining for Gfap at E16 and could not observe any activation in the cKO (Figure 4-3A,B). Furthermore, microglial cells, labelled by Iba1 immunostaining at E16, appeared comparable in number and morphology in controls and cKO (Figure 4-3C,D). However, in 1 month old mice we did observe Gfap activation in the cKO, which is probably a result of reactive gliosis due to neuronal death (Figure 4-3E,F).

These results suggest that neurons and glia are generated in an appropriate manner in the cKO and control during embryonic stages.

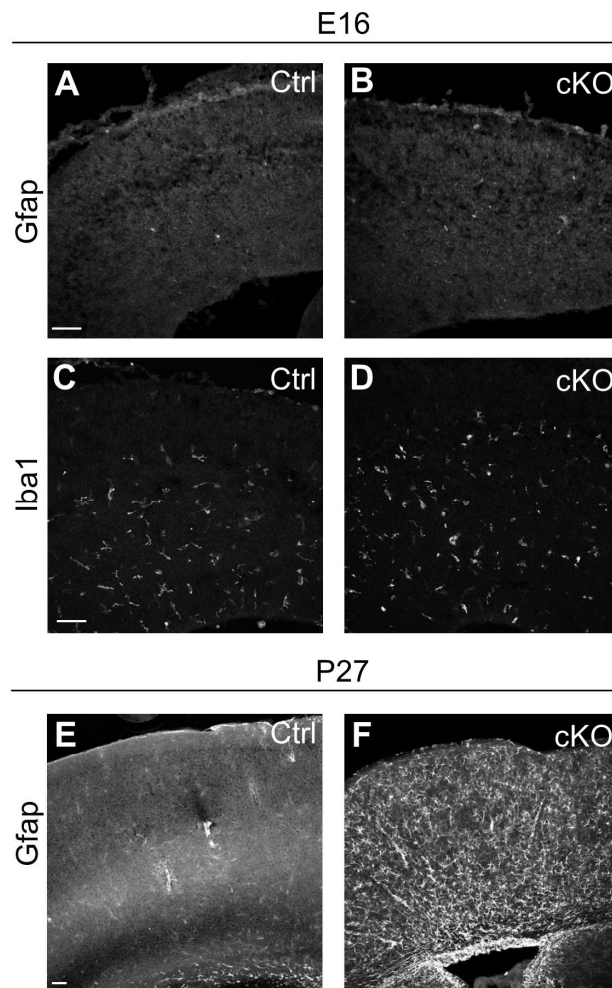


Fig.4-3 Absence of glial cell activation in E16 cKO cortices with reactive gliosis at later stages

A-D. Confocal images of coronal sections of the cerebral cortex at E16 of controls (A,C) and cKO (B,D) immunostained for Gfap (A,B) to label astrocytes and Iba1 (C,D) to label microglia. Note the absence of Gfap staining in both cKO and controls and comparable Iba1 staining in cKO and control.

E,F. Confocal images of coronal sections of the cerebral cortex at P27 of controls (E) and cKO (F) immunostained for Gfap. Note the reactive gliosis at in 1-month old cKO cerebral cortex. Scale bar = 50 μ m

4.2.2 Cortical layering at embryonic and postnatal stages appeared normal in the cKO

As generation of neurons was not impaired in the cKO, we next sought to determine if the neuronal layers of the cortex were specified in the appropriate manner. We performed immunostaining for Ctip2 to label upper layer neurons and Tbr1 to label lower layer neurons at E18 and could not detect any abnormalities in the cKO as compared to the control (Figure 4-4A,B). Furthermore, we also performed Ctip2 immunostaining at P2 and observed analogous staining in controls and cKO (Figure 4-4C-D). These results suggest that neurons are generated and specified correctly into the layers of the cerebral cortex of *Uhrf1* cKO animals.

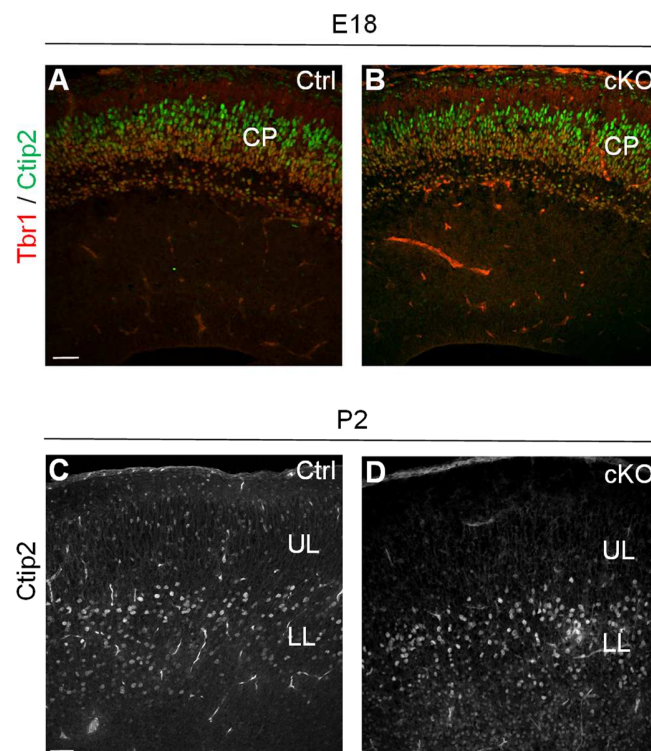


Fig.4-4 Upper layer and lower neuronal identity is maintained in *Uhrf1* cKO cortices

A-D. Confocal images of coronal sections of cerebral cortex of controls (A,C) and cKO (B,D) immunostained for Ctip2 and Tbr1 at E18 (A,B) and Ctip2 at P2 (C,D)

Note that the cortical layers in controls and cKO appear intact in all stages. Scale bar = 50 μ m. Abbreviations: CP – cortical plate; LL – lower layers; UL – upper layers

4.2.3 Cell death peaks in the postnatal *Uhrf1* cKO

As mentioned previously, conditional knockout of *Uhrf1* in the cerebral cortex exhibited cell death in embryonic stages. We sought to determine the onset of cell death by performing TUNEL staining as early as E12 (Figure 4-5A,B). We observed significantly higher TUNEL positive cells at E12, with about 4-fold higher in the cKO cortices (Figure 4-5C). Thus, the onset of cell death was observed at E12, at similar levels to later embryonic stages (Ramesh,Bayam et al. 2016).

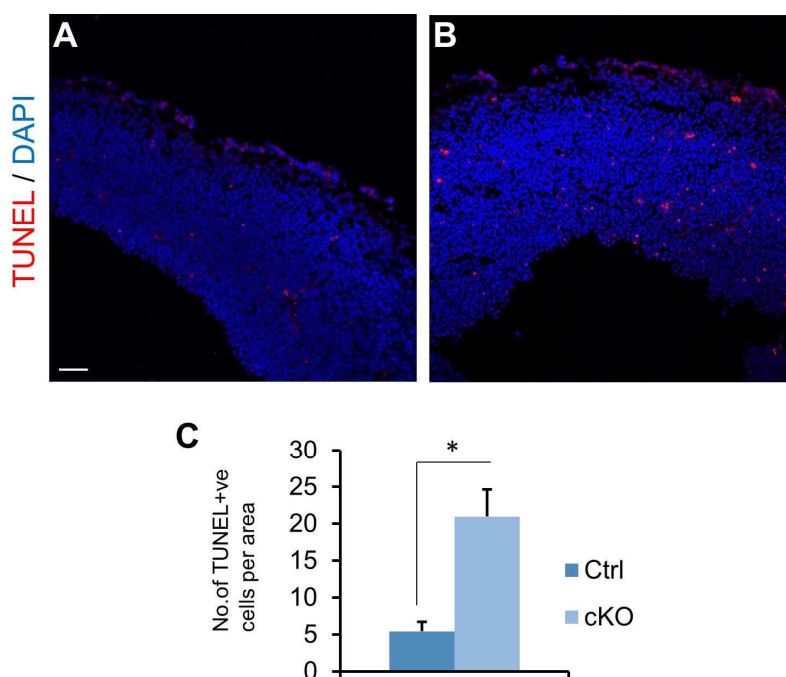


Fig.4-5 Onset of cell death was observed to be at E12 in cKO

A-C. Confocal images of coronal sections of cerebral cortex at E12 of controls (A) and cKO (B) immunostained for TUNEL (A,B). Increase in TUNEL+ve cells was observed in the cKO compared to control.

C. Quantifications of TUNEL+ve cells per area from A,B indicating 4-fold higher in the cKO. * indicates significance with Mann-Whitney test with p-value = 0.03, n=4. Error bars indicate standard error of mean. Scale bar = 50 μ m.

Although cell death was observed from early embryonic stages, a reduction in cortical thickness was not detected until P7 (Figure 4-6A,B). We sought to determine the peak of cell death, by analyzing postnatal stages. We performed TUNEL analysis at P2 and P7 and observed up to 11-fold higher cell death in P2 cKO (Figure 4-6C,D,G) as opposed to 6-fold higher at P7 (Figure 4-6E,F,G). Thus, we could detect higher levels of TUNEL positive cells at early postnatal stages leading to a discernible reduction in cortical tissue at P7.

In summary, deletion of *Uhrf1* in embryonic neural stem cells showed no cell fate change or changes in proliferation and differentiation. The significant phenotype was an increase in cell death beginning at embryonic stages and escalating at postnatal timepoints.

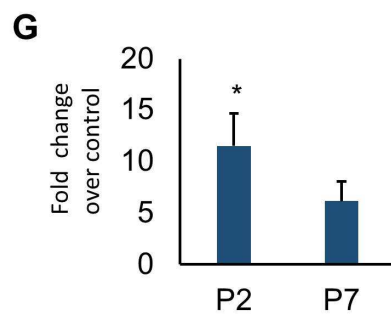
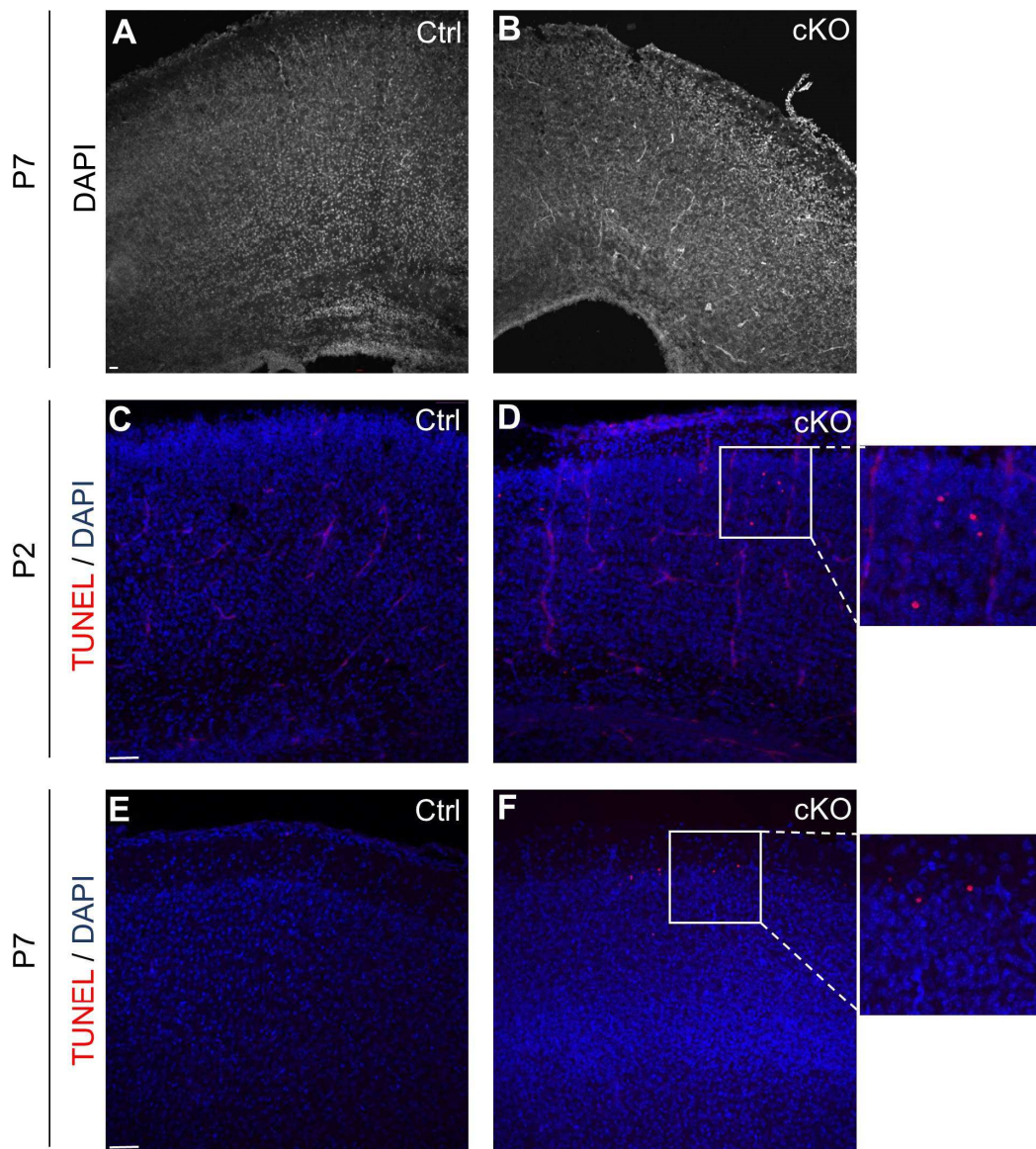


Fig.4-6 Cell death peaks at postnatal day 2 in the cKO cortex

A,B. Confocal images of coronal sections of cerebral cortex of P7 control (A) and cKO (B) stained with DAPI to indicate a reduction in cortical thickness in the cKO.

C,D,E,F. Confocal images of coronal section of cerebral cortex of controls (C,F) and cKO (D,G) stained with the TUNEL kit at P2 (C,D) and P7 (F,G), indicating increased number of TUNEL+ve cells in the cKO.

G. Quantifications of fold change of TUNEL+ve cells per area in P2 and P7 sections from C,D,E,F showing a significant increase in the cKO. * indicates significance with Mann-Whitney test with p-value = 0.01, n=4 for P2 and N=2 for P7. Error bars indicate standard error of mean. Scale bar = 50 μ m

4.3. Transcriptional profiling of Uhrf1 cKO

4.3.1 Activation of cellular stress genes at E16 and P5 Uhrf1 cKO

To understand the underlying molecular mechanisms contributing to the observed cell phenotype in *Uhrf1* cKO, we performed transcriptional profiling to uncover deregulated genes. Firstly, we focused on the region wherein *Uhrf1* is expressed and thus dissected the germinal zones (GZ) of *Uhrf1* cKO and controls and performed RNAseq (Figure 4-7A). We observed 68 upregulated genes and 30 downregulated genes (Fold change > 2 and p-value < 0.05) (Figure 4-7B, Table 1). Of these, 52 genes were derepressed (Table 1, highlighted in red). We defined a derepressed gene to have < 0.1 RPKM value in the control and > 2 fold change upregulation in the cKO.

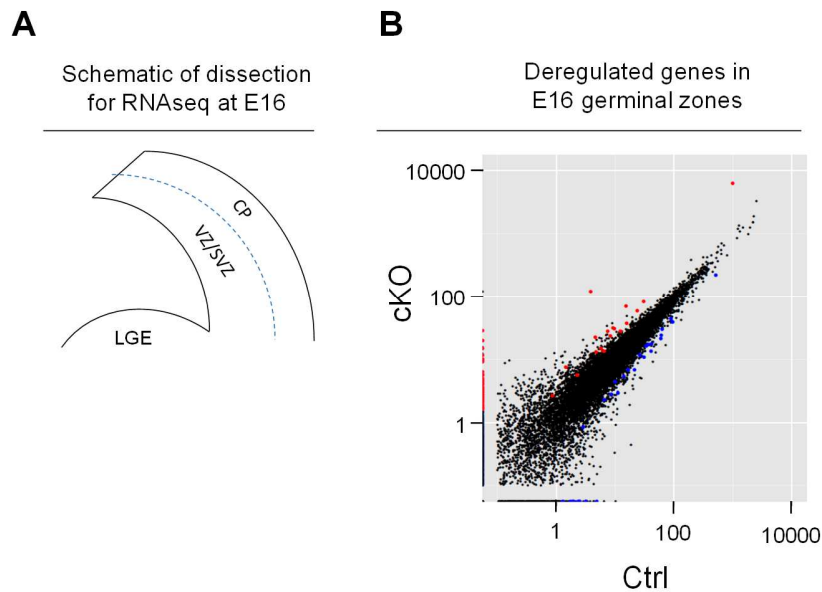


Fig.4-7 Transcriptional profiling in E16 germinal zones in cKO and controls

A. Schematic drawing showing microdissection of germinal zones (GZ) at E16 for the RNAseq. Blue dotted line indicates dissection cut. The tissue below the dotted line in the cortex was used for the RNAseq as *Uhrf1* is expressed in this region.

B. Expression plot of differentially regulated genes in the cKO compared to the control at E16 in the germinal zones. Red dots indicate upregulated genes, black dots indicate genes not changed in expression and blue dots indicate downregulated genes in the cKO. Fold change > 2 and p value < 0.05. X-axis and Y-axis values are FPKM (Fragments per million bases) from 100bp paired end RNAseq.

Table 1 – E16 cortex germinal zones RNAseq

Upregulated genes		Downregulated genes			
Gene name	FC	Gene name	FC	Gene name	FC
Serpinb1c	29.20	Nxf3	3.95	Apol7d	0.17
Corn4l	25.01	Xlr4b	3.94	Rsg1	0.24
Xlr3c	20.73	Pidd1	3.78	Gm2109	0.24
4930550L24Rik	20.52	Tex13	3.70	5830454E08Rik	0.29
Mnd1	15.81	Sifn4	3.69	Nnmt	0.29
4930500J02Rik	12.58	Gm773	3.67	Bcl2l10	0.30
Cdh19	10.97	Mtfp1	3.52	Kcnv1	0.32
Mia	10.84	Cd53	3.48	Cd79b	0.34
Rhox5	10.51	Ddr2	3.46	Hat1	0.34
Uba1y	9.97	Tuba3b	3.44	4930447C04Rik	0.35
Ccdc163	7.32	Dnajc6	3.36	Arhgap29	0.35
Col6a5	6.69	Nrtn	3.36	Pnliplr1	0.36
Sectm1a	6.65	Ly86	3.33	Bend6	0.36
E330017A01Rik	6.60	Klrb1b	3.20	Rorb	0.37
Rnf183	6.54	Slc15a2	3.12	Rgs8	0.39
Rpph1	6.39	Cdkl4	3.11	Gap43	0.40
Ccnb1ip1	5.92	Nkx2-3	3.08	Arpp21	0.42
Sohlh2	5.76	Slc25a18	2.93	Amer3	0.42
Ulbp1	5.61	Asns	2.90	Atpif1	0.43
Gfap	5.52	Fmo1	2.82	Csmd3	0.43
Mnd1-ps	5.32	Mbl2	2.82	Apoa1	0.43
Hamp2	5.06	Cacng1	2.75	Syn3	0.44
Crabp2	5.02	Batf3	2.68	B3galt2	0.44
Xlr4c	4.95	Trib3	2.66	Nfe2l3	0.46
Mgl2	4.61	Tmc3	2.65	Tceal8	0.47
Xlr4a	4.54	Hsd17b12	2.63	Lrp1b	0.48
Apoh	4.44	Ext2	2.62	Insig1	0.48
Tex101	4.31	Ptafr	2.62	Scn1a	0.49
Syce1	4.29	Ccnd1	2.46	Cat	0.49
Pnpt1	4.29	Tnc	2.37	Ypel5	0.50
Ptprq	4.23	Adcyap1r1	2.35		
Slc47a1	4.16	Sec61a1	2.26		
Atp6ap1l	4.12	Ak3	2.16		
Kntc1	4.07	Arhgef17	2.04		

Table 1. Table of upregulated and down regulated genes in E16 germinal zones

Table depicting upregulated and downregulated genes from Fig.4-7B at E16 in the germinal zones. Red indicates derepressed genes.

Secondly, we performed RNAseq on the total E16 cortex of controls and *Uhrf1* cKO to detect transcriptional changes in all cell types including neurons. We observed 89 upregulated genes and 20 downregulated genes (Figure 4-8, Table 2), of which 30% were derepressed (Table 2, highlighted in red). Having detected more upregulated than down regulated genes with many being derepressed, these data suggest that *Uhrf1* could play a more prominent role in transcriptional repression as opposed to activation.

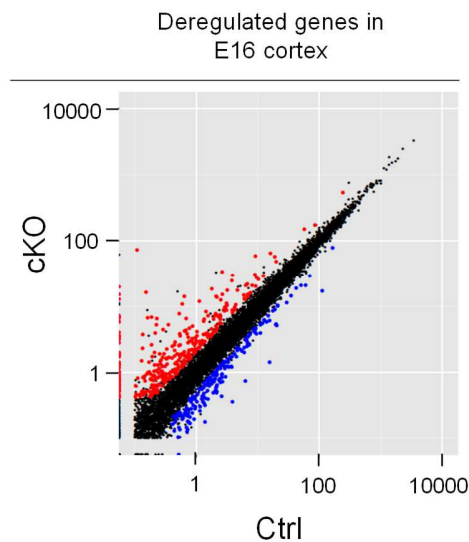


Fig.4-8 Transcriptional profiling in E16 full cortex in cKO and controls

Expression plot of differentially regulated genes in the cKO compared to the control at E16. Red dots indicate upregulated genes, black dots indicate unregulated genes and blue dots indicate downregulated genes in the cKO. Fold change > 2 and p value < 0.05. X-axis and Y-axis values are FPKM (Fragments per million bases) from 100bp paired end RNAseq.

Table 2 – E16 cortex RNAseq

Upregulated genes				Downregulated genes	
Gene name	FC	Gene name	FC	Gene name	FC
Ccrn4l	21.60	Pnpt1	2.77	Vaultc5	0.17
Sectm1a	13.54	Mbl2	2.76	Lst1	0.23
Mnd1	10.41	Arhgap15	2.72	Uhrf1	0.30
Al662270	9.97	Crif1	2.68	Hddc3	0.34
Wfdc9	9.84	Ulbp1	2.66	Dynlt1c	0.34
Trpc6	9.03	Myo1a	2.60	Scoc	0.34
Tuba3b	8.81	Zfp69	2.55	Nefl	0.36
Pet2	7.23	Capn11	2.55	Hbb-y	0.40
Gm9866	6.29	Chac1	2.50	Crym	0.41
493050J02Rik	5.72	Gfap	2.48	Smc2os	0.42
Gm773	5.68	Xlr3b	2.47	Gstt1	0.42
Xlr3a	5.63	Phlda3	2.46	2610507I01Rik	0.43
Slc47a1	5.48	Trap1a	2.43	Plin2	0.48
Kntc1	5.43	Ddn	2.43	Gm8773	0.48
Kcnh1	5.31	Nxph4	2.38	3110039M20Rik	0.48
Uba1y	4.87	Msx3	2.36	Ublcp1	0.49
Gpat2	4.81	Slc1a5	2.36	Tst	0.49
Ccnb1ip1	4.73	Cldn1	2.29	Dio2	0.49
Xlr4c	4.72	Cilp2	2.28	5730408K05Rik	0.49
Hamp2	4.65	Hsf2bp	2.28	Morf411	0.50
1700017N19Rik	4.39	Arl10	2.28		
Ctsh	4.08	Rhox2d	2.27		
Tspo2	4.07	Relb	2.26		
Slc7a3	3.95	Ptprh	2.25		
Sohlh2	3.95	Ecel1	2.25		
Ddr2	3.93	Dmrt2	2.23		
Mia	3.90	Gramd1c	2.23		
Crabp2	3.87	Casq1	2.23		
Cep112	3.69	Tex19.1	2.23		
Nxf3	3.69	Cdkn1a	2.20		
Mnd1-ps	3.66	Egfr	2.20		
Tfpi	3.52	Ptprq	2.20		
Eif4ebp1	3.43	Dcn	2.18		
Olfml2a	3.41	Acrbp	2.14		
Ifi27	3.38	Trank1	2.13		
Slc20a2	3.32	Gprin3	2.12		
Bfsp1	3.31	Acpp	2.12		
Cyct	3.17	Slc6a9	2.09		
Hspb3	2.95	Olf194	2.08		
Tex13	2.94	Stbd1	2.08		
Cdkl4	2.90	Gm5635	2.07		
Nrgn	2.84	Fam160a1	2.07		
Efcab6	2.80	A330102I10Rik	2.05		
Dact2	2.80	Gm6880	2.04		
		Pdgfc	2.02		

Table 2. Table of upregulated and down regulated genes in E16 full cortex

Table depicting upregulated and downregulated genes from Fig.4-8B at E16. Red indicates derepressed genes.

To detect significantly altered pathways, our collaborator, Dr. Schotta (BMC, Munich), utilized the Gene Set Enrichment Analysis (GSEA) tool. GSEA is a method used to determine if a defined set of genes is statistically different between 2 biological states. In the E16 germinal zone dataset, we observed an overrepresentation of genes involved in interferon alpha signaling (Figure 4-9A) and an underrepresentation of genes involved in oxidative phosphorylation (Figure 4-9B). Interestingly, in the E16 full cortex dataset, we did not observe any alteration in interferon signaling, suggesting that the proliferating cells are mainly altered in this pathway in *Uhrf1* cKO. However, we did observe an underrepresentation of oxidative phosphorylation genes and DNA repair genes in the cKO (Figure 4-9C,D). Thus, loss of *Uhrf1* in cortical NSCs, largely led to deregulation of cellular stress pathways.

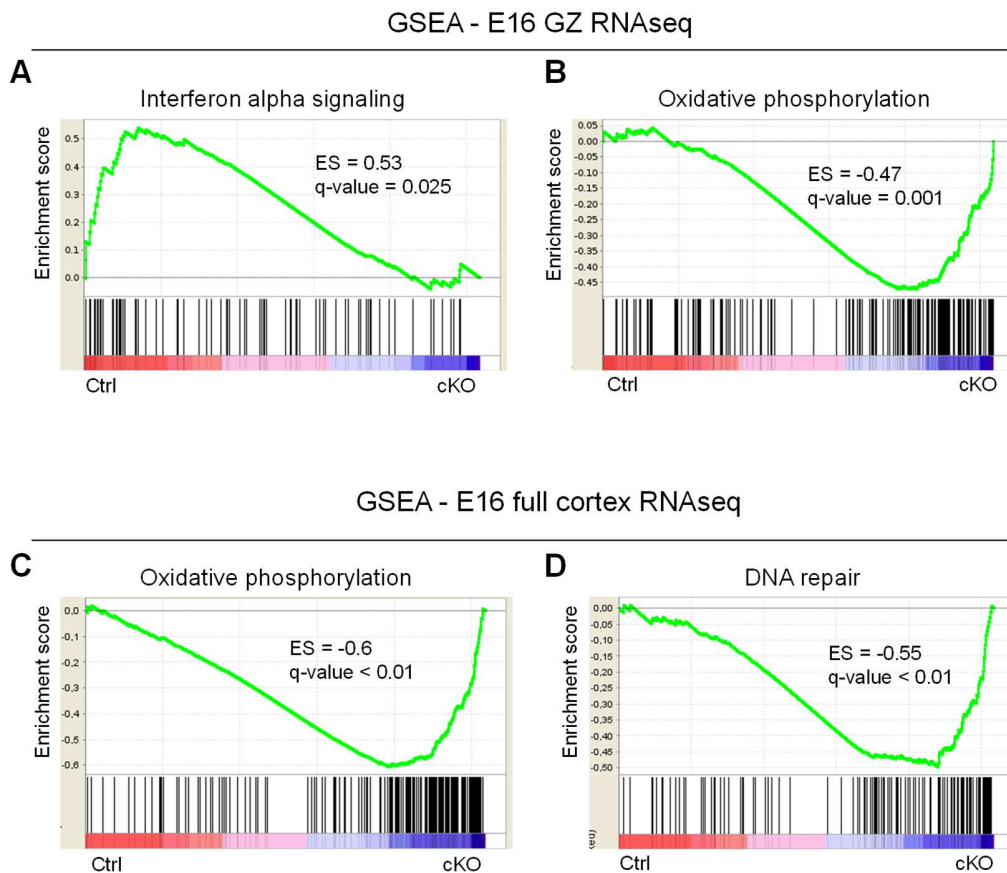


Fig. 4-9 GSEA analysis at E16 detect deregulation of cellular stress pathways

A-D. Graphs showing gene set enrichment analysis at E16 germinal zones (A,B) and full cortex (C,D), on gene expression datasets. *Uhrf1* cKO showed underrepresentation of genes involved in oxidative phosphorylation for both datasets. However, only the germinal zones show upregulation of interferon signaling and only the full cortex shows an underrepresentation of DNA repair genes in the cKO, suggesting that the former occurs in NSCs and the latter in neurons. FDR < 25%.

To understand, if these pathway alterations are maintained into later stages, we performed RNAseq in the entire cerebral cortex at postnatal day 5 (P5) in cKO and controls and observed 96 upregulated and 40 downregulated genes (with 43 derepressed genes) (Figure 4-10A and

Table 3). We observed that interferon signaling was upregulated also at this later stage, in addition to the unfolded protein response (Figure 4-10B,C). Thus, there appeared to be an exacerbation of the cellular stress phenotype in postnatal stages. Additionally, we observed an underrepresentation of genes belonging to the LEIN_neuron markers dataset which are genes expressed the adult brain (Figure 4-10D). These data suggest that either maturation of neurons is impaired or the slight reduction of neurons at this stage could cause this dataset to be underrepresented. However, as we do not observe a clear reduction in cortical thickness at P5, we favor the former hypothesis as a more likely cause.

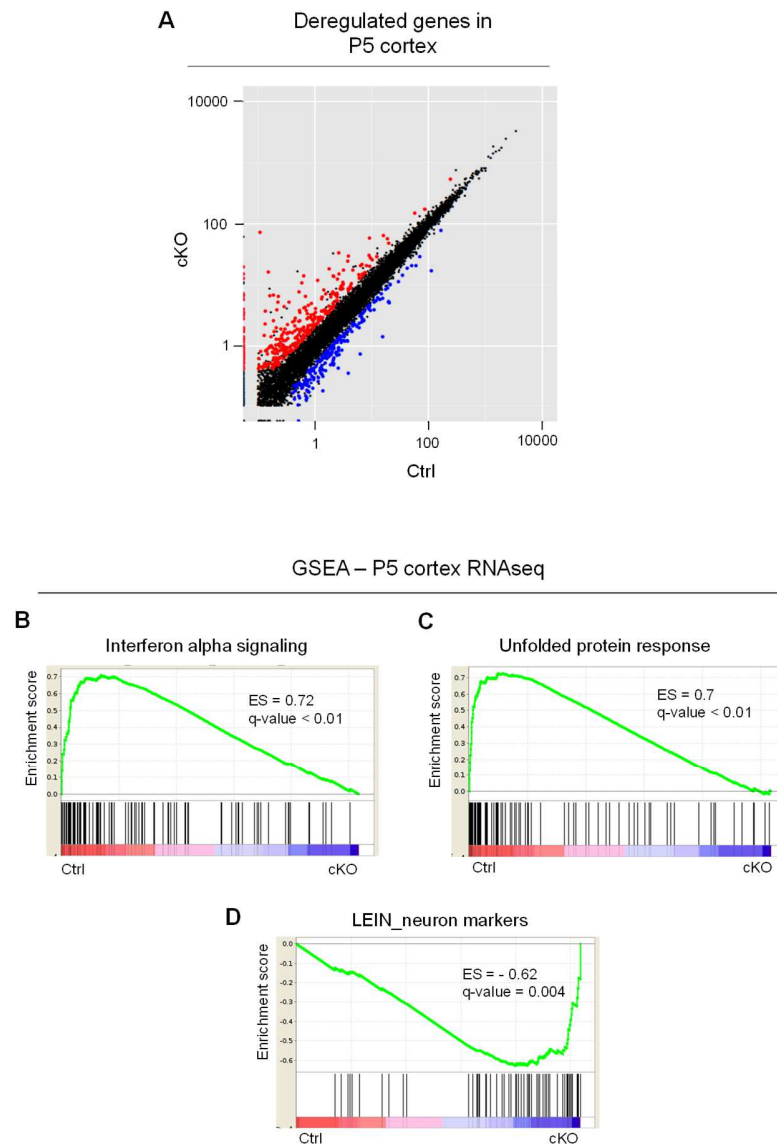


Fig. 4-10 GSEA analysis at E16 detect deregulation of cellular stress pathways

A. Expression plot of differentially regulated genes in the cKO compared to the control at P5. Red dots indicate upregulated genes, black dots indicate unregulated genes and blue dots indicate downregulated genes in the cKO. Fold change > 2 and p value < 0.05. X-axis and Y-axis values are FPKM (Fragments per million bases) from 100bp paired end RNAseq.

B-D. Graphs showing gene set enrichment analysis at P5 on hallmark and curated datasets. Uhrf1 cKOs show underrepresentation of genes involved LEIN_neuron markers and an overrepresentation of genes involved in interferon signaling and unfolded protein response in the cKO. FDR < 25%.

Table 3 – P5 cortex RNAseq

Upregulated genes				Downregulated genes			
Gene name	FC	Gene name	FC	Gene name	FC	Gene name	FC
Rhox5	65.47	Apoc1	3.09	H2bfm	2.29	Tshz2	0.14
Gm773	20.63	Bfsp1	3.07	Ogn	2.29	Nefl	0.16
Xlr3c	15.91	Tdrd9	3.00	Igtp	2.29	Lefty2	0.24
AI662270	14.89	Cd74	2.99	Tcfl5	2.28	Fam163a	0.28
E330017A01Rik	13.67	Wfdc12	2.99	Pgam2	2.28	Nefm	0.28
Slc47a1	11.09	A330049N07Ril	2.98	Prss45	2.28	Gpr88	0.30
Uba1y	9.34	Piwil2	2.95	Olfr1054	2.28	Scd1	0.31
Cox6a2	9.33	Atp6ap1l	2.93	Gm11413	2.27	Rprml	0.35
Mnd1	9.10	Magea10	2.90	Bst2	2.26	Nxn12	0.40
Pet2	7.97	Atf5	2.90	Pnpt1	2.24	Nts	0.40
Sectm1a	7.71	Efcab6	2.89	PspH	2.24	Ntf3	0.40
ApoH	7.59	Hsf2bp	2.89	Cilp2	2.21	Gsto1	0.42
4930500J02Rik	7.31	Lgals9	2.89	Ddr2	2.21	Crym	0.42
Myl4	6.85	Gm6268	2.88	Arhgap30	2.21	Sowaha	0.42
Hamp2	6.71	Rabggta	2.86	Psmb8	2.20	Itpka	0.42
Ccnb1ip1	6.58	Cyb5r1	2.86	H2-Aa	2.20	Grp	0.42
Cox7b2	6.51	Rhox2a	2.85	Gm13826	2.19	Pcbd1	0.43
Slc7a3	6.27	Olfr194	2.84	Adad2	2.18	Gstt1	0.45
Gpat2	6.04	Mia	2.79	Hk2	2.16	Resp18	0.45
Kntc1	6.03	Col6a3	2.78	Foxs1	2.16	Met	0.45
Il15	5.99	Dpep1	2.71	Mbl2	2.15	Lynx1	0.45
Ptgds	5.81	Tmem184a	2.70	Eda2r	2.15	Slc16a11	0.46
Ptprh	5.61	H2-K1	2.70	Dhrs3	2.12	Rxrg	0.46
Eif4ebp1	5.24	Ly86	2.68	Pnma5	2.11	Zdbf2	0.46
Gpr97	5.00	Arhgef18	2.67	AI848285	2.10	Trim16	0.47
Tuba3b	4.99	Plb1	2.67	H19	2.09	Plcd3	0.47
Cep112	4.81	Sesn2	2.67	Isg15	2.09	Rasgrf1	0.47
Trpc6	4.61	H2-Ab1	2.63	Serpinb1a	2.05	Fam132a	0.47
Xlr3a	4.60	Npy	2.57	Eif2s3y	2.04	Tmem212	0.47
1700017N19Rik	4.54	Capn11	2.55	C1qb	2.03	Lmo4	0.48
Mrgprx2	4.51	Ifitm3	2.53	A10006H16Ri	2.02	Cartpt	0.48
Sema3b	4.42	Nupr1	2.52	Acpp	2.01	Krt222	0.49
Chac1	4.41	Tspo	2.51	Gpc3	2.01	Phyhip	0.49
Tfpi	4.34	Irgm1	2.48	Rhox2d	2.01	Mchr1	0.49
Wfdc9	4.34	Slc6a13	2.47	Hmx1	2.01	Tekt5	0.49
6720468P15Rik	4.14	Ccdc3	2.47	Mmp21	2.01	A010300C02Ril	0.49
Ugt3a2	4.11	Pnlcd1	2.46			Coro2a	0.50
Mnd1-ps	4.10	Pnmt	2.46			Arhgef15	0.50
Gbgt1	4.02	Avil	2.44			Slc10a4	0.50
Mageb4	3.77	Mfap5	2.42			Ntng2	0.50
Suv39h2	3.77	Svs5	2.42				
Xlr3b	3.77	Gpr98	2.41				
Ccrn4l	3.76	Igf2	2.40				
Cdh19	3.40	Mgp	2.39				
E330020D12Rik	3.24	Grhl2	2.36				
Ifi27	3.24	Ddit3	2.36				
Dcn	3.15	Cdkn1c	2.35				
Pdlim2	3.14	B2m	2.32				
Stc2	3.14	Olfr193	2.32				
Mitf	3.13	1700048O20Ril	2.32				
Mthfd2	3.13	Lyz2	2.31				
Cdkn2b	3.13						

Table 3. Table of upregulated and down regulated genes at P5

Table depicting upregulated and downregulated genes from Fig.4-10A in P5 cerebral cortex.

4.3.2 Specific ERVs are activated in the developing cerebral cortex of Uhrf1 cKO

Upregulation of interferon signaling has previously been described to be a consequence of retroviral activation (Chiappinelli et al. 2015). Therefore, we analysed the RNAseq datasets for deregulation of transposable elements. Indeed, we could observe a strong upregulation of a specific ERVs, namely IAPs, in all datasets, with IAPEz subtype exhibiting the strongest activation (Figure 4-11A-C, Table 4 and 5). Moreover, we did not detect other classes of transposable elements to be misregulated (Figure 4-11A-C). We interrogated the dataset further to identify deregulation of single transposable elements. Interestingly, we could observe upregulation of individual transposable elements in the P5 dataset (Figure 4-11D).

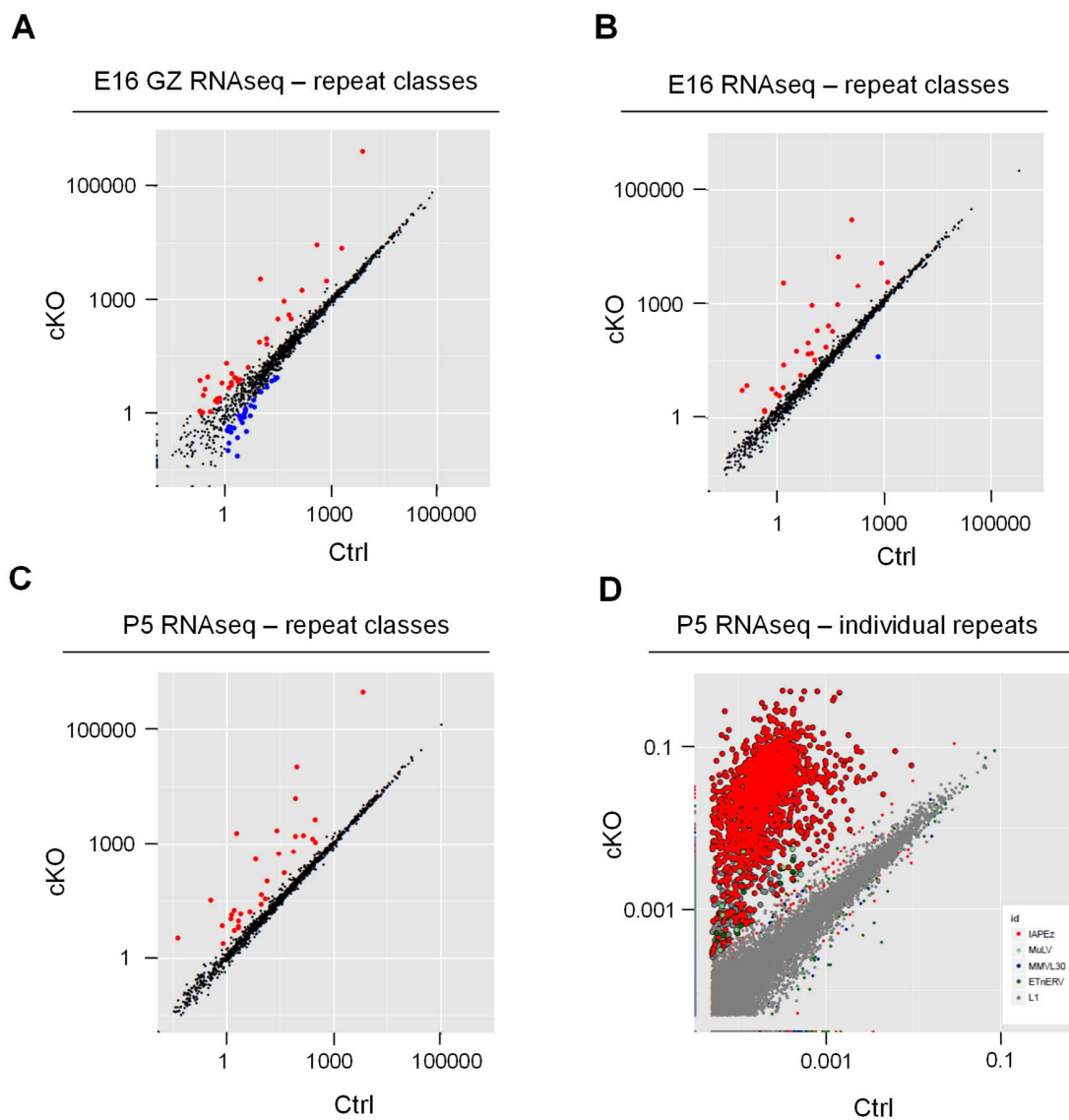


Fig. 4-11 IAP activation in Uhrf1 cKO in embryonic and postnatal stages

A-C. Graph depicting activation of classes of repeat elements in E16 germinal zones (A), E16 full cortex (B) and P5 cerebral cortex (C). Red dots indicate repeat classes with significantly increased expression and blue dots indicate repeat classes with significantly downregulated expression in the cKO cerebral cortex compared to controls. X-axis and Y-axis values are FPKM (Fragments per million bases) from 100bp paired end RNAseq.

D. Graph depicting individual repeat elements in E16 germinal zones (D), full cortex (E) and P5 cerebral cortex (F). X-axis and Y-axis values are FPKM (Fragments per million bases) from 100bp paired end RNAseq.

E16 GZ RNaseq – repeat classes

Repeat classes	FC Ratio of cKO over Ctrl
IAPEz-int LTR ERVK	103.13
IAPA_MM-int LTR ERVK	51.17
IAPLTR1_Mm LTR ERVK	17.24
ERVB2_1-I_MM-int LTR ERVK	11.18
MER110 LTR ERV1	9.30
IAPEy-int LTR ERVK	7.23
IAPEY5_I-int LTR ERVK	7.11
RLTR9A3A LTR ERVK	6.37
RLTR46 LTR ERVK	5.20
MMERGLN-int LTR ERV1	5.14
IAPLTR1a_Mm LTR ERVK	5.14
MMERVK10D3_I-int LTR ERVK	4.56
IAPLTR3-int LTR ERVK	4.01
RLTR30C_MM LTR ERV1	3.86
RLTR46A2 LTR ERVK	3.73
MMERGLN_LTR LTR ERV1	3.40
RLTR6C_Mm LTR ERV1	3.32
RLTR44-int LTR ERVK	3.28
DNA1_Mam DNA TcMar	2.84
MER50 LTR ERV1	2.75
Ricksha_a DNA MULE-MuDR	2.73
MMVL30-int LTR ERV1	2.70
IAPLTR4_I LTR ERVK	2.65
RLTR44B LTR ERVK	2.63
IAP1-MM_I-int LTR ERVK	2.61
LTR80A LTR ERV1	2.53
MMERVK10D3_LTR LTR ERVK	2.52
(CTTTG)n Simple_repeat Simple_repeat	2.50
LTRIS4A LTR ERV1	2.39
(TAGTG)n Simple_repeat Simple_repeat	2.35
MER65D LTR ERV1	2.34
RLTR9C LTR ERVK	2.31
(TATAG)n Simple_repeat Simple_repeat	2.28
RLTR46A LTR ERVK	2.21
MLT1A1-int LTR ERV1-MaLR	2.04
MLTR32C_MM LTR ERVK	2.04
(ATAAG)n Simple_repeat Simple_repeat	2.02
(GTATG)n Simple_repeat Simple_repeat	0.50
Chap1_Mam DNA hAT-Charlie	0.50
MamGypLTR3 LTR Gypsy	0.50
MER92A LTR ERV1	0.50
GCCTAA)n Simple_repeat Simple_repeat	0.49
LTR85b LTR Gypsy?	0.48
(GGTTG)n Simple_repeat Simple_repeat	0.48
MLT1L-int LTR ERV1-MaLR	0.48
LTR106_Mam LTR LTR	0.48
LTR108d_Mam LTR ERV1	0.46

Table 4. Table depicting repeat elements classes in E16 germinal zones

Table showing upregulated and downregulated classes of transposable elements in E16 germinal zones of cKO compared to controls.

P5 RNAseq – repeat classes

Repeat classes	FC Ratio of cKO over Ctrl
IAPEz-int LTR ERVK	126.90
IAPLTR1_Mm LTR ERVK	107.64
IAPA_MM-int LTR ERVK	101.72
IAPLTR1a_Mm LTR ERVK	32.79
ERV2_1-I_MM-int LTR ERVK	20.67
IAPEy-int LTR ERVK	19.57
RLTR12F LTR ERVK	18.89
IAPLTR3-int LTR ERVK	15.69
IAPLTR2a2_Mm LTR ERVK	7.21
MMERVK10D3_I-int LTR ERVK	7.20
MMERGLN-int LTR ERV1	5.93
IAPLTR2_Mm LTR ERVK	5.20
MMERVK10D3_LTR LTR ERVK	5.04
IAPLTR3 LTR ERVK	4.66
IAPEY5_I-int LTR ERVK	4.59
IAPEY3-int LTR ERVK	4.12
Ricksha_0 DNA MULE-MuDR	4.09
IAPEY_LTR LTR ERVK	3.98
RLTR44B LTR ERVK	3.22
IAPEY4_I-int LTR ERVK	3.11
MMERGLN_LTR LTR ERV1	2.93
IAPLTR4_I LTR ERVK	2.74
RLTR44-int LTR ERVK	2.64
RLTR10-int LTR ERVK	2.41
RLTR10D2 LTR ERVK	2.40
RLTR46A2 LTR ERVK	2.21
MER31-int LTR ERV1	2.16
RLTR6C_Mm LTR ERV1	2.11
TAGGG)n Simple_repeat Simple_repea	2.09
RLTR46A LTR ERVK	2.09
IAPLTR4 LTR ERVK	2.01

Table 5. Table depicting repeat elements classes in P5 full cortex

Table showing upregulated and downregulated classes of transposable elements in P5 cortex of cKO compared to controls

The transcriptional upregulation of IAPs (about 100-fold) was confirmed by qRT-PCR at E16 and P5 with no activation of LINE-1 and SINE-B1 as an entire class (Figure 4-12A-C). To investigate the onset of IAP activation, we performed qRT-PCR from cerebral cortex tissue of control and cKO at E12 and E14. About 35 fold IAP activation at E12 was observed (Figure 4-12D) which steeped to about 70 fold at E14 (Figure 4-12E).

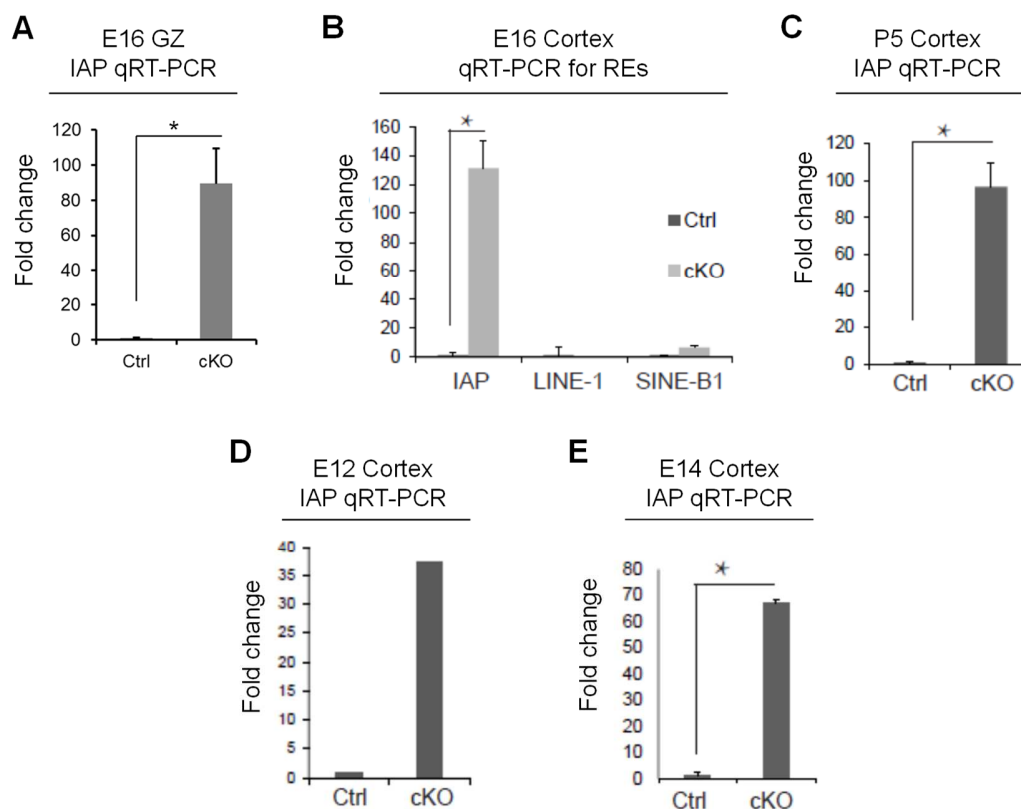


Fig. 4-12 qRT-PCR showing IAP activation in the cKO

A-E. RT-qPCR graph for IAP in control and cKO cerebral cortex in the E16 germinal zones (A), E16 full cortex (B), P5 cortex (C), E12 (D) and E14 (E) and for LINE-1 and SINE-B1. * indicates significance with p -value < 0.05 ($n=4$ for A,B,C,E; $n=2$ for D) Error bars indicate standard error of mean.

We investigated the correlation between deregulated genes and activated IAP transcripts. We could observe a low correlation, ranging 15-30% between activated IAP transcripts and deregulated genes (Table 6). These data suggest that activated IAP transcripts led to transcriptional activation of neighbouring genes and transposable elements in some instances.

Correlation between activated IAP transcripts and proximal genes

Dataset		% of deregulated genes in proximity to activated IAP transcripts			
E16 GZ		16			
E16 Cortex		19			
P5 Cortex		33			

E16 RNAseq		P5 RNAseq			
Gene name	IAP	Gene name	IAP	Gene name	IAP
Ccrn4l	,i.s	2010005H15Rik	,d.as	Mnd1	,i.s
Sectm1a	,i.as	Cypt12	,d.as	Mrgprx2	,i.s
Mnd1	,i.s	Hcst	,d.as	Slc20a2	,i.s
Trpc6	,i.s	Klhl33	,d.as	Trpc6	,i.s
Slc47a1	,u.as	Mypn	,d.as	Zfp69	,i.s
Kcnh1	,u.s	Trim34a	,d.as	Cep112	,i.s,u.s
Hamp2	,u.s	Ulbp1	,d.as	Mitf	,i.s,u.s
1700017N19Rik	,u.s	Cldn11	,d.s	Casq1	,u.as
Ddr2	,u.as	D630041G03Rik	,d.s	Ddr2	,u.as
Cep112	,i.s,u.s	Ecel1	,d.s	Eif2s3y	,u.as
Tfpi	,u.as	Fam160a1	,d.s	Foxd1	,u.as
Slc20a2	,i.s	Olfr498	,d.s	Slc47a1	,u.as
Efcab6	,i.as,u.as	Psemb8	,d.s	Tfpi	,u.as
Pnpt1	,u.s	Scel	,d.s	1700017N19Rik	,u.s
Ulbp1	,d.as	Tap1	,d.s	1700080O16Rik	,u.s
Zfp69	,i.s	Tap2	,d.s	Arhgef18	,u.s
Capn11	,i.as	Apoh	,i.as	BC035044	,u.s
Ecel1	,d.s	Capn11	,i.as	Dhrs3	,u.s
Gramd1c	,u.s	Cped1	,i.as	E330017A01Rik	,u.s
Casq1	,u.as	Enpp1	,i.as	Gramd1c	,u.s
Olfr194	,u.s	F13a1	,i.as	Gsdma3	,u.s
Fam160a1	,d.s	Mageb18	,i.as	H2-Ab1	,u.s
Arhgef18	,u.s	Mei4	,i.as	H2-Q4	,u.s
		Sectm1a	,i.as	Hamp2	,u.s
		Efcab6	,i.as,u.as	Ikzf2	,u.s
		A330049N07Rik	,i.s	Kcnh1	,u.s
		Ccrn4l	,i.s	Olfr1054	,u.s
		Cdh19	,i.s	Olfr193	,u.s
		Itgbl1	,i.s	Olfr194	,u.s
		Mmp1b	,i.s	Olfr43	,u.s
				Pnpt1	,u.s

Table 6. Deregulated genes in proximity to deregulated IAP transcripts

Table depicting percentage and list of genes in proximity to IAPs, upregulated in Uhrf1 cKO. as – antisense; s – sense; i – intergenic; u – upstream from gene.

To determine if the upregulated IAP transcripts were being translated to protein, we performed immunostaining for IAP Gag protein at different embryonic and postnatal stages (Figure 4-13). We could not detect Gag staining at E12 (Figure 4-13A,B) while from E14 and upto P5 Gag staining was present in the cKO cerebral cortex (Figure 4-13C-H).

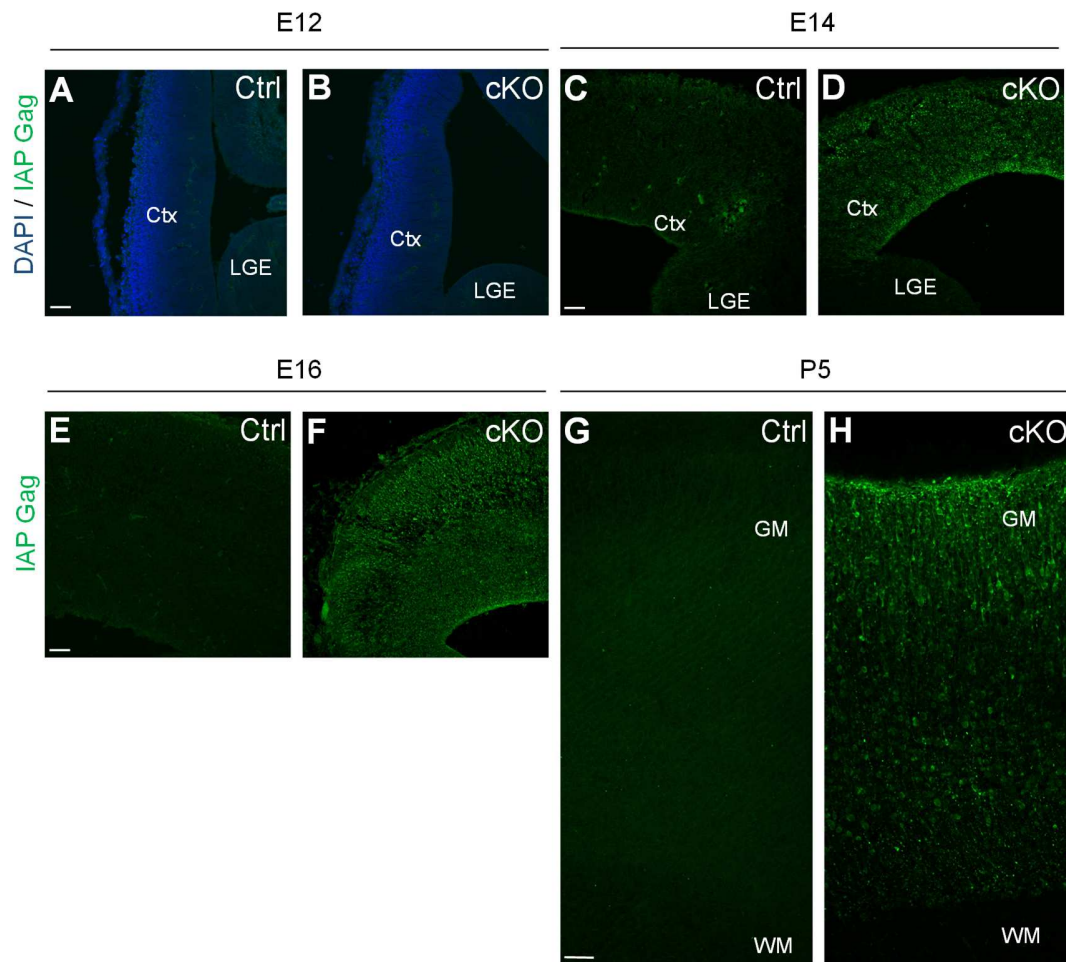


Fig. 4-13 IAP Gag immunostaining in embryonic and postnatal stages

A-H. Confocal images of coronal sections of cerebral cortex of controls (A,C,E,G) and cKO (B,D,F,H) at E12 (A,B) E14 (C,D), E16 (E,F) and P5 (G,H) cerebral cortex immunostained for IAP gag and DAPI .

Scale bar = 50 μ m; LGE – lateral Ganglionic Eminence; Ctx - cerebral cortex

GM – grey matter; WM – white matter

4.4. Alterations in methylation and chromatin marks in Uhrf1 cKO

4.4.1 Loss of DNA methylation in Uhrf1 cKO

As Uhrf1 has been previously described to be involved in DNA methylation in ES cells, we sought to investigate this process in controls and *Uhrf1* cKO. We assessed global DNA methylation by employing 2 restriction enzymes – MspI and HpaII which recognize CCGG sequences. When the internal cytosine is methylated in such sequences, HpaII cannot cleave the DNA, whereas MspI enzyme can cleave the internal CG. Thus, we performed restriction digests with both enzymes on genomic DNA extracted from E16 controls and *Uhrf1* cKO cortices. Although MspI could digest both conditions comparably, HpaII could digest the cKO more than the control (Figure 4-14).

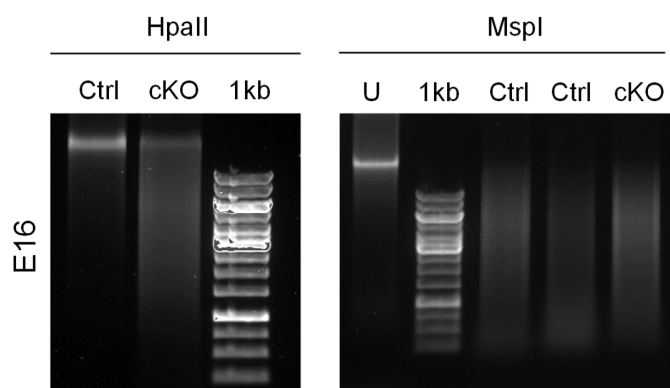


Fig. 4-14 Uhrf1 cKO exhibit global hypomethylation at E16

Restriction digests of E16 genomic DNA obtained from controls and *Uhrf1* cKO cerebral cortex digested for HpaII and MspI. Note that both enzymes recognize CCGG sequence, however HpaII is unable to cut DNA when the internal cytosine is methylated. As more DNA was cut in the Uhrf1 cKO samples this indicates less DNA methylation upon Uhrf1 deletion. 1kb is the 1kb DNA ladder and U is undigested DNA.

To further ascertain if there is a loss of global methylation, we performed immunostaining for 5-methyl cytosine (5mC) in embryonic stages. At E14 we could observe a severe loss of 5mC

immunoreactivity in the cKO cortex (Figure 4-15A,B). Interestingly, we detected some cells in the cKO cortex to persist in 5mC immunostaining. We performed co-stainings for Tbr2 (Figure 4-15C), Tbr1 (Figure 4-15D) and Pax6 (Figure 4-15E) with 5mC at E14 to identify the population of cells with persisting 5mC staining in the cKO. Some of the 5mC immunopositive cells did not colocalize with these markers, suggesting that these could be other cell types such as interneurons, glia or endothelial cells which did not arise from *Emx1*-Cre recombination. Thus, data from the restriction digests and immunostaining suggest a global loss of 5mC in *Uhrf1* cKO.

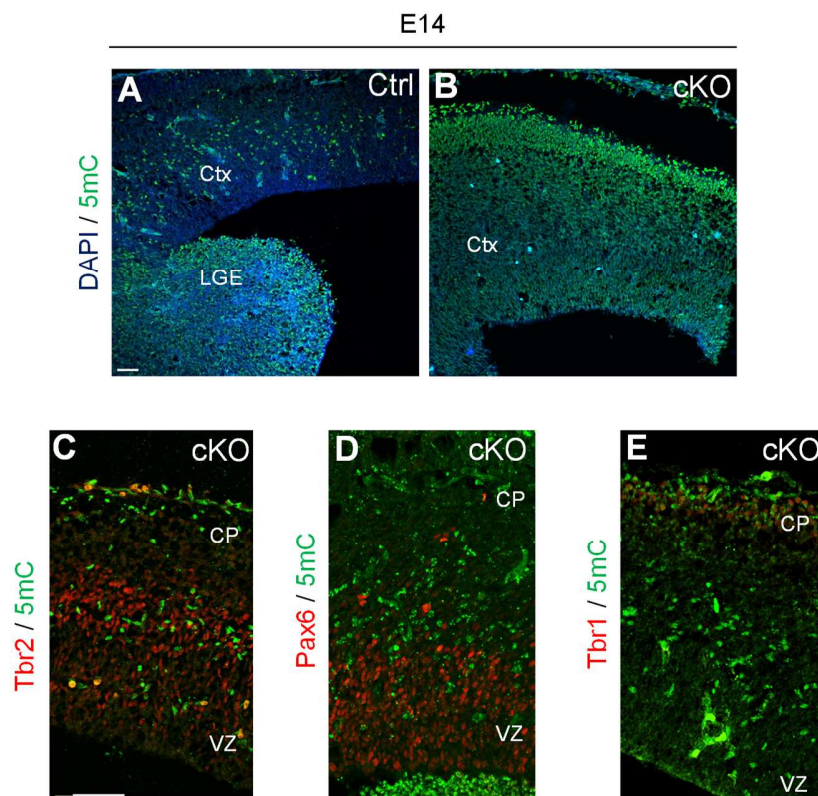


Fig. 4-15 Reduced 5mC immunostaining in the *Uhrf1* cKO

A-I. Confocal images of coronal sections of cerebral cortex of controls (A) and cKO (B,C,D,E) at E14 immunostained for 5mC and DAPI and Tbr2 (C), Tbr1 (D) and Pax6 (E). Note that at 5mC staining is noticeably reduced in the cortex of cKO but not in the LGE wherein *Uhrf1* was not deleted. Scale bar = 50µm.

Abbreviations: LGE – lateral ganglionic eminence; Ctx – cortex; VZ – ventricular zone; CP – cortical plate

4.4.2 Loss of 5mC in specific genes and transposable elements in *Uhrf1* cKO

To identify specific loci with reduced levels of 5mC, we employed Oxidative Reduced Representation Bisulfite Sequencing (Ox-RRBS) in collaboration with Dr. Reimenschneider (Regensburg University). In this technique, DNA is oxidized prior to treatment with bisulfite such that 5-hydroxy methyl cytosine (5hmC) is converted to 5-formyl cytosine (5fC). 5fC behaves in a similar manner to C during bisulfite treatment, as opposed to 5mC. This oxidation step thus allows an accurate measurement of 5mC levels in the relevant genomic DNA, differentiating between C, 5mC and 5hmC. Therefore, we performed Ox-RRBS on genomic DNA isolated from E16 cortex of controls and *Uhrf1* cKO. We observed a global loss of 5mC with all chromosomes exhibiting at least 40% of loci with reduced 5mC levels (Figure 4-16A). Moreover, we detected alterations in 850 differentially methylated promoters (DMRs) with at least 25% loss of 5mC (FDR and q-value) (Table 7). We overlapped the DMRs at E16 with the deregulated genes from the E16 RNAseq dataset. An extremely low overlap of genes with loss of 5mC and deregulated transcripts was detected (Figure 4-16B). We further interrogated the dataset for transposable elements and could observe loss of 5mC in most classes, particularly IAP, LINE-1 and SINE-1 (Figure 4-16C). These data suggest that loss of DNA methylation is not deterministic for transcriptional activation for most genes, with the only exception being IAP ERVs.

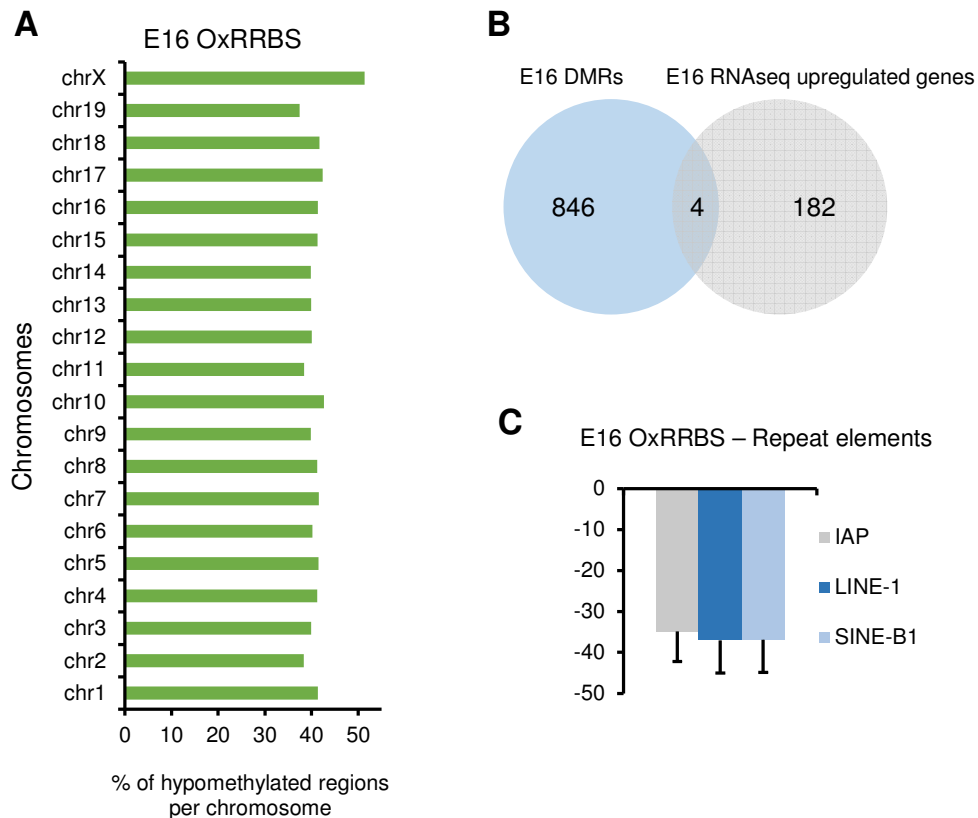


Fig. 4-16 Ox-RRBS at E16 showing hypomethylated DMRs and REs in the cKO

A. Graph depicting the percent of regions per chromosome with hypomethylation in the cKO cerebral cortex compared to the control. X-axis is the % of hypomethylated regions per chromosome and Y-axis is each chromosome. Note that every chromosome has a fairly equal level of hypomethylated regions. N=3

B. Venn diagram overlapping the 850 DMRs from the E16 Ox-RRBS dataset with the E16 full cortex RNAseq upregulated genes (Fold change > 1.5). Note the minor overlap between the 2 datasets.

C. Graph showing percentage of hypomethylation in IAP, LINE-1 and SINE-B1 repeat classes in the E16 Ox-RRBS dataset. Note that all classes are equally hypomethylated.

E16 OxRRBS – top 100 DMRs

Gene name	% loss of 5mC	Gene name	% loss of 5mC
Gm10913	-57.76	Gcn111	-45.23
Klhl36	-55.00	Man2c1	-45.10
Fgfr1	-54.56	Cdhr4	-45.07
Mybl2	-52.98	Ip6k1	-45.07
Ttc7	-52.90	Uba7	-45.07
Tchp	-51.75	Cirbp	-45.02
Fam167a	-50.47	ENSMUSG00000095332	-44.99
Mllt6	-50.43	Hps4	-44.82
EG666887	-50.27	Acaa1a	-44.74
Carkd	-50.16	L3mbtl2	-44.67
Kctd13	-49.92	Galnt10	-44.63
Sez6l2	-49.92	Gcn111	-44.50
Sez6l2	-49.92	Dnajb11	-44.42
Kctd13	-49.92	Asap3	-44.40
Fem1a	-49.55	Daxx	-44.36
4930467D21Rik	-49.38	Stat6	-44.32
Gpn2	-49.06	Kdelr3	-44.24
Gm9883	-48.81	Hnrnp1	-44.21
H2afy2	-48.71	Itgal	-44.20
Aifm2	-48.71	Lgl1	-44.20
Entpd2	-48.16	Yipf1	-44.13
Npdc1	-48.16	AK149779	-44.05
Exosc10	-48.12	Pex11b	-44.02
Hdgf	-48.07	Itga10	-44.02
Rere	-47.64	4931417G19	-43.97
Nlgn3	-47.57	4930594O21Rik	-43.94
2900075N08Rik	-47.57	Ttpal	-43.82
Med12	-47.57	Ube3b	-43.54
Zbtb7a	-47.34	Nosip	-43.38
ENSMUSG000000938	-46.99	Lrrc47	-43.32
Dmpk	-46.97	Zfand3	-43.25
Fam132b	-46.90	E2f7	-43.17
Ank3	-46.76	Lep	-43.15
Scap	-46.71	Dhx16	-43.14
Dlg4	-46.66	Cxxc1	-43.12
Rgs11	-46.59	Pitpna	-43.12
Nek4	-46.49	Gm12338	-43.12
Bahcc1	-46.49	1700003E16Rik	-43.11
Actg1	-46.30	H2-DMa	-43.09
AK089428	-46.26	Pank4	-43.05
Katnb1	-46.09	Pgs1	-42.99
Rltpr	-46.07	Nphs1	-42.98
Rltpr	-46.07	Atp13a2	-42.92
Tmem140	-46.00	Ptp4a3	-42.84
Dppa3	-45.84	AK136829	-42.70
Tshz3	-45.83	Phrf1	-42.69
Pygo2	-45.51	Zc3h12d	-42.57
Irf9	-45.49	Slc4a8	-42.48

Table 7. Table showing DMRs in the E16 Ox-RRBS dataset

Table depicting the 100 most DMRs in the E16 cKO compared to control and their percentage of hypomethylation.

Moreover, we also investigated the correlation between individual LINE-1 elements and upregulated IAP transcripts. Interestingly, we observed the few upregulated LINE-1 transcripts to be in proximity to upregulated IAP transcripts (Figure 4-17).

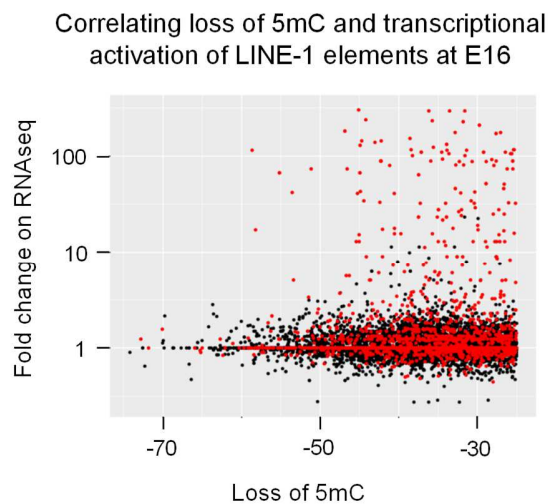


Fig. 4-17 Activated LINE-1 elements are in proximity to activated IAPs

Graph depicting the correlation between hypomethylated LINE-1 elements and transcriptionally activated LINE-1 elements and IAPs at E16 in the cerebral cortex of controls and cKO. Fold change of LINE 1 elements from RNAseq is plotted against the Ox-RRBS data. The data shows few hypomethylated elements with high fold change in mRNA. Red dots indicate LINE-1 elements in proximity to IAP elements and black dots are all remaining LINE-1 elements.

To confirm the specific loss of 5mC on retrotransposable elements, we employed bisulfite sequencing coupled with MiSeq. This method uses PCR amplification following oxidative bisulfite treatment of regions of interest. The PCR fragment is sequenced by next generation sequencing technology. In our case, we amplified a 500bp sequence of the IAP Gag region and a 200bp sequence of LINE-1 from controls and cKO cortex at E16. We could identify 27 CpGs in the IAP region with nearly 95% 5mC levels in the control which decreased to about 70% 5mC levels in the cKO (Figure 4-18A). In the case of LINE-1 we identified 9 CpGs in the control to also have about 80% 5mC levels which dropped to about 50% in the cKO (Figure 4-18B).

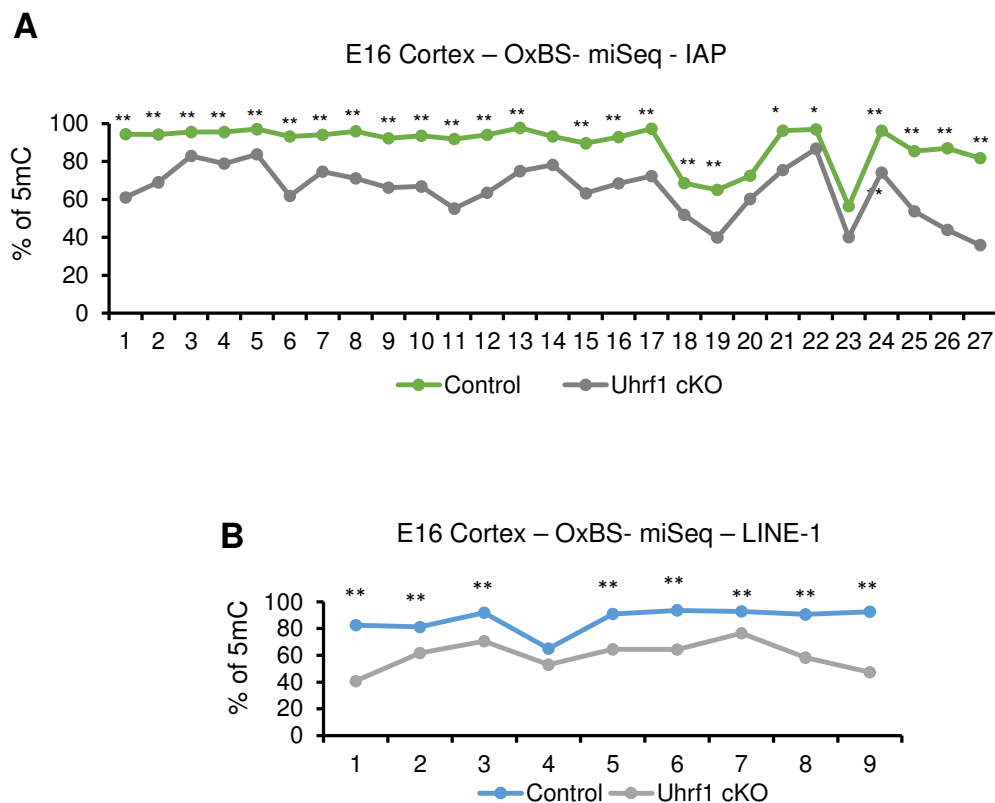


Fig 4-18 Ox-BS-Miseq analysis revealed hypomethylated CpGs in IAP and LINE-1 in the Uhrf1 cKO at E16

A,B. Graphs depicting the percentage of methylation per CpG in the IAP (A) and LINE-1 (B) loci for cKO and control cerebral cortex. Y-axis indicates % of methylation and X-axis indicates individual CpGs. * indicates significance with a Fisher's test with ** having p-value < 0.0001 and * with p-value < 0.001. N=1.

4.4.3 Gain of 5hmC in Uhrf1 cKO on IAP elements

Uhrf1 has been previously described to bind 5hmC (Frauer et al. 2011). Moreover, transcriptional activation has been associated with a gain of 5hmC (Wu et al.). Thus, to further shed light on the mechanisms governing IAP activation, we explored the 5hmC mark in the cKO. We first performed immunostaining against 5hmC at E12, E14 and E16 in controls and cKO cortices (Figure 4-19A-

F). At E12, we did not observe any difference in 5hmC (Figure 4-19A,B). However, both at E14 and E16, we detected cells in the germinal zones to ectopically express 5hmC (Figure 4-19D,F). This was in contrast to the control wherein 5hmC was only observed in the cortical plate where neurons reside (Figure 4-12C,E). This distribution in the control was in concordance with previous observations (Hahn et al.2013).

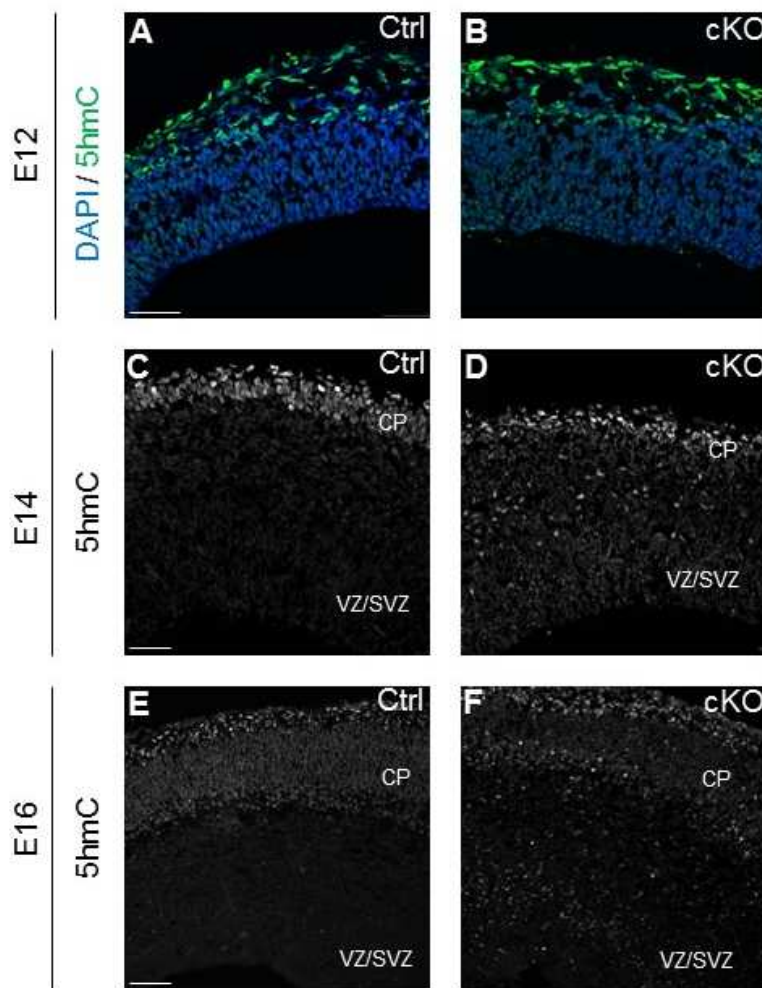


Fig.4-19 Ectopic 5hmC immunolabelled cells in the cKO at embryonic stages

A-F. Confocal images of coronal sections of controls (A,C,E) and cKO (B,D,F) immunostained for 5hmC at E12 (A,B), E14, (C,D) and E16 (E,F). Note the presence of ectopic 5hmC cells in the cKO at E14 and E16. Scale bar = 50 μ m.

Abbreviations: CP- cortical plate; VZ – ventricular zone; SVZ – subventricular zone

We investigated this increase in 5hmC by exploring the genomic loci which had accumulated 5hmC levels in the cKO compared to control. To address this question, we performed hydroxy methylated DNA immunoprecipitation followed by next generation sequencing (hmeDIPseq) on E16 controls and cKO. In order to enrich for the cells ectopically expressing 5hmC in the cKO, we subdissected the cortex to remove the cortical plate and enrich for the germinal zones as was previously described for the E16 RNAseq experiment. hmeDIPseq was performed on the tissue enriched for the germinal zones. Interestingly, we did not observe any significant changes of 5hmC in coding regions between control and cKO. However, when we investigated 1200 repetitive element classes for 5hmC levels, we observed 4 subtypes of IAP elements to have at least 2-fold enrichment of cKO over control (normalized to input) (Figure 4-20A and Table 8). Cumulative coverage plots were generated for all IAP elements in cKO and control, showing an increase in 5hmC peaks at the SHIN region of the Gag portion of IAP sequence (Figure 4-20B). The SHIN region or Short Heterochromatin Inducing Region is a sequence which has been previously described to induce the formation of heterochromatin in ES cells (Sadic et al. 2015). Some additional peaks were also observed on the LTR region which acts as promoters for IAP (Figure 4-20B). These data were confirmed with hmeDIP-RT-qPCR for IAP and negative regions (Figure 4-20C).

Moreover, we utilized the data from the Ox-BS-Miseq experiment to deduce relative levels of 5hmC in the control and cKO at E16 on IAP and LINE-1. We observed an increase of about 1.4% 5hmC in IAP in the cKO compared to the control (Figure 4-20C). Interestingly, we observed an increase of only 0.4% 5hmC for LINE-1 in the cKO compared to the control (Figure 4-20C). These data also indicate the actual levels of 5hmC might be relatively low in the cKO, although higher than the control.

Thus, in summary, the above data indicate a significant accumulation of 5hmC specifically on IAP in Uhrf1 cKO.

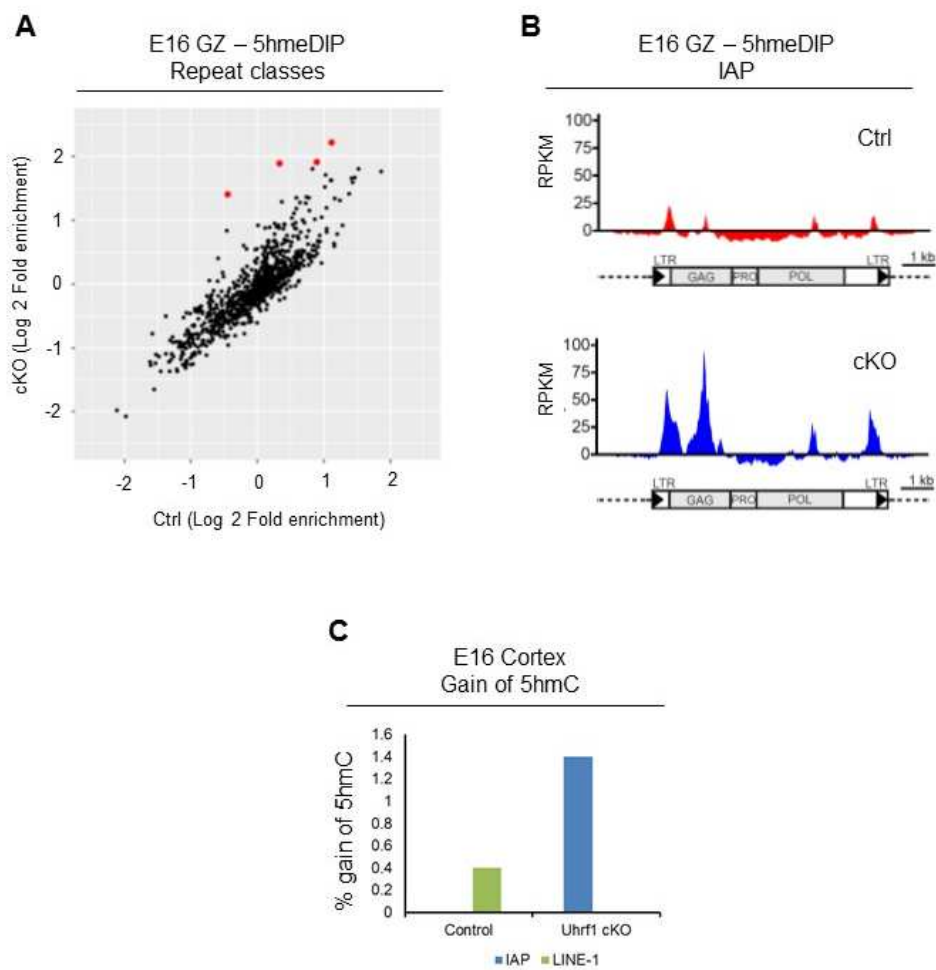


Fig.4-20 Ectopic accumulation of 5hmC is specifically on IAPs in the cKO

A. Graph depicting 1200 repeat elements classes from the E16 germinal zones hmeDIPseq dataset of control and cKO cerebral cortex. X-axis and Y-axis are log fold enrichment of control and cKO over input from 50bp single end sequencing. Red dots indicate repeat classes with > 2 fold higher 5hmC in cKO over control. P-value < 0.05. RPKM is reads per million bases.

B. Cumulative coverage plots of RPKM reads for IAP in control and cKO from the hmeDIPseq dataset. Note that the cKO has an accumulation of peaks in the Gag and LTR regions compared to the control.

C. Graph depicting the relative increase in 5hmC in controls and cKO on the IAP and LINE-1 loci from the Ox-BS-MiSeq experiment from Figure 4-18.

E16 GZ 5hmeDIP – repeat classes with
upregulated 5hmC in cKO

IAPEY_LTR|LTR|ERVK
IAPA_MM-int|LTR|ERVK
IAPLTR1_Mm|LTR|ERVK
IAPLTR1a_Mm|LTR|ERVK

Table 8. Table depicting the repeat elements classes with upregulated 5hmC from the hmeDIPseq dataset

4.4.4 Assessing changes in histone marks in the cKO

Data from the RNAseq and DNA methylation analysis revealed differences in the behavior of repeat classes. More specifically, although both IAP and LINE-1 elements lost 5mC in the Uhrf1 cKO, only IAP showed activation on the transcript level. Thus, we hypothesized that the two loci could differ in chromatin marks such as histone methylation. It has been described that the H3K9me3 can act as a repressive modification (Volpe et al. 2002). Thus, we speculated that levels of H3K9me3 could differ between IAP and LINE-1 in the control and cKO cortices, thus translating into transcriptional activation for one and not the other. Therefore, in collaboration with Dr. Cernilogar at the Biomedical Center, Munich, we performed ChIP experiments for H3K9me3 in control and cKO cortices at E16. Contrary to our hypothesis, we did not observe a significant change in H3K9me3 between cKO and control for IAP and LINE-1 (Figure 4-21).

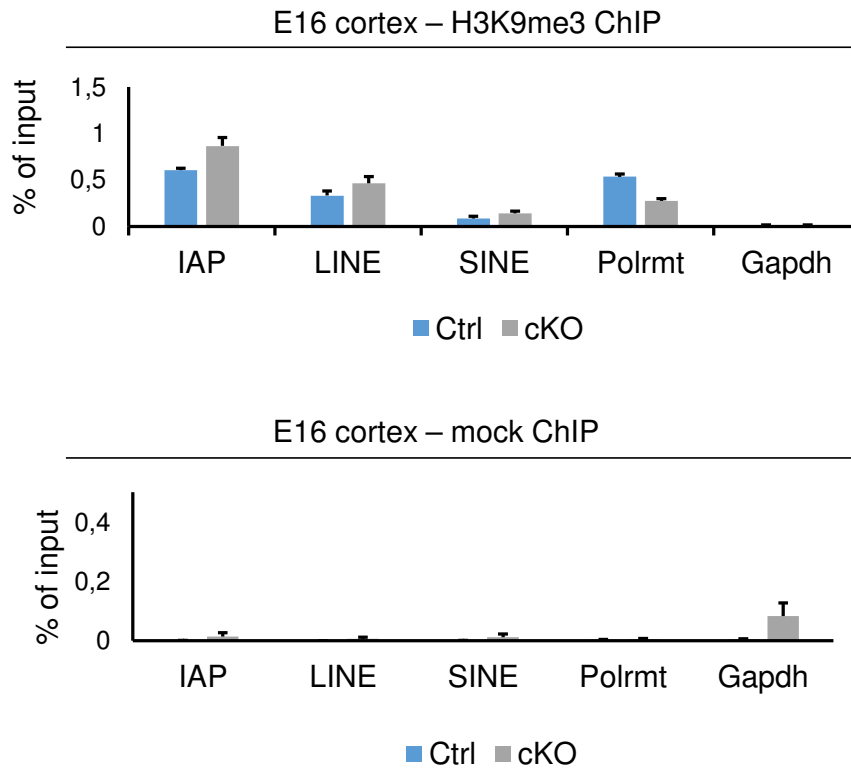


Fig. 4-21 Comparable repressive histone marks in the cKO and control at E16

Graph depicting percentage of input in control and cKO at E16 following ChIP for H3K9me3 on IAP, LINE-1 and Polrmt (positive controls) and Gapdh (negative controls). Note that there is no significant difference between controls and cKO on the loci. Error bars indicate standard error of mean. n=3

4.5. Manipulation of Tet enzymes to rescue IAP activation

4.5.1 In vivo knockdown of Tet enzymes by in utero electroporation of the cKO cortex

Tet enzymes have been described to be responsible for converting 5mC to 5hmC. Since we observed a specific increase in 5hmC on IAPs only, we hypothesized that the increase in 5hmC could be causative for the observed IAP transcriptional activation. Thus, we sought to knockdown *Tet* enzymes in the cKO cortex to test whether this would reduce IAP transcripts. We focused on *Tet2* and *Tet3* as it had been previously described to be the most highly expressed Tet genes in

the embryonic cerebral cortex (Hahn et al. 2013). We obtained previously published shRNA constructs and a scrambled control construct (Hahn et al. 2013). Using in utero electroporation, we electroporated a combination of *Tet2/Tet3* shRNA into cKO embryos at E13. Firstly, we observed no significant difference in the distribution of GFP positive cells in cKO embryos electroporated for Scrambled or *Tet2/Tet3* shRNA (Figure 4-22A,B). Moreover, we did not observe any difference in GFP distribution of cKO and control embryos electroporated for *Tet2/3* shRNA (Figure 4-22B,C). These data suggest that the Tet knockdown does not result in any obvious changes in cell fate. It is also interesting to note, that the distribution of GFP+ve cells in the cKO embryos indicates that neurons are migrating adequately to their final destination, the cortical plate (Figure 4-22A,B). We isolated GFP+ve and GFP-ve cells by FACS from embryos electroporated for *Tet2/3* in cKOs at E16 (Figure 4-22D) and performed qRT-PCR for the IAP region (Figure 4-22E). Paired t-test analysis was carried out on these samples as the 2 population of GFP+ve and GFP-ve cells were derived from the same embryo in each experiment. The analysis showed a significant reduction of IAP mRNA levels in the cells electroporated for Tet constructs as compared to the surrounding non-electroporated cells (Figure 4-22E). Importantly, IAP was already activated in the cKO at the time of electroporation. Thus, the small degree of IAP reduction after *Tet* knockdown is hence expected as only the further increase of IAP can be blocked.

In utero electroporation E13 to E16

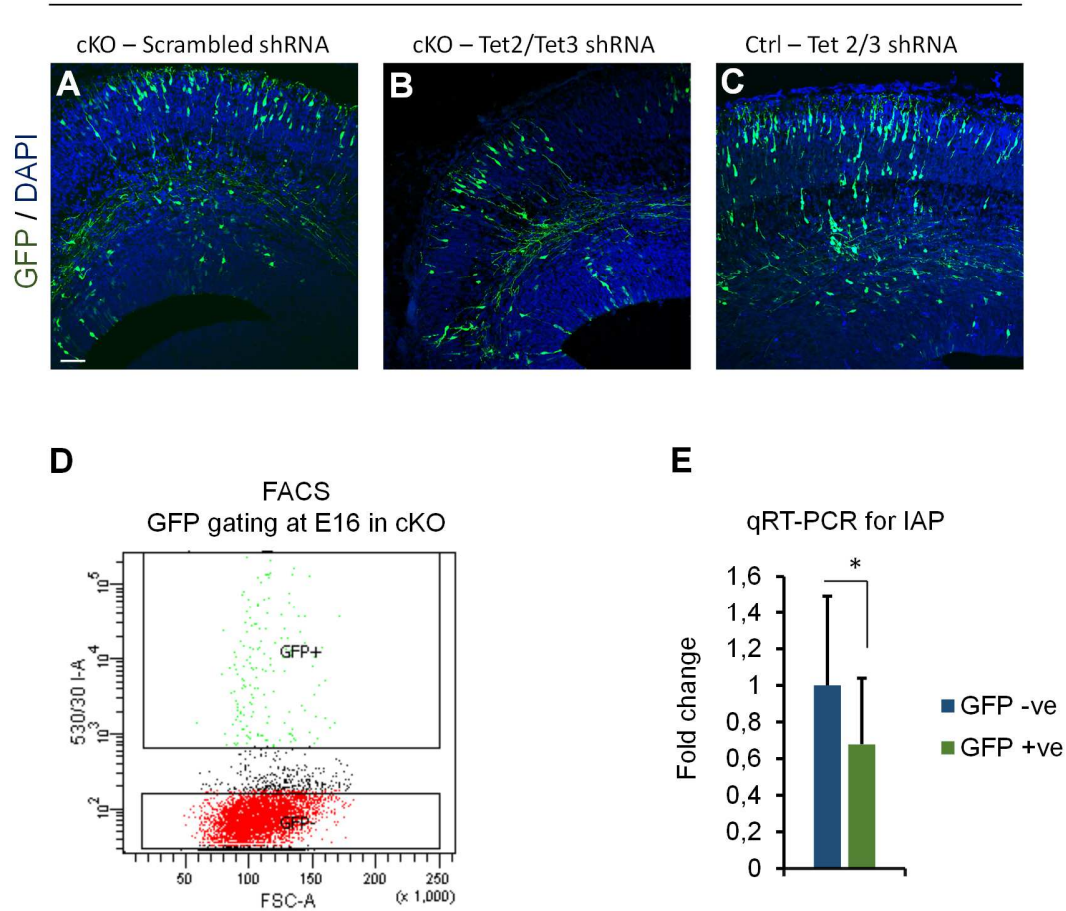


Fig. 4-22 Tet knockdown in the cKO partially rescued IAP transcriptional activation

A-C. Confocal images of coronal sections of cerebral cortex of E16 cKO (A,B) and control (C) embryos electroporated for Tet2/3 shRNA with GFP (B,C) and Scrambled shRNA with GFP (A) at E13 and immunostained for GFP and DAPI. Scale bar =50 μ m.

D. FACS plots showing gating for GFP+ve (green dots) and GFP -ve (red dots) cells in E16 cKO embryos electroporated at E13 for Tet2/3 shRNA.

E. Graph depicting qRT-PCR for *Uhrf1* in E13 cKO embryos electroporated for *Tet2/3* shRNA showing significantly less IAP mRNA in GFP+ve cells compared to GFP-ve cells. * indicates significance with a paired t-test with p-value < 0.05. Error bars indicate standard error of mean. N=3.

We performed additional experiments to understand if a downregulation of the IAP gag protein could be observed following Tet knockdown. We electroporated cKO embryos at E13 and analysed sections of the cerebral cortex at E16. In addition to electroporating *Tet2/Tet3* shRNA, we also electroporated Scrambled shRNA in other cKO and control embryos. We performed an immunostaining for IAP Gag in the cKO embryos and quantified the proportion of Gag in the GFP+ve cells for the Scrambled and Tet shRNA conditions (Figure 4-23A,B). We separated the quantifications between cortical plate and the rest of the cortex (VZ, SVZ and IZ). This is because we hypothesized that the knockdown would be more pronounced in the germinal zones compared to the differentiated cortical plate. Although we could observe a trend towards a slight decrease in the IAP Gag immunostaining in cKO embryos electroporated for *Tet2/3* shRNA, the difference was not statistically significant (Figure 4-23C). Thus, further time might be needed for reduction in Gag protein to become detectable.

In utero electroporation E13 to E16

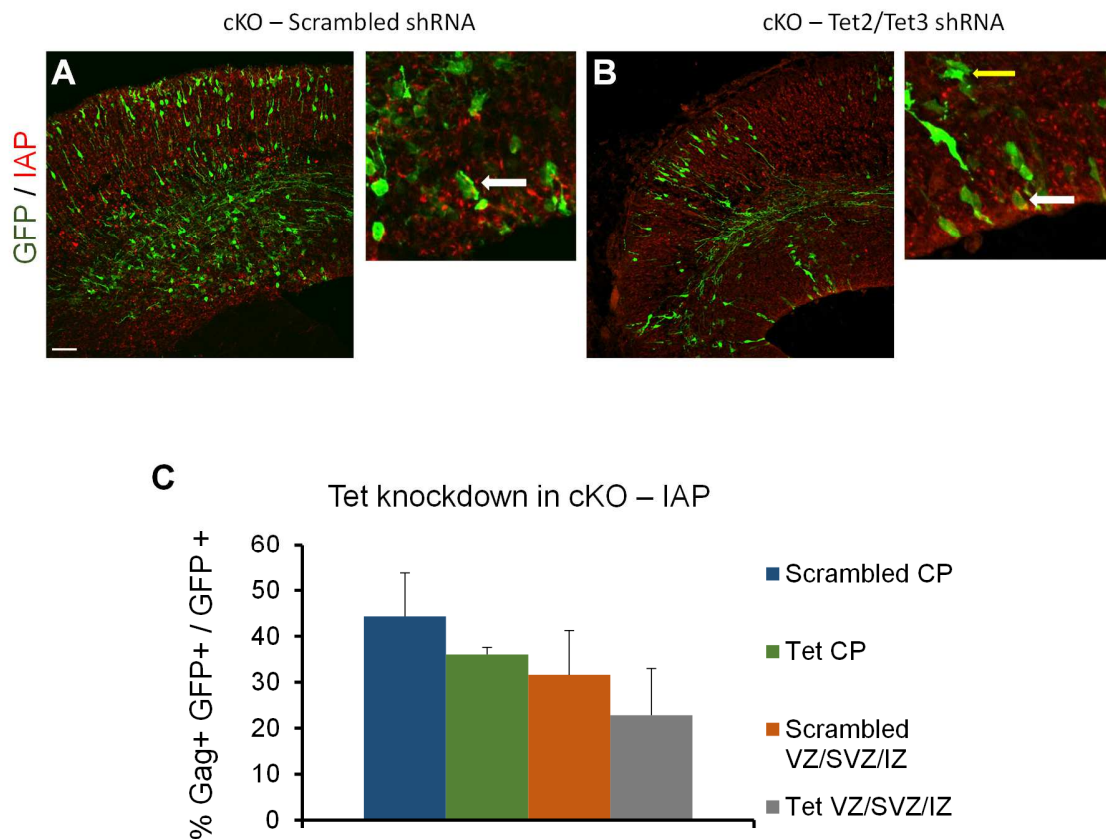


Fig. 4-23 Assessing changes in IAP Gag immunostaining following Tet knockdown in the cKO

A,B. Confocal images of coronal sections of E16 cerebral cortex cKO embryos electroporated for Scrambled shRNA (A) and Tet2/3 shRNA (B) at E13 and immunostained for GFP and DAPI and IAP Gag. Scale bar =50 μ m. White arrows indicate cells positive for IAP Gag and yellow arrows indicate cells negative for IAP Gag.

C. Graph depicting quantification of the percentage of IAP Gag +ve cells over GFP+ve cells from A,B sections. Error bars indicate standard error of mean. n=3

VZ – ventricular zone; SVZ – subventricular zone; IZ – intermediate zone; CP – cortical plate

4.5.2 Generating an in vitro system to investigate the relationship between Tet enzymes and IAP activation

The IAP transcript activation was evident already from E12 and could have started prior to this stage. Thus, it was technically not possible to downregulate the *Tet* enzymes prior to IAP activation, by in vivo electroporation. Thus, we sought out to generate an in vitro system wherein the *Tet* hypothesis regarding IAP activation could be better tested, wherein *Tet* enzymes could be manipulated simultaneously as *Uhrf1*. We generated an in vitro system of self-renewing multipotent neural stem cells from *Uhrf1* floxed E13 cortices, as previously established (Conti et al. 2005; Onorati et al 2010). To stably knockout *Uhrf1* in these *Uhrf1* NS cells, we added Cre protein to the media and analysed the cells after 4 days by immunostaining for Uhrf1. We could observe that in the condition without Cre, all cells were positive for Uhrf1 (Figure 4-24A). However, in the condition with Cre, some cells lost or downregulated Uhrf1 protein levels (Figure 4-24B). Also, qRT-PCR indicated a 20-fold reduction of *Uhrf1* mRNA (Figure 4-24C). We first characterized the system by assessing cell death with the Annexin-V assay. NS cells treated with and without Cre were harvested after 4 days in vitro and analysed using the FACS with the Annexin V kit. We observed a trend towards an increase in cells expressing Annexin-V in the condition with Cre (Figure 4-24D). However, the increase was not statistically significant, possibly due to the high variation between experiments. These data indicate that at least part of the cellular phenotypes observed in vivo could be recapitulated in vitro.

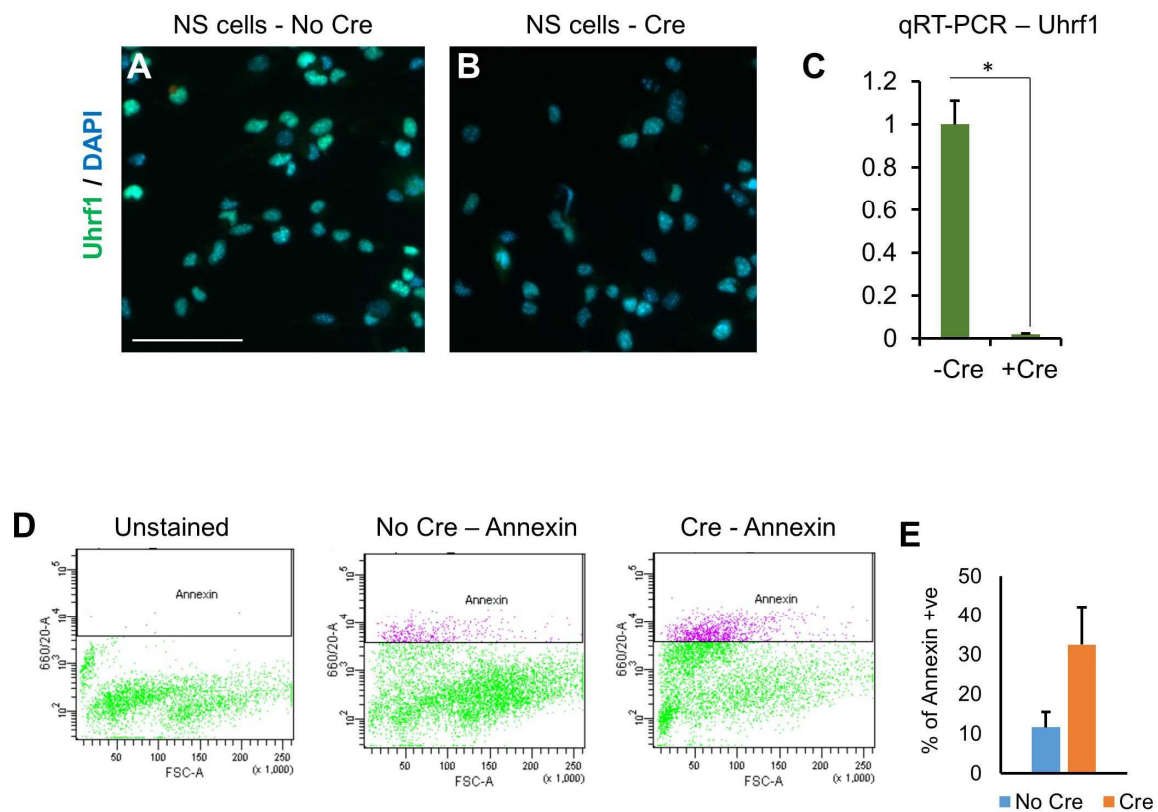


Fig. 4-24 Establishing an in vitro system of Uhrf1 KO NS cells

A-B. Epifluorescence images of *Uhrf1* floxed NS cells without Cre induction (A) and with with Cre induction (B). After 4 days in vitro, the cells were immunostained for Uhrf1 and DAPI. Scale bar = 50 μ m.

C. qRT-PCR for Uhrf1 in *Uhrf1* floxed cells after 4 days in vitro with and without Cre induction. Error bars indicate standard error of mean. * indicates significance with unpaired t-test with p-value = 0.02. N=4 for –Cre and n=8 for + Cre.

D. FACS plots for *Uhrf1* floxed NS cells analysed for cell death with the Annexin-V assay kit. Cells were treated with and without Cre and analysed after 4 days in vitro. Annexin gates were set using unstained cells.

E. Graph indicating increase in annexin +ve cells in the Cre condition. Note that the standard error shows high variation between replicates and thus the data is not significant. N=4.

To characterize if the molecular aspect of the phenotype was replicated *in vitro*, we first probed the cells for expression of IAP, LINE-1 and SINE-B1 elements. Indeed, we could observe about 25-fold induction of IAP in cells treated with Cre with only a mild upregulation of LINE and SINE compared to untreated controls (Figure 4-25A). In order to assess changes in methylation, we performed stainings for 5mC and observed a loss of 5mC in cells treated with Cre as expected from the *in vivo* data (Figure 4-25B,C). We further confirmed the changes in 5mC using the Oxidative Bisulfite Sequencing method coupled with MiSeq, as was performed for the *in vivo* tissue. Indeed, we could observe a significant loss of 5mC (about 15% loss) on some of the CpGs in both the IAP and LINE-1 loci (Figure 4-25D,E). We could also infer the levels of 5hmC from this experiment and detected a gain of 4.3% for IAP with only 0.2% for LINE-1 in the condition upon Cre application compared to cells without Cre (Figure 4-25F). Thus, in summary, we could also recapitulate some of the molecular phenotypes of the *in vivo* phenotype in this *in vitro* system.

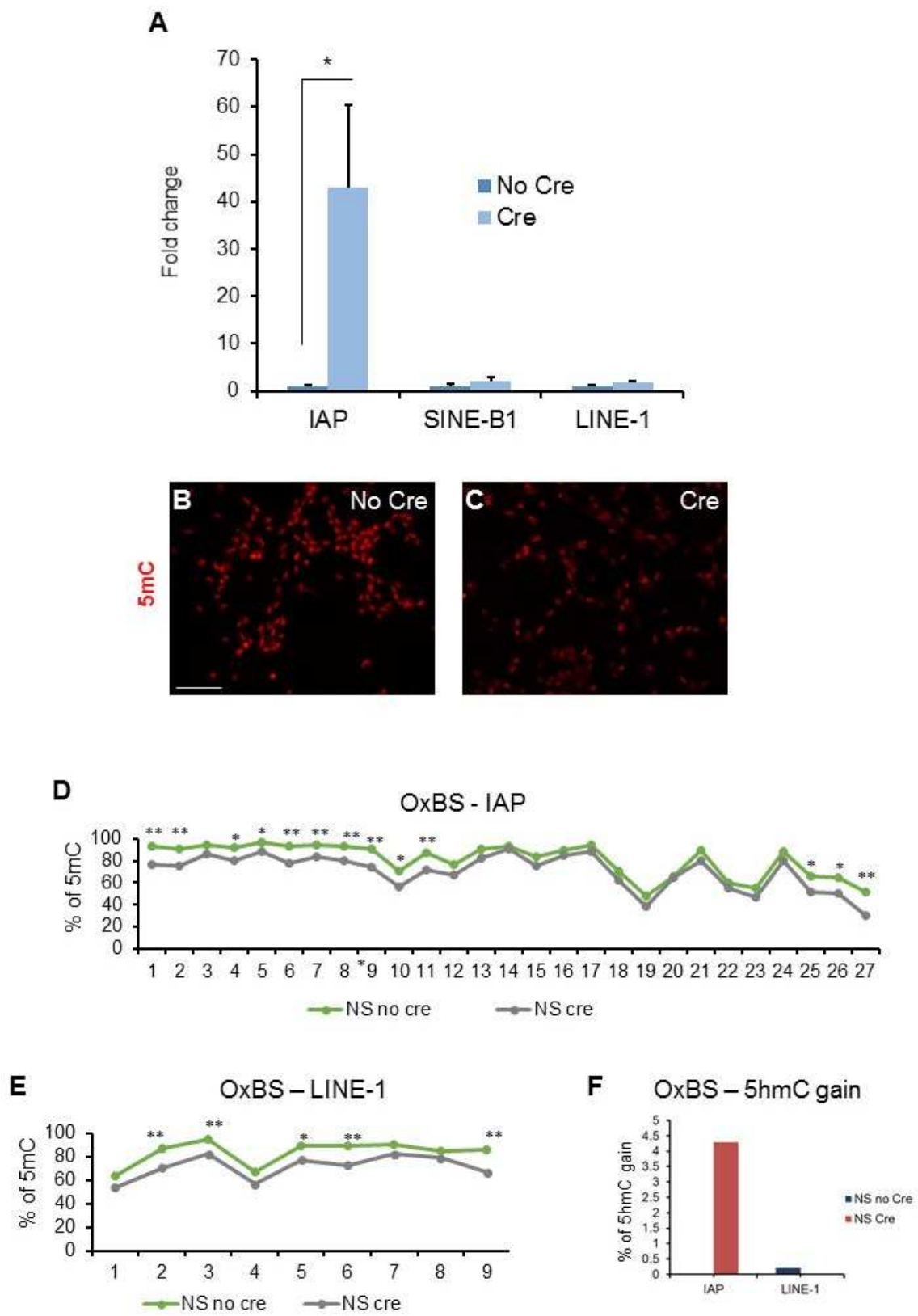


Fig. 4-25 Molecular characterization of the Uhrf1 floxed in vitro system

A. qRT-PCR for IAP, LINE-1 and SINE-B1 in *Uhrf1* floxed NSCs treated with and without Cre and analysed after 4 days in vitro. Note the increase of IAP mRNA in the Cre condition. Error bars indicate standard error of mean. * indicates significance with unpaired t-test with p-value. N=3.

B,C. Epifluorescence images of *Uhrf1* floxed NSCs treated with (C) and without Cre (B) immunostained for 5mC. Observe loss of 5mC staining in the Cre condition. Scale bar = 50µm.

D,E. Graphs depicting the percentage of methylation per CpG in the IAP (D) and LINE-1 (E) loci in *Uhrf1* floxed NSC treated with and without Cre and analysed by Ox-BS-MiSeq after 4 days in vitro. Y-axis indicates % of methylation and X-axis indicates individual CpGs. * indicates significance with a Fisher's test with ** having p-value < 0.0001 and * with p-value < 0.001. N=1

F. Graph depicting the relative increase in 5hmC in *Uhrf1* floxed NSCs treated with and without Cre on the IAP and LINE-1 loci from the Ox-BS-MiSeq experiment from D,E.

Having successfully established an in vitro system for *Uhrf1* cKO, we performed knockdown experiments for the *Tet* enzymes. We transfected shRNA constructs for *Tet2/Tet3* and Scrambled in *Uhrf1* NS cells and simultaneously treated the cells with and without Cre recombinant protein. After 4 days in vitro, we harvested all the cells in both conditions and assessed IAP expression. We observed a significant difference in IAP mRNA in the *Tet* shRNA plus Cre condition as compared to the Scrambled shRNA plus Cre (Figure 4-26). We performed paired t-test analysis since the same pool of cells were electroporated and treated with Cre.

Thus, in summary, we observed that downregulation of *Tet* enzymes in *Uhrf1* floxed NS cells treated with Cre could partially suppress the IAP mRNA upregulation.

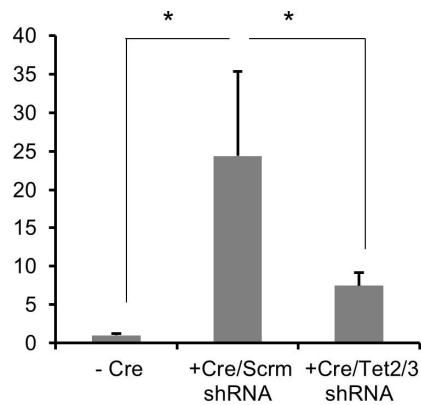


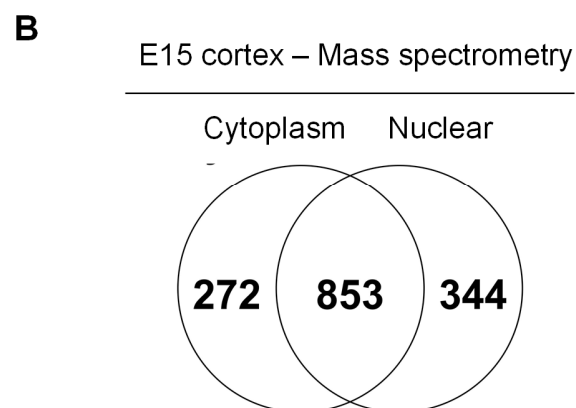
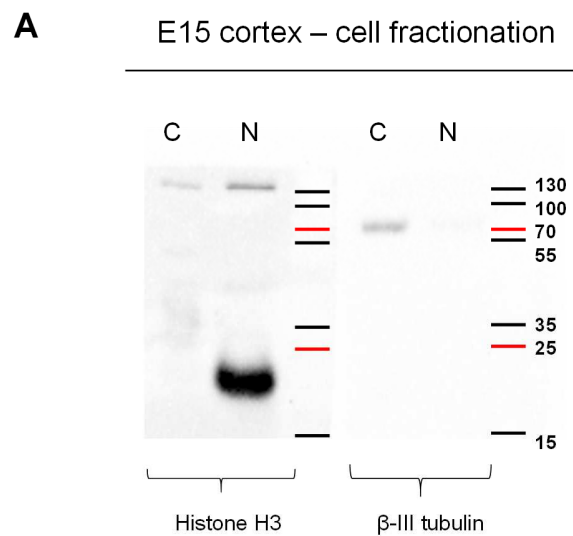
Fig. 4-26 Tet knockdown in Uhrf1 floxed NSCs could partially rescue IAP activation

qRT-PCR for IAP in *Uhrf1* floxed NSCs treated with and without Cre and electroporated for Scrambled or *Tet2/Tet3* shRNA. Note the significantly less IAP mRNA levels in *Uhrf1* floxed NSCs treated with Cre and electroporated for *Tet2/Tet3* shRNA compared to the Scrambled shRNA condition. Error bars indicate standard error of mean. * indicates significance with a paired t-test with p-value = 0.02 and 0.04 respectively. N=3.

4.6 Investigating changes in the proteasome of cKO cortices and controls

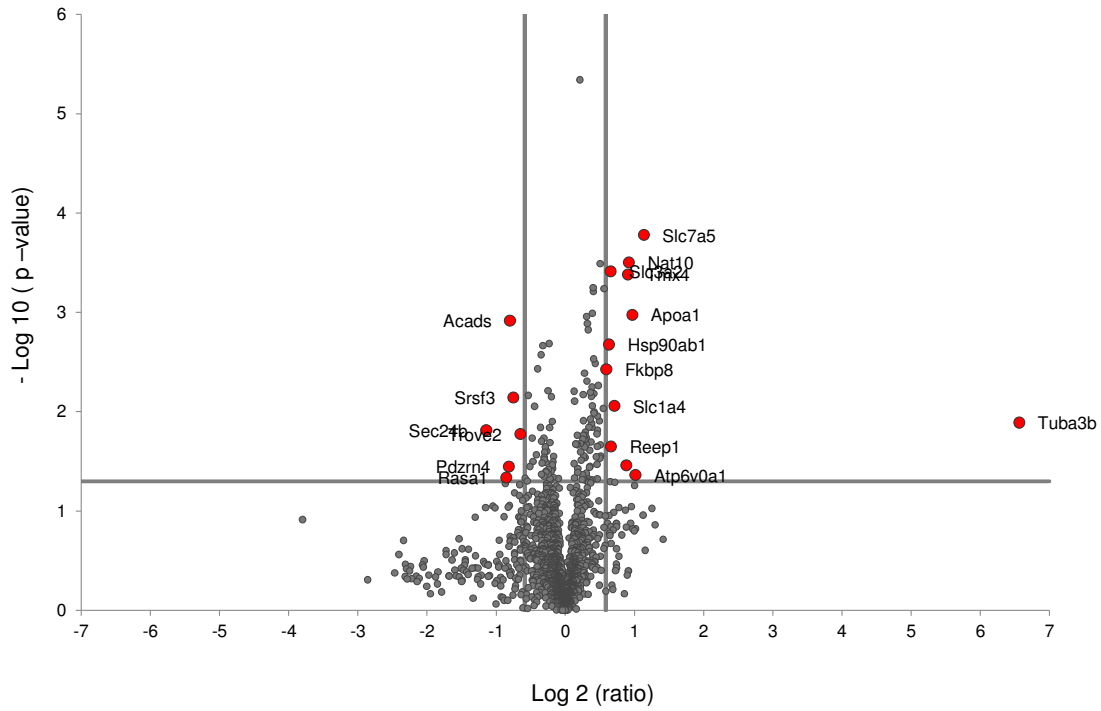
As described in the introduction, Uhrf1 protein has several domains, one of which is the RING domain. This domain can act as an E3 ubiquitin ligase, thereby controlling the stability of certain (proteins. This was observed in the case of the protein Pml (Guan et al. 2013). Thus, we investigated the proteasome of the cKO and control cortices by performing mass spectrometry at E16 of the protein lysates. As Uhrf1 is present in the nucleus, we used a cellular fractionation protocol to separate the nucleus and cytoplasm. Indeed, the nuclear fraction was highly enriched for nuclear proteins, as observed by a western blot for histone H3 and the other fraction was highly enriched for cytoplasmic proteins, as observed by a western blot for beta III tubulin (Figure 4-27A). First, we performed a test experiment of a wild-type E15 cerebral cortex lysate to ascertain the extent and nature of proteins which could be detected via mass spectrometry in this cell type. We could detect about 1400 proteins from this experiment with about 300 protein specific for each fraction (4-27B). Following this, we performed mass spectrometry on lysates from the cKO and control cortices at E16. We could observe several proteins to be significantly upregulated in the cKO as compared to the control in both the nucleus (Figure 4-27C) and the cytoplasm (Figure 4-

28D; Table 9). The most upregulated protein was Nox3, a NADPH oxidase with a nearly 100-fold upregulation in the mutant. This would be consistent with the loss of a E3 ubiquitin ligase mediating degradation, hence increasing Nox3 levels. Interestingly, we had evidence for oxidative stress also from the RNAseq data in the cKO and now found a protein increasing reactive oxygen species which could be a potential cause for the oxidative stress.



C

E16 cKO/Ctrl Mass spectrometry
Nuclear proteins



Cytoplasmic proteins

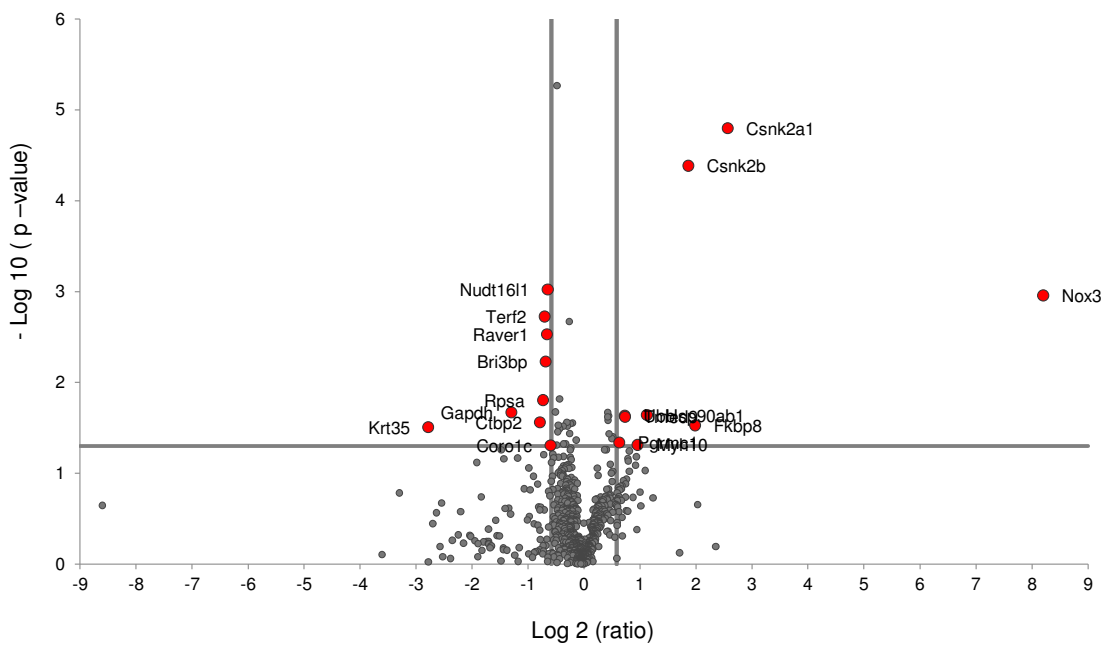


Fig. 4-27 Proteasome analysis of Uhrf1 cKO mutants at E16

A. Western blots for Histone 3 and Beta III tubulin in E15 cortical lysates fractionated for the nucleus and cytoplasm. Note the presence of Histone H3 only in the nuclear fraction and beta III tubulin only in the cytoplasmic fraction.

B,C. Volcano plots of the proteasome analysis of cerebral cortex of E16 cKO and controls by mass spectrometry depicting proteins between the controls and cKO in the nuclear (B) and cytoplasmic (C) fractions.

E16 Cortex – Mass spectrometry data

Nuclear fraction

Name	Ratio of cKO/Ctrl	Unique peptides	Anova (p)
Tuba3b	94.65	1	0.0129
Slc7a5	2.20	1	0.0002
Atp6v0a1	2.02	1	0.0434
Apoa1	1.96	1	0.0011
Nat10	1.89	2	0.0003
Tmx4	1.87	1	0.0004
Hsp90ab1	1.84	1	0.0346
Slc1a4	1.64	1	0.0087
Reep1	1.58	1	0.0224
Slc3a2	1.58	6	0.0004
Hsp90ab1	1.55	18	0.0021
Fkbp8	1.51	2	0.0037

Cytoplasmic fraction

Name	Ratio of cKO/Ctrl	Unique peptides	Anova (p)
Nox3	293.86	1	0.0011
Csnk2a1	5.93	6	0.0000
Fkbp8	3.95	1	0.0298
Csnk2b	3.64	3	0.0000
Hsp90ab1	2.18	4	0.0229
Myh10	1.94	9	0.0488
Tmed9	1.67	1	0.0239
Ubb	1.66	4	0.0234
Pgrmc1	1.55	4	0.0459

Table 9. Table depicting deregulated proteins in E16 Uhrf1 cKO and control lysates detected by label-free mass spectrometry

Table enlisting upregulated and downregulated proteins in the Uhrf1 cKO compared to controls at E16.

4.7. Generating neural stem cells from Uhrf1 KO ES cells

Previous studies have shown that loss of Uhrf1 in ES cells resulted in activation of IAPs (ref). Moreover, in our study we could also determine IAP activation in a *Uhrf1* KO of neural stem cells both in vivo and in vitro. Thus, we sought to determine if neural stem cells derived from *Uhrf1* KO ES cells still maintained IAP activation and exhibited any cellular phenotype. In collaboration with Dr. Fabio Spada at the LMU, we received NS cells which had been derived from *Uhrf1* KO ES cells and corresponding controls. Firstly, we immunostained these cells for IAP Gag and could observe a strong activation of IAP in the KO cells compared to WT controls (Figure 4-28A,B). Interestingly, we also observed a strong upregulation of H2AX staining in the KO cells compared to controls (Figure 4-28C,D). As H2AX has been described to label DNA double stranded breaks, this result could indicate genomic instability in the *Uhrf1* KO NS cells.

Thus, these data further indicate that once IAPs are ectopically activated certain cell types, in this case ES cells, they are maintained in all subsequent generations (such as NS cells in this case and neurons in the cKO cerebral cortex).

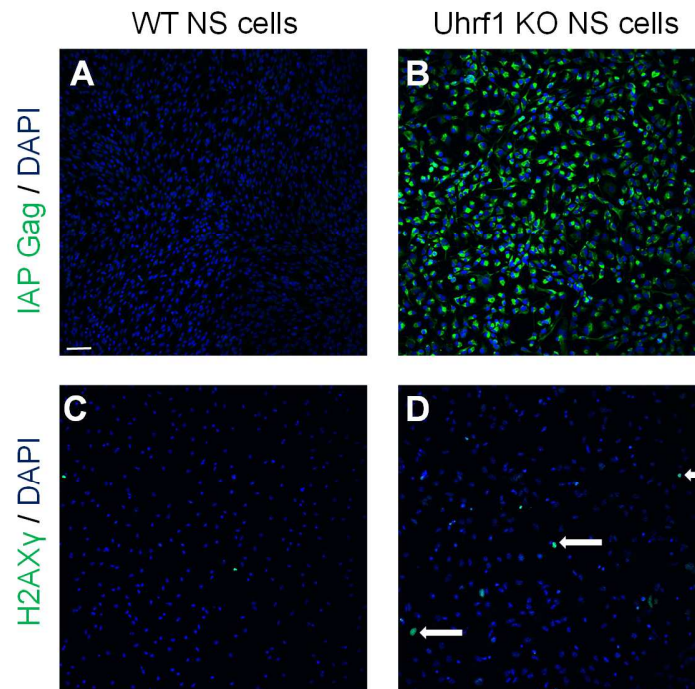


Fig. 4-28 IAP is activated in NSCs derived from Uhrf1 ES KO cells

A-D. Epifluorescence images of wild-type and *Uhrf1* KO NSCs immunostained for IAP Gag (A,B) and H2AX (C,D) indicating IAP activation and genomic instability.

4.8. Conditional knockout of Uhrf1 in adult neurogenic niches

4.8.1 Loss of Uhrf1 in the adult subependymal zone and dentate gyrus – further characterization of the cellular phenotype

Previous data from our lab (Bayam 2014) has shown that loss of Uhrf1 in the adult neurogenic niches (subependymal zone and dentate gyrus) have resulted in reduced proliferation of transit-amplifying progenitors (TAPs) and neuroblasts. The adult cKO was generated by using *Glax1^{CreERT2}; Uhrf1 flox*; CAG mice wherein Cre was activated with Tamoxifen induction (Mori et al. 2006). The reduction in proliferation was previously assessed by immunostaining for Ki67 and 1 hour BrdU pulses.

To understand if the reduction in neuroblasts in the SEZ and DG was due only because of reduced proliferation or due to increased cell death, we first performed TUNEL analysis at 9dpi post induction in the DG (Figure 4-29A). We did not observe a significant difference in % of TUNEL+ve cells over GFP+ve at 9dpi in the DG (Figure 4-29B). We also analysed 4 weeks pi in the SEZ. Although we observed a mild increase in TUNEL+ cells in the adult cKO SEZ, in total there were very few in the SEZ of both the cKO and control (Figure 4-29C). Thus, we concluded that although cell death could contribute towards the reduction in TAPs and neuroblasts, it is not the main cause.

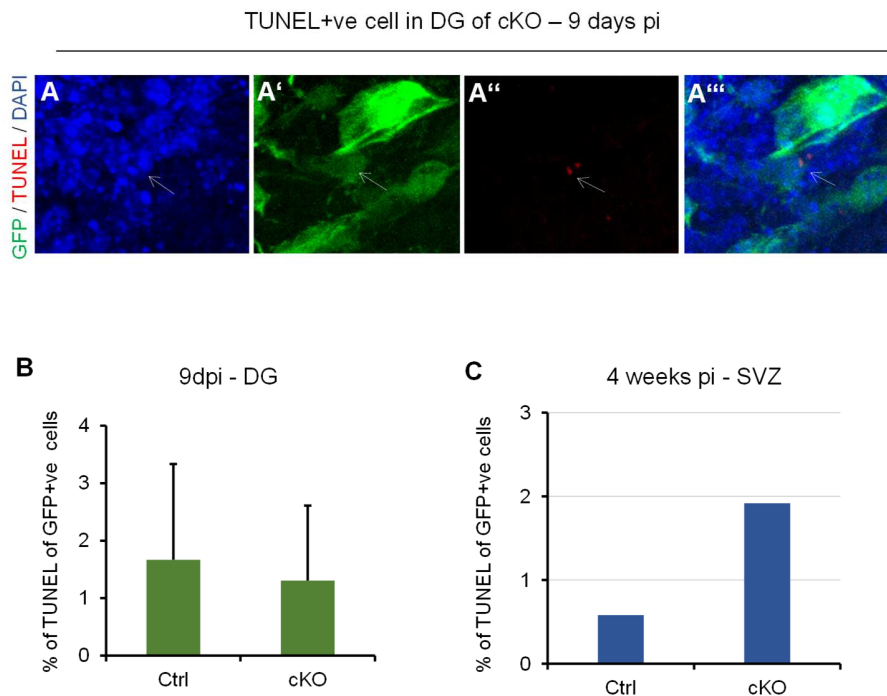


Fig-4-29 Cell death analysis in the adult cKO of the SEZ and DG

A. Confocal images of sagittal sections of the adult DG of cKO stained with the TUNEL kit to label apoptotic cells, GFP to label recombined cells and DAPI at 9 days post tamoxifen induction.

B. Graph depicting quantifications for numbers of TUNEL+ve cells per GFP+ve cells in adult control and cKO at 9dpi in DG, showing no difference in TUNEL+ve cells in the adult control and cKO. Error bars indicate standard error of mean. n=2.

C. Graph depicting quantifications for numbers of TUNEL+ve cells among GFP+ve cells per area in adult control and cKO from at 4 weeks post induction in the SEZ showing a slight increase in the adult cKO. n=1 for cKO and 2 for Ctrl.

Although a reduction in GFP+ve cells was previously also observed in the SEZ (Bayam 2014), the numbers of GFP+ve cells in the olfactory bulb appeared unchanged at 4 weeks post induction.

Thus, we investigated if the recombined cells in the adult cKO and controls were changed in the olfactory bulb at 4 months post induction. We quantified numbers of GFP+ve cells in different layers of the olfactory bulb in the cKO compared to the control but observed no significant change in numbers (Figure 4-30A-C).

Therefore, we concluded that although loss of Uhrf1 in the adult SEZ resulted in impaired proliferation and a reduction in cell types in the SEZ, there was a compensation for this loss in the olfactory bulb, resulting in comparable number of neurons generated from the recombined GFP+ve cells that migrated to and survived in the OB.

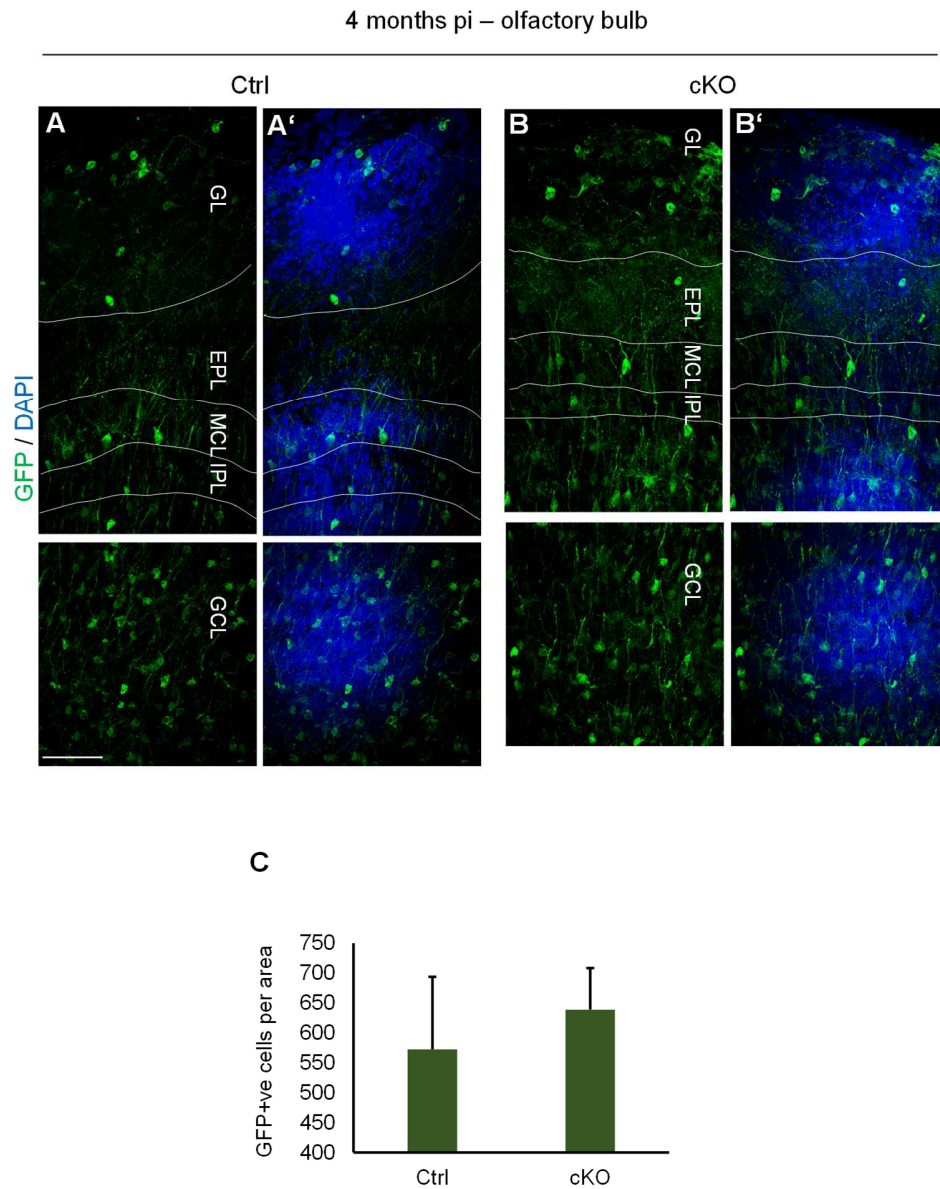


Fig-4-30 Comparable recombined cells in the olfactory bulb of the adult control and cKO of the SEZ

A,B. Confocal images of sagittal sections of the adult olfactory bulb of control (A) and cKO (B) stained with GFP to label recombined cells and DAPI at 4 months post tamoxifen induction. Scale bar = 50 μ m

C. Graph depicting quantifications for numbers of GFP+ve cells per area in adult control and cKO from A,B, showing no difference in the control and adult cKO. Error bars indicate standard error of mean. n=2.

4.8.2 Differences in IAP activation in the adult cKO of the SEZ and dentate gyrus

To investigate the molecular mechanisms underlying the phenotypes in the adult cKO, we first examined if there were any changes in DNA methylation. We performed immunostaining for 5mC and 5hmC in the SEZ at 9 days post induction. We could not observe any significant changes in 5mC in GFP+ve cells in the cKO and control SEZ (Figure 4-31A,B).

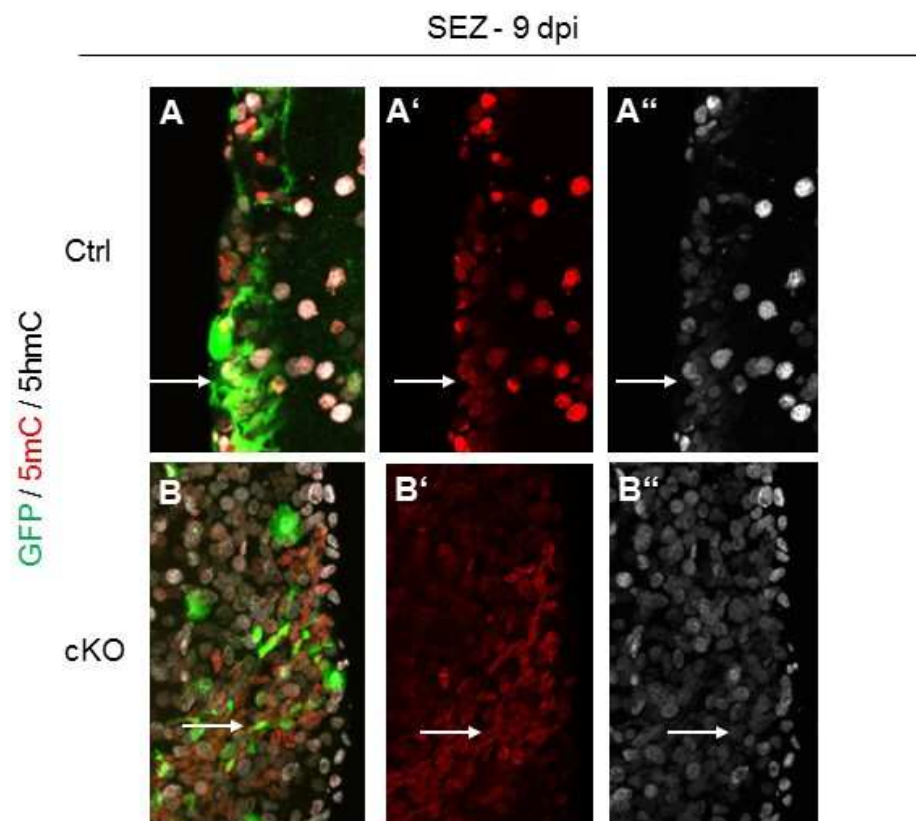


Fig. 4-31 Assessing changes in methylation marks by immunostaining in adult cKO of SEZ and dentate gyrus

A-B. Confocal images of sagittal sections of the SEZ control (A) and adult cKO (B) immunostained for 5mC and 5hmC at 9 days post induction in the SEZ. Immunostaining for 5mC and 5hmC appear largely unchanged between controls and cKO. White arrows indicate GFP+ve cells positive for 5mC and 5hmC. Scale bar = 50 μ m.

In order to ascertain if IAP is activated in the adult cKO, we performed immunostaining for IAP Gag protein at 9 days and 4 weeks post induction (Figure 4-32) in both SEZ and dentate gyrus. At 9 days post induction, we mainly observed IAP to be activated in the SEZ (Figure 4-32A,B). The NSCs from the SEZ migrate through the RMS and to the OB so at 4 weeks post induction we performed IAP Gag staining. We detected IAP additionally in the rostral migratory stream and olfactory bulb of the adult cKO (Figure 4-32C,D).

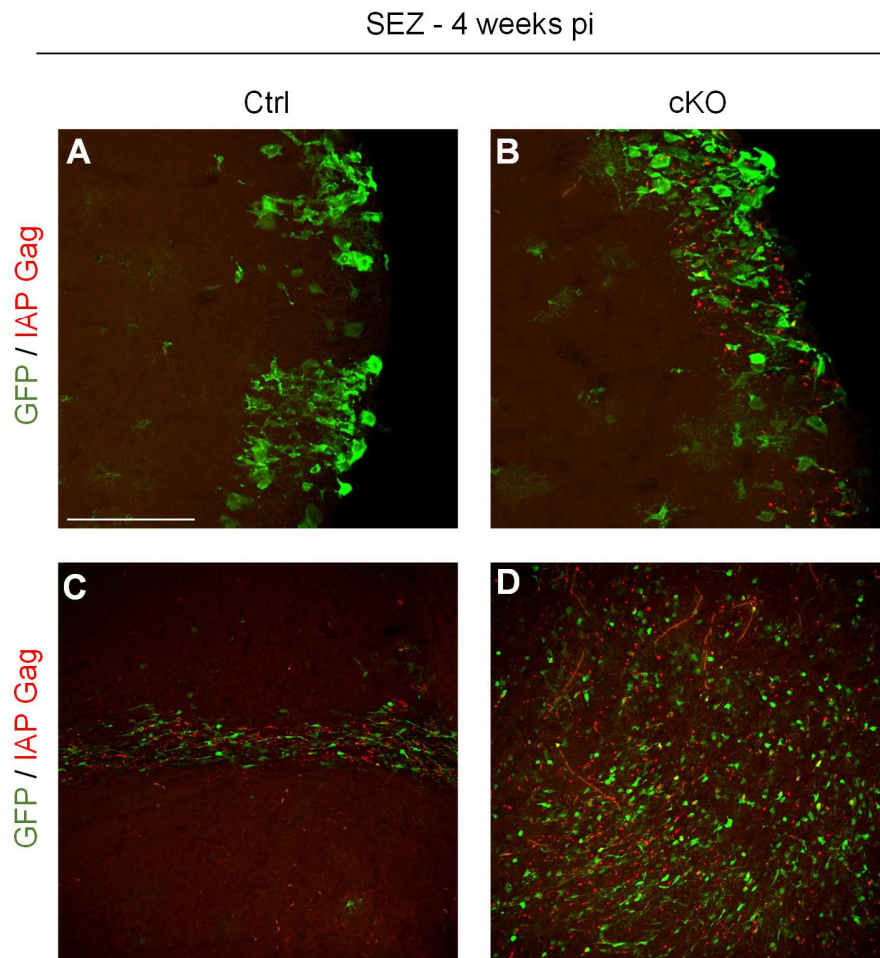


Fig. 4-32 IAP activation in the adult SEZ cKO

A-D. Confocal images of sagittal sections of control (A) and adult cKO (B,C,D) immunostained for IAP Gag at 9 days post induction (A,B) and 4 weeks post induction (C,D) in the SEZ. Note that IAP Gag immunostaining is detectable only in the cKO. Scale bar = 50 μ m

Surprisingly, we did not observe IAP activation in the adult cKO of the dentate gyrus, even at 4 weeks post induction (Figure 4-33A,B). Thus, these data indicate specificity for Uhrf1 in IAP regulation in different neurogenic niches.

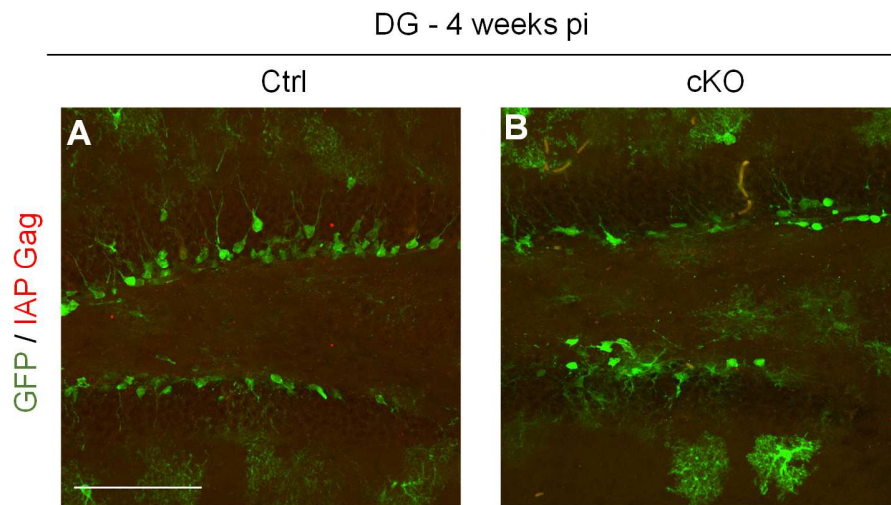


Fig. 4-33 IAP is not activated in the adult dentate gyrus cKO

A-D. Confocal images of sagittal sections of control (A) and adult cKO (B) immunostained for IAP Gag at 4 weeks post induction in the dentate gyrus. Note that IAP Gag immunostaining is not detectable in the control and cKO. Scale bar = 50 μ m

5. Discussion

5.1. Expression of Uhrf1 in the developing cerebral cortex

Comprehensive analysis of Uhrf1 expression in the embryonic cortex provided several insights. From mRNA and immunohistochemistry, we could observe that Uhrf1 is largely present as protein and mRNA in early stem cells of the neurogenic lineage and is strongly downregulated in later differentiated cells. Uhrf1 was found to be expressed highly by embryonic radial glia and Uhrf1 immunostaining was prominent in the ventricular zone wherein radial glial cells reside. Interestingly, Uhrf1 protein was mostly downregulated in the intermediate progenitors labelled by Tbr2, with only few Tbr2+ve cells having low levels of Uhrf1 (Ramesh et al. 2016). Intermediate progenitors could not be isolated via FACS with current protocols and thus it is still unclear the extent of Uhrf1 mRNA present in these cells. Finally, we examined newborn neurons in the embryonic cortex for Uhrf1 expression and immunostaining. Uhrf1 expression in newborn neurons was extremely low (about 40-fold lower than radial glia). Moreover, Uhrf1 immunostaining was largely absent in the differentiated zones at E12. We could also observe Uhrf1 immunostaining in the ventricular zone of the LGE, suggesting a role for Uhrf1 in GE radial glia proliferation and differentiation. In the adult neurogenic niches, we detected Uhrf1 mRNA in the SEZ, indicating that it is expressed in aNSCs and progenitors. These data support published findings from our lab, wherein Uhrf1 is largely detected in TAPs and to a lower extent in aNSCs (Ramesh et al. 2016). Thus, the expression of Uhrf1 differs between embryonic and adult neurogenesis, wherein embryonic NSCs have high levels of Uhrf1 and the embryonic TAPs have low levels and the contrast is observed for the adult SEZ.

The expression of Uhrf1 in the neurogenic lineage is similar to that observed in other lineages wherein Uhrf1 is largely present in proliferating cells such as in skin stem cells (Sen et al. 2010), in regulatory T-cells (Obata et al. 2014), T-cell progenitors (Cui et al. 2016) and in hematopoietic stem cells (Zhao et al. 2016). Additionally, Uhrf1 was shown to be downregulated during skin stem cell differentiation (Sen et al. 2010) and this was also observed by us in the developing cortex, with its low levels in intermediate progenitors and near absence in neurons.

5.2. Cellular function of Uhrf1 in the embryonic cerebral cortex

Uhrf1 null mice are embryonically lethal, probably due to mid-gestational lethality (Muto et al. 2002). Thus, in order to study Uhrf1 function, only conditional knockout mice can be utilized. Since

we were interested in studying Uhrf1 function specifically in cortical neurogenesis we employed a Cre specific to the dorsal telencephalon, namely, Emx1-Cre (Iwasato et al. 2000; Cappello et al. 2006). Moreover, since we observed Uhrf1 immunostaining in radial glia of both the developing cerebral cortex and the ganglionic eminence, we could monitor loss of Uhrf1 using the GE as an internal control. We observed loss of Uhrf1 only in the dorsal telencephalon at E12, with no loss in the GE. Previous data have shown that loss of Uhrf1 in the embryonic cortex leads to loss of cortical neurons at 1 month of age with no apparent changes in embryonic radial glia and progenitors (Bayam. 2014). We probed for defects in proliferation with Ki67 staining at E16 and observed no changes in numbers. However, we did detect an increase in non-apical Ki67+ve cells in the cKO compared to the control. As we did not observe defects in proliferation of cortical progenitors, we hypothesized that the reduction in cortical neurons could arise from premature neuronal differentiation. We performed Tuj1 and Tbr1 staining at E16 to address this question. We could not detect any ectopic neurons in the germinal zones or any difference in the numbers of Tbr1+ve cells between the cKO and controls. These phenotypes are in contrast to that which was studied in T-regulatory cells and hematopoietic stem cells wherein loss of Uhrf1 lead to defects in stem cell or progenitor proliferation (Obata et al. 2014; Zhao et al. 2016). Thus, although Uhrf1 is known to be expressed primarily in proliferating cells, it does not always play an active role in proliferation and differentiation in the cell type of its expression. These findings are in contrast to those which were observed for Uhrf1 in other systems. In the T-regulatory cells, loss of Uhrf1 resulted in defects in proliferation due to the upregulation of p27kip1, a cell cycle inhibitor (Obata et al. 2014). In the zebrafish lens, loss of Uhrf1 and Dnmt1 led to defect in lens development and maintenance (Tittle et al. 2011). Moreover, loss of Uhrf1 in HSCs and skin stem cells impaired their self-renewal (Sen et al. 2010; Zhao et al. 2016). Thus, ours is the first study wherein conditional loss of Uhrf1 in multipotent stem cells (cortical radial glia) did not result in a significant aberration of self-renewal, proliferation of initial differentiation.

To further understand the underlying cause for the reduction in cortical neurons in 1 month old mice, we probed the cKO for cell death. We hypothesized that the reduction in neurons could arise from increase cell death. In fact, previous data have indicated some cell death at mid-neurogenic stages in the Uhrf1 cortical cKO compared to controls (Bayam. 2014). We investigated the onset of cell death by examining the cKO for TUNEL+ve cells at E12. Indeed, we observed about a 4-fold increase in TUNEL+ve cells at E12 in the cerebral cortex of the cKO compared to controls. This extent of increase in TUNEL+ve cells in the cKO at E12 was similar to that which was observed at E14 and E16 (Bayam 2013). Thus, although some cell death occurs at embryonic stages, this is not translated into a detectable reduction in either progenitors or neurons. These

data suggest that the cerebral cortex of the cKO is able to compensate the cell death without resulting in significant changes in progenitors or neurons.

Loss of Uhrf1 has been shown to cause apoptotic death in certain cell types such as cancer cells and human cell lines (Dai et al. 2013; Ge et al. 2016; Matsushita et al. 2016). One of the described mechanisms involves the interaction of Uhrf1 with Tip60 wherein loss of this binding facilitates binding of Tip60 to p53 to acetylate it and activate its downstream targets for apoptosis (Dai et al. 2013). However, it has also been shown that loss of Uhrf1 in cancer cells can lead to an increase in caspase-8 dependent apoptotic cell death, which occurs in a p53-independent manner (Tien et al. 2011). Thus, it is possible that the cell death we are observing might be occurring in a p53 dependent or independent manner. Additionally, we detected an increase in Nox3, a NADPH oxidase which increases reactive oxygen species in cells. Thus, it is likely that Nox3 upregulation can lead to ferroptosis, a form of cell death related to increased ROS (Yu et al. 2016).

As we did not observe defects in radial glia/progenitor proliferation or initial neuronal differentiation, we investigated early postnatal stages wherein terminal neuronal differentiation occurs. Indeed, we could only observe a decrease in the thickness of the cortex from P7. At E16 and even P2, we could not detect a significant change in cortical thickness. Thus, we hypothesized that cell death was possibly aggravated during early postnatal cortical development. We investigated TUNEL staining at P2 and P7 of the cKO compared to controls. At P2 we detected almost an 11-fold increase in TUNEL+ve cells of the cKO and at P7 it reduced to about 6-fold higher in the cKO. These data suggest that loss of Uhrf1 resulted in a late neurodegenerative phenotype wherein postnatal cell death was the possible primary cause for the severe reduction of cortical neurons.

In fact, conditional deletion of Dnmt1 in the developing cerebral cortex using also Emx1-Cre resulted in a highly comparable phenotype to that of Uhrf1 (Hutnick et al. 2009). Dnmt1 cKO exhibited a severe reduction of cortical thickness with massive cell death occurring at embryonic stages (Hutnick et al. 2009). On the contrary, conditional deletion of genes regulating histone marks displayed a range of phenotypes. ESET (involved in setting the H3K9me3 mark) cKO in the cerebral cortex (using Emx1-Cre) led to defects in proliferation and initial neurogenic differentiation (Tan et al. 2012), suggesting differing roles for genes involved in H3K9 methylation and DNA methylation. In fact, as observed by our H3K9me3 ChIP experiments, loss of Uhrf1 did not significantly change this histone mark. Interestingly, conditional deletion of G9a, a histone methyltransferase which is involved in setting H3K9me2, led to a similar phenotype as was observed here with Uhrf1 (Kumar 2014). This could be due to the fact that Uhrf1 has been shown to

bind G9a (Kim et al. 2009), suggesting an interplay between these molecules also in the embryonic cortex.

We also investigated changes in gliogenesis in the cKO cortices. We did not observe any activation of Gfap in the Uhrf1 cKO, which is in contrast to that observed in Dnmt1 cKO, wherein precocious astroglial differentiation was detected (Fan et al. 2005). This premature Gfap activation in Dnmt1 cKO NSCs was attributed to deregulated Jak-Stat signaling pathway (Fan et al. 2005). This pathway was not deregulated in our Uhrf1 cKO study, suggesting some differing transcriptional targets for Uhrf1 and Dnmt1. However, we did observe some genes expressed in the germline and some x-linked genes to be commonly regulated in both the Dnmt1 and Uhrf1 cKO RNAseq datasets at P5. The only time point wherein we observed Gfap activation in the cerebral cortex was in 1-month old cKO mice. Gfap activation, as part of reactive gliosis, has been linked to neurodegeneration (Maragakis and Rothstein 2006). Thus, the observed Gfap activation is probably due to neuronal death observed in the Uhrf1 cKO. We also analysed microglia activation in our Uhrf1 cKO and did not observe any major differences in number or morphology at embryonic stages.

In summary, loss of Uhrf1 in the developing cortex leads to a late neurodegenerative phenotype wherein a majority of cortical neurons are lost in postnatal stages. Significant defects in radial glia and progenitor proliferation and differentiation were not observed (this study and Bayam. 2014).

5.3. Transcriptional control of Uhrf1 in the embryonic cortex

Transcriptional profiling of Uhrf1 cKO was performed to understand the molecular triggers of the cellular phenotype. This revealed that Uhrf1 is primarily involved in controlling cellular stress genes and retroviral elements. It is important to note that in support of our cellular phenotypic analysis, we did not observe transcriptional changes in cell fate genes such as Pax6, Ngn2 and Ascl1. Moreover, we also did not observe changes in genes related to self-renewal, also in concomitance to our phenotypic analysis. These data further indicate that loss of Uhrf1 does not trigger a change in neuronal fate. This is particularly in contrast to loss of Uhrf1 in HSCs, wherein KO cells exhibited deregulation of HSC self-renewal and differentiation genes (Zhao et al. 2016) and also its role in the zebrafish lens and T-regulatory cells (Tittle et al. 2011; Obata et al. 2014). These data suggest a highly cell-type specific role for Uhrf1.

Transcriptional profiling in E16 germinal zones (comprising mainly progenitors) primarily resulted in mild upregulation of interferon signaling and downregulation of oxidative phosphorylation genes. Surprisingly, transcriptional profiling in E16 progenitors and neurons did not uncover a change in interferon signaling but only that of oxidative phosphorylation. These data suggest that at E16, the neurons have still not activated interferon signaling and that it is largely present only in progenitors. Moreover, at postnatal day 5, interferon signaling is activated again, suggesting that by this time the neurons have also upregulated this pathway. In addition, P5 cKO cells also upregulated the unfolded protein response and downregulate genes expressed in adult mature neurons (LEIN_neuron markers).

In general, three main pathways seem to be deregulated in the cKO – interferon signaling, oxidative phosphorylation and unfolded protein response. Each of these pathways have been known to cause cellular stress which could eventually lead to cell death, especially in neurodegenerative diseases (Johri and Beal 2012; Chen et al. 2014; Diaz-Castro et al. 2015; Pasquarella et al. 2016). Besides these pathways, we also observed genes related to germ-cells and x-linked genes to be upregulated. Similar groups of genes were also upregulated in the cerebral cortex Dnmt1 cKO (Hutnick et al. 2009), suggesting a link to DNA methylation changes. Interestingly, we could also detect some cell-cycle genes such as Cdkn1a and Cdkn1b to be mildly upregulated in the cKO. As mentioned previously, postmitotic neurons still express cell-cycle related proteins after terminal neuron differentiation (Yoshikawa 2000) which is considered relevant for their terminal maturation. However, studies have shown that when neurons are subjected to certain injury or stress, such as oxidative stress for example, they upregulated certain cell-cycle proteins which in turn can cause a block at the G1/S cell cycle checkpoint, ultimately leading to their death (Frade and Ovejero-Benito 2015). Moreover, this type of cell cycle re-entry can also be observed in neurodegenerative diseases, wherein it can also lead to genome instability (Frade and Ovejero-Benito 2015).

Uhrf1 possess E3 ligase activity which has been shown to be involved in the protein turnover of Promyelocytic leukemia protein (Pml) in primary human umbilical vein endothelial cells, HEK293 and cancer cells (Guan et al. 2013). Therefore, we investigated if Uhrf1 could perform a similar function in the developing cerebral cortex. We assessed proteomic changes in controls and cKO at E16 and could identify a few upregulated and downregulated proteins in the cKO. In particular, we observed a 300 fold upregulation of the protein Nox3, a NADPH oxidase, in the cKO. Nox3 belongs to the Nox family of genes, which contribute towards the production of reactive oxygen species. Increased ROS can lead to oxidative stress which has been described to be an

underlying mechanism of neurodegeneration (Gandhi and Abramov 2012). Thus, it is possible that Nox3 is contributing towards the cell death phenotype observed in the cerebral cortex Uhrf1 cKO.

Oxidative phosphorylation (OxPhos) is a metabolic process occurring in mitochondria, whereby energy is produced in an aerobic manner. Aberrations in this process can lead to the production of reactive oxygen species which can cause cellular stress and prove detrimental. In particular, production of ROS due to defects in oxidative phosphorylation can cause oxidative stress in neurodegenerative diseases such as Alzheimer's disease, Amyotrophic Lateral Sclerosis, Huntington's disease and Parkinson's disease (Sayre et al. 2001). Conditional loss of SDHD in the neocortex, an important gene involved in mitochondrial function, resulted in a highly similar phenotype as that was observed here for Uhrf1 (Diaz-Castro et al. 2015). In particular SDHD cKO mice did not exhibit major defects in embryonic cortical neurogenesis or neurogenic cell fate and appeared largely normal until birth. However, they did display severe brain defects in later postnatal stages, with reduction in cortical tissue size, among other brain regions (Diaz-Castro et al. 2015). Moreover, our observed upregulation of Nox3 could be a function of the RING finger domain of Uhrf1, involved in protein turnover, exacerbating the defects in OxPhos and contributing towards oxidative stress. These data are consistent with our findings, suggesting that mitochondrial defects could prove more deleterious in postnatal cell types as compared to embryonic progenitors and neurons.

Interferon signaling acts as an immune response against viral infections mediated by interferons. Interferons, which are cytokines, can be of different types such as interferon- α , interferon- β , interferon- γ and others, each binding to specific receptors. Viruses often trigger interferon signaling via their dsRNA or viral proteins (Haller et al. 2006). Moreover, interferon signaling is crucial to combat viral infections as IFN- α , β knockout mice can quickly succumb to viral infections (Muller et al. 1994; Hwang et al. 1995; van den Broek et al. 1995; Grieder and Vogel 1999; Ryman et al. 2000; Bouloy et al. 2001; Bray 2001). Additionally, It has been shown that endogenous retroviral elements can trigger interferon signaling due to the presence of dsRNA from ERV activation (Chiappinelli et al. 2015). Interferon signaling can lead to cell death via apoptosis (Chawla-Sarkar et al. 2003).

Unfolded protein response (UPR) is a cellular stress mechanism which occurs in response to an accumulation of misfolded proteins in the endoplasmic reticulum. This excess of protein load can often lead to cell death (Sano and Reed 2013). In fact, ER stress has been described to be an important contributor towards accumulation of β -amyloid plaques and α -synuclein leading to

neuronal death in the neurodegenerative Parkinson's and Alzheimer's disease (Sano and Reed 2013). ER stress can also be triggered by endogenous retroviral elements which produce high levels of viral proteins, as has been shown for B-cells (Pasquarella et al. 2016).

LEIN_neuron markers comprise those genes expressed in adult neurons and we observed many genes related to terminal neuronal differentiation to be underrepresented in the cKO. These data suggest that either the cKO neurons are hampered in their neuronal maturation processes which is consistent with persisting cell cycle gene expression or that the slight loss of neurons at this stage could be reflected with a transcriptional reduction in these genes. However, as we do not observe a significant difference in the cortical thickness at this stage, and we do not observe cell death as a clear deregulated pathway, we think it's unlikely that a few less neurons in the cKO can be detected with a deregulated pathway. Thus, it is most likely that the postnatal neurons in the cKO are defective in their terminal differentiation and maturation processes.

The transcriptional changes on coding genes were comparatively mild as compared to the major transcriptional changes observed on a set of RNA transposable elements, IAPs. IAPs, specific to the mouse genome, are a type of endogenous retroviral elements. Although we observed some individual LINE-1 and SINE-B1 elements (other ERVs) to be activated, the entire class was not significantly upregulated. We could observe about 25-30% of deregulated genes to be near activated IAPs. It has been shown that activated IAPs in proximity to genes can affect their nearby gene transcription (Fasching et al. 2015). Moreover, we also observed a major proportion of the individual activated LINE-1 elements to be in near activated IAPs. Thus, it is likely that the activated IAPs are regulating local transcription in the Uhrf1 cKO.

Activation of transposable elements has been previously reported in knockouts of the DNA methylation machinery. Dnmt1 cKO of the developing cortex also led to a strong activation of IAP gag protein, however, the other REs were not analysed (Hutnick et al. 2009). Uhrf1 and Dnmt1 KO ESCs significantly upregulate both IAPs and LINE element transcripts, with a higher activation in Dnmt1 KO (Sharif et al. 2007; Sharif et al. 2016). Conditional deletion of Uhrf1 at early development (about E9) in the whole embryo did not lead to a major increase in IAP and LINE activation, compared to a similar cKO of Dnmt1 (Sharif et al. 2016). These data indicate that loss of Uhrf1 could either be compensated for with regard to DNA methylation, or that Dnmt1 has other adapters for this process. Since we observe a strong activation of IAP in the developing cortex, which is not observed in the rest of the embryo, these data indicate a clear specificity for Uhrf1 in IAP regulation in the neocortex.

Besides proteins involved in the DNA methylation process, the histone methylation machinery has also been implicated in ERV regulation. Conditional loss of Setdb1 and Kap1, both involved in setting the H3K9me3 mark, in the neocortex led to IAP and other RE activation (Tan et al. 2012; Fasching et al. 2015). However, in both cases, the level of IAP activation was much lower than that observed in our Uhrf1 cKO. In both Setdb1 and Kap1 cKOs, H3K9me3 was reduced but DNA methylation was not altered significantly (Tan et al. 2012; Fasching et al. 2015). These data indicate that both DNA methylation and histone methylation can control ERV regulation. It remains to be elucidated if these machineries are exclusive or function together in such regulation. Uhrf1 itself has been shown to bind both DNA and histones, providing a link between the two epigenetic pathways.

We could observe that the activation of IAPs is sustained over a long period of time, wherein even weeks after Uhrf1 deletion, high levels of IAP mRNA and protein were detected in the postnatal cortical neurons, although Uhrf1 is not expression in these cells. Thus, IAP activation could not be re-silenced by other proteins and Dnmts/Tet enzymes expressed in cortical neurons. The implications of ERV activation in cellular process have largely been linked to being detrimental in nature. In general, ERVs have been heavily implicated in diseases such as cancers, neurological diseases and diabetes (Blomberg et al. 2000-2013). Overexpression of HERVK (a human ERV) in motor neurons causes neuronal death (Li et al. 2015). Moreover, this ERV has also been implicated in ALS, a neurodegenerative disease (Li et al. 2015). IAP activation has also been linked to cell death in primordial germ cells (Liu et al. 2014).

In summary, we observed that Uhrf1 cKO exhibit early transcriptional changes which increase and accumulate into postnatal stages. Additionally, the cell death phenotype we detected is also progressive over time. We suggest two possible mechanisms which could cause this 'late neurodegenerative phenotype' – 1) a) The accumulation of deregulated genes and the nature of them causes the phenotype to deteriorate and 2) certain phenotypes are not deleterious at embryonic stages, but become critical at later stages when neurons mature and become functional.

As discussed above, in support of our first theory, we observe activation of the OxPhos pathway in both progenitors and neurons, following which interferon signaling is activated (first in progenitors and then neurons) and finally UPR and a reduction in genes involved in neuronal maturation is detected (in postnatal neurons). Additionally, the IAP elements accumulate in all the cells as mRNA and protein, acting as possible cause and consequence of both the deregulated genes and subsequent cell death. Our second hypothesis stems from our finding that although

strong transcriptional changes are observed as early as E12, it takes several weeks for the cKO to exhibit a detrimental phenotype.

5.4. Molecular mechanism of Uhrf1 in the developing neocortex

The methylation changes we observed upon loss of Uhrf1 were broadly of two categories. In the first category, we observed that most of the loci which had lost methylation in the cKO, namely the differentially methylated promoters (DMRs), did not incur transcriptional changes. Some of the ERVs and other transposable elements such as LINE-1 and SINE-B1 also fell into this category. The second category comprised mainly of the IAP family of ERVs which had both lost methylation and had upregulated transcripts in the cKO. Thus, our two main conclusions from these data are that – 1) Uhrf1 has a great deal of specificity in regulating methylation of its target loci and 2) Loss of methylation does not have to be a necessary trigger for transcriptional activation in the developing neocortex.

Global methylation was analyzed by immunostaining, DNA restriction digests and RRBS and indicated that about 50% of the genome lost methylation upon Uhrf1 deletion in the developing cortex. The data from the DNA restriction digests with HpaII indicated that there was higher levels of demethylation in the cKO at E16, which is in accordance with the immunostainings. Loss of Uhrf1 in ES cells and the zebrafish lens also resulted in hypomethylation with restriction digests (Tittle et al. 2011; Sharif et al. 2007). From the immunostainings for 5mC at E14, we observed a severe reduction of 5mC in the cKO cerebral cortex. However, some cells still retained 5mC upon Uhrf1 deletion. Some of these remaining cells colocalized with Pax6, Tbr2 and Tuj1. These cells could have arisen from radial glia prior to Cre recombination and Uhrf1 loss, however this is probably unlikely as the Emx1 recombination occurs prior to neurogenesis. Some of 5mC positive cells in the cKO did colocalise with Calbindin-interneurons (data not shown) which would arise from the GE where Uhrf1 is not deleted, and migrate into the cortex. We could also detect the ectopic 5hmC in the cKO at E14, which increased at E16 in the germinal zones of the cKO cortex. We did not observe ectopic 5hmC at E12 in the cKO, although we already detected some IAP transcript activation. Thus, it could be that E12 is the onset of IAP activation in the cKO, with some low levels of 5hmC which cannot yet be detected by immunostaining. At E14 and E16, the level of IAP activation increases greatly, along with the presence of 5hmC positive cells in the cKO.

In fact, a study wherein G9a was also deleted in the neocortex with Emx1-Cre, the loss of H3K9me2 observed was in a highly similar pattern to the reduced 5mC levels in our Uhrf1 cKO

(Kumar. 2013) The cells which had retained H3K9me2 upon G9a deletion were in a similar distribution as those cells which retained 5mC after Uhrf1 deletion, at E14. As mentioned before, G9a is a histone methyltransferase which can bind Uhrf1. It is interesting to speculate that these two molecules could be working in conjunction in cortical radial glia.

The RRBS analysis uncovered specific loci in the genome which had lost methylation in the cKO. Firstly, it revealed that on every chromosome of the cKO, about 40-60% of loci had lost at least 25% of 5mC compared to controls. This data indicates that Uhrf1 has a wide range of target loci, but that it is not required for methylation of all the loci. The remaining loci which have retained methylation could be regulated by other factors, either acting in conjunction with Dnmt1 or Dnmt3a/b. There could also be compensation by another factor on loss of Uhrf1. Although Uhrf2 also binds DNA, there have been no reports yet of its expression in neural stem cells. It is also important to note that the RRBS analysis was carried out on the entire cortical tissue, comprising radial glia, progenitors and neurons. Thus, we cannot ascertain which loci are methylated in which cell types. Therefore, it is possible that the loci which lost methylation in the cKO are specifically methylated only in proliferating cells and were thus affected when Uhrf1 was deleted. Further analysis using pure cell populations can shed light on these points.

Loss of Uhrf1 in the developing cortex led to 850 loci losing at least 25% of 5mC at E16. We could not align these 850 regions with a specific pathway or cellular mechanism, suggesting a random function for Uhrf1 in gene silencing in the neocortex. This finding contrasts slightly with the HSC system, wherein loss of Uhrf1 led to loss of methylation on specific loci related to self-renewal and HSC differentiation, which reflected the cellular phenotype (Zhao et al. 2016). Also, loss of Uhrf1 in regulatory T-cells led to derepression of p27kip1, a cell cycle regulator which in turn caused defects in T-cell proliferation (Obata et al. 2014). Thus, although the DNA methylation function of Uhrf1 is retained in the cerebral cortex, its target genes vary, thus affecting different cellular processes.

From the 850 affected loci in the cKO, only 4 genes had upregulated transcripts at E16, from the full cortex RNAseq data. These data clearly suggest that loss of 5mC is not sufficient for transcriptional activation in the developing cerebral cortex. There is evidence from literature which suggests that promoter methylation can regulate transcription directly or that additional layers of regulation such as histone marks might be necessary to regulate transcription from loci (Hackett and Surani 2013).

In addition to these 850 loci, we also observed many transposable elements to lose methylation in the cKO. In particular, we observed about 35% loss of 5mC on all IAPs, LINE and SINE elements. The loss of 5mC on IAP and LINE-1 was further confirmed with OxBS coupled with miSeq on specific CpGs on IAP Gag region and LINE-1 ORF1. Loss of methylation on repeat elements has also been reported for the Dnmt1 cKO of the cerebral cortex (Hutnick et al. 2009).

The rather surprising finding in our methylation data was the ectopic increase in 5hmC in Uhrf1 cKO. This result has not been previously reported in a Dnmt1 knockout or Uhrf1 knockout of another system. Reports have claimed that Uhrf1 can bind to 5hmC (Frauer et al. 2011; Spruijt et al. 2013). However, there is also a study claiming that Uhrf1 only binds 5mC and not 5hmC (Hashimoto et al. 2008). We observed a clear increase in 5hmC only from E14 at the level of immunostaining, which is after IAP is activated on mRNA. It is possible that 5hmC is increased on IAP also at E12, especially since we observed their transcriptional activation at this stage. However, it could also be that loss of 5mC leads to slight IAP transcriptional activation, which further exacerbates due to the accumulation of 5hmC. Ours and data from the literature is still preliminary to understand the exact dynamics of loss of 5mC and 5hmC in Uhrf1 cKO.

To identify the specific loci with increased 5hmC in the cKO, we performed 5hmeDIP in E16 germinal zones. The reason we excluded the cortical plate is because the control cortex also contains high levels of 5hmC in this region (Hahn et al. 2013). 5hmeDIP relies on enriching the levels of 5hmC but it is not an absolute quantitative technique, as compared to RRBS. Thus, it is less sensitive in its detection of changes of 5hmC in a sample. Nevertheless, we could identify a significant increase of 5hmC on IAPs in the cKO compared to the control. The increase was primarily on the Gag and LTR region of IAP. The LTR region can act as the promoter of the IAP, and thus this accumulation could potentially facilitate binding of transcription factors to the LTR to activate its transcription. Moreover, in the Gag region, the increased 5hmC was specific to a region called SHIN, which is a small sequence capable of inducing heterochromatin in ESCs (Sadic et al. 2015). Demethylation of this region could reduce levels of heterochromatin, allowing transcription. In fact, increased 5hmC levels have been described to lead to transcriptional activation (Wu et al. 2011).

In order to obtain a better understanding of the absolute levels of 5hmC, among all CpGs on IAPs, we utilized the OxBS-miSeq data. In this experiment, we could deduce levels of 5hmC in control and cKO cerebral cortices at E16. We could only see a 1.6% increase in 5hmC on IAP and 0.4% for LINE-1 in the cKO compared to the control. Thus, the 5hmeDIP and miSeq data in conjunction revealed that although there is a significant increase in 5hmC on IAP, the absolute levels of 5hmC

are quite low. Due to this reason, it might be that other genes and loci have also increased 5hmC on the cKO, however, we may have missed this change with 5hmeDIP. Thus, further genome wide deep sequencing such as TAB-seq (Tet assisted BS) might shed more light on this point.

Our working hypothesis for IAP regulation from the above data was that loss of Uhrf1 could lead to increased access for Tet enzymes to convert existing 5mC to 5hmC. Since we did not observe an increase in Tet mRNA in the cKO, we concluded that the levels of Tet are unaltered. Thus, Uhrf1 and Tet could compete for the IAP locus to regulate its transcription. We tested this hypothesis in vivo by employing in utero electroporation of the developing cerebral cortex (Saito et al. 2005; Stahl et al. 2013). Tet2 and Tet3 have been described to be expressed highly in the embryonic cerebral cortex compared to Tet1 (Hahn et al. 2013). Thus, we employed Scrambled, Tet2 and Tet3 shRNAs from this. We electroporated a Tet2/3 shRNA cocktail into cKO embryos at E13 and analysed the GFP+ve and GFP-ve cells for IAP mRNA. We could observe a significant reduction of IAP mRNA in GFP+ve cells compared to the surrounding GFP-ve cells for each analysed cKO embryo. These data suggested that downregulating Tet enzymes could alleviate some of the IAP activation in the cKO.

We deduced that this action of Tet enzymes probably occurs in the radial glia stage, since Uhrf1 is expressed in these cells and IAP regulation should occur in them. It would also be interesting to understand if Uhrf1 directly binds to IAP and other REs in the developing cortex. It has been shown in ESCs that both Dnmt1 and Uhrf1 can bind the IAP locus (Sharif et al. 2016).

Thus, we decided to focus on the NSCs or radial glia to investigate and strengthen our in vivo Tet data. We generated an in vitro NSC system to delete Uhrf1 wherein several molecular aspects of the in vivo data could be recapitulated here. We observed activation of IAPs, with no significant change in LINE-1 and SINE-B1 mRNA. We analyzed methylation with immunostainings and OxBS-miSeq and observed a significant reduction of 5mC in the Cre treated cells. Importantly, from the OxBS-miSeq experiment, we detected an increase of about 3.8% in 5hmC on IAP compared to a 0.2% increase on LINE-1. Although we could observe a trend for increased Annexin V staining in the Cre treated cells, the increase was not significant due to high variability between replicates. It could be that the passage number affects the level of cell death in these NSCs as they are quite vulnerable compared to immortalized cell lines. We employed the same shRNAs for Tet2/3 and Scrambled in this NSC system. In accordance with our in vivo data, we observed that NSCs deleted for Uhrf1 with Tet2/3 knockdown had a significantly lower level of IAP activation to those only deleted for Uhrf1.

In summary, our data strongly suggest that in the absence of Uhrf1 in cortical radial glia, Tet enzymes are playing a key role in IAP activation, probably by increasing 5hmC levels on these elements, which can allow key transcription factors to drive transcription from these loci. In physiological conditions, where Uhrf1 is present in radial glia, Tet might be spatially blocked from binding IAP and regulating 5hmC levels and thus its transcription. This in turn keeps IAP elements silenced.

5.5. Uhrf1 function in adult neurogenesis

Uhrf1 is expressed by a small proportion of adult NSCs, most of the TAPs and some neuroblasts in the adult SEZ (Bayam. 2014). In the dentate gyrus, Uhrf1 is expressed by TAPs and some neuroblasts as well. However, in both OB neurons and hippocampus neurons, Uhrf1 protein is not detected (Bayam. 2014). Thus, in contrast to the embryonic cortex, Uhrf1 is expressed mainly by TAPs in the adult neurogenic niches. Conditional deletion of Uhrf1 in adult NSCs using *Glast-CreERT2; Uhrf1 flox; CAG mice*, led to clear defects in proliferation and differentiation (Bayam. 2014). In *Uhrf1* adult cKO, Ki67+ve cells (labelling proliferating TAPs and neuroblasts primarily) were significantly reduced in both the SEZ and DG (Bayam. 2014). Moreover, recombined cells were generally reduced as well as neuroblasts in both the SEZ and DG (Bayam. 2014). We investigated mitotic cells in the SEZ and could observe a reduction of pH3+ve cells in the adult SEZ cKO. These defects in proliferation are in accordance with other studies wherein Uhrf1 was deleted in non-cancer cell types and cell cycle defects were observed (Bonapace et al. 2002; Arima et al. 2004; Sadler et al. 2007; Tittle et al. 2011) but in contrast to our data in the developing cerebral cortex.

A reduction in recombined cells could be due to either a reduced generation of TAPs and neuroblasts (via aberrant proliferation) or due to increased cell death. We investigated cell death with TUNEL assay and could not observe a significant upregulation of TUNEL in the cKO. Thus, we favor the hypothesis that in the adult cKO, proliferation is hampered leading to fewer TAPs and neuroblasts. Interestingly, this reduction of neuroblasts in the SEZ does not affect the number of OB neurons in the cKO. This could suggest compensation by the SEZ-OB system to ensure more neuroblasts survive in the OB and mature into neurons. This feature has been previously reported for the SEZ and OB (Petreanu and Alvarez-Buylla 2002; Mouret et al. 2008; Mouret et al. 2009).

Although Dnmt1 has not been studied in the adult neurogenic niches, Dnmt3a is expressed in the postnatal SEZ and DG (Feng et al. 2005; Feng et al. 2010; Wu et al. 2010). As mentioned previously, Uhrf1 can also bind Dnmt3a (Meilinger et al. 2009). In fact, Dnmt3a null mice display defects in both SEZ and DG neurogenesis which are similar to those observed in the adult Uhrf1 cKO (Wu et al. 2010) (Bayam. 2014). The underlying mechanism was uncovered to be related to DNA methylation wherein Dnmt3a was shown to methylate promoters of gliogenic genes and genes bodies of neurogenic genes (Wu et al. 2010). It is likely that in our Uhrf1 cKO, the methylation of these regions is similarly affected, resulting in neurogenic defects. Another molecule which Uhrf1 binds, namely HDAC1 (Unoki et al. 2004), has also been implicated in SEZ neurogenesis. HDAC1 is expressed by GFAP+ve cells which comprise of aNSCs in the postnatal SEZ and inhibitors against HDAC1 and 2 reduced SEZ neurosphere formation (MacDonald and Roskams 2008; Montgomery et al. 2009; Zhou et al. 2011; Foti et al. 2013).

Although we could not ascertain a clear change in methylation, we examined IAP gag immunostaining in the SEZ and DG. To our surprise, although IAP is activated in the adult SEZ cKO, we did not observe this activation in the adult DG cKO. These data further describe a cell-type specific role for Uhrf1 in IAP regulation.

In summary, Uhrf1 plays a more conventional role in adult neurogenesis, affecting progenitor proliferation and neurogenesis, similar to that observed in other cellular systems. This contrasts with our embryonic findings, clearly exhibiting different roles for Uhrf1 in embryonic and adult neurogenesis.

5.6. Conclusions and prospects

Our study has introduced Uhrf1 to be an important epigenetic player in cortical and adult neurogenesis. Conditional deletion of Uhrf1 elucidated a unique function of Uhrf1 in ensuring appropriate postnatal cortical neuron numbers. In general, we detected a 'late neurodegenerative' phenotype which has not been observed previously for transcription factor or cell cycle regulators. This finding has elucidated a new type of transcriptional control wherein early molecular programs in radial glia can play critical roles in later stages of the neurogenic process, such as in terminal differentiation and maturation and neuronal survival. Our findings are supported by data from Dnmt loss of function of studies wherein Dnmt1 and Dnmt3a were deleted in either radial glia or only in neurons. Only loss of Dnmt1 in progenitors affected neuronal survival (Hutnick et al. 2009), whereas loss of Dnmt1 and Dnmt3a in postmitotic neurons did not affect neuronal survival (Feng

et al. 2010). Thus, there is strong evidence that this type of transcriptional control is related to the DNA methylation maintenance function of Uhrf1.

Moreover, our data have implicated a critical role for the maintenance of DNA methylation on retroviral elements, IAPs, in this above process. We have uncovered a layer of specificity in the regulation of transposable elements, in this case Uhrf1 for IAP. Although Uhrf1 does regulate IAP, this process is also not ubiquitous to every cell as was observed in the adult DG and in the early conditional deletion of the whole embryo (Sharif et al. 2016). Another crucial finding in our study was the lack of correlation between DNA methylation and transcription, strongly suggesting that loss of 5mC is not deterministic for transcriptional activation. Additional mechanisms are necessary in order to allow transcription from highly methylated and silenced loci, which in our case was observed to be Tet regulated 5hmC production.

Our differences in Uhrf1 phenotypes in the embryo and adult indicate a cell-type specific role for this protein. Although expressed by proliferating cells in all tissues studied till date, it does not appear to always control self-renewal and differentiation. It would be interesting to study the role of Uhrf1 in the context of reprogramming and neuronal injury, to further understand the multiple mechanisms of this protein. In fact, Uhrf1 has been reported to be upregulated in cortical injury (Bayam. 2014).

Our study has generated several interesting and important future directions. Firstly, the underlying mechanism of the adult cKO should be understood to elucidate if DNA methylation is impaired and which genes are transcriptionally altered. It would be important to look at 5hmC in this system and investigate if the Tet competition would exist here as well.

Secondly, additional experiments towards a better understanding of 5hmC and Tet/Uhrf1 interplay is quite crucial. 5hmC levels can be analysed in the Dnmt1 cKO of the cerebral cortex and of Uhrf1/Dnmt1 KO ESCs. Furthermore, next generation deep sequencing coupled with TABseq can be carried out to assess the exact levels of 5hmC in the Uhrf1 cortical cKO, especially on coding genes. Moreover, ChIP-seq experiments for Uhrf1 and Tet in this system would add relevant information on the binding sites of these proteins - which genes and transposable elements.

Thirdly, the implication of IAP activation on cellular processes can be studied more extensively. It would be useful to perform next generation sequencing of cKO DNA with high coverage to discover if IAP transcriptional activation can also lead to its transposition. Moreover, tools such

as CRISPR can be used to manipulate individual IAP elements and study the resulting phenotypes, if they lead to neurodegeneration for example.

In general, our study has enlightened the unique mechanisms of epigenetic players in neurogenesis. Further studies examining other epigenetic modifications and relevant proteins would provide us with important answers towards understanding the key molecular mechanisms of neurogenesis, which is crucial for steps towards neuronal repair.

6. Materials and Methods

6.1 Materials

6.1.1 Chemicals

Chemical	Company
Acetic Acid	Merck
Actinomycin D	Sigma
Acrylamide/Bis solution	Sigma
Agarose	Biozym
Ammonium persulfate (APS)	Thermo Fisher Scientific
Ampicillin	Roth
Aqua Poly / Mount	Polyscience Inc.
Corn oil	Sigma
Chloroform	Sigma
DAPI (4,6-dasmindino-2-phenylindol)	AppliChem
Difco LB-Agar	Hartenstein Labor.
DNA Ladder (Generuler 1kb)	Fermentas
EDTA	Merck
Ethanol	Merck
Fast Green	Sigma
Glycerol	Sigma
Glycine	Sigma
HEPES	Roth
Hydrochloric acid	Merck
Isopropanol	Merck
Methanol	Merck
Normal goat serum (NGS)	Vector Lab.

Orange G	Sigma
Paraformaldehyde (PFA)	Merck
PCR buffer (10X Taq Buffer)	Qiagen
PCR dNTP Mix (25mM each)	Fermentas
PCR reagent: MgCl ₂ (25mM)	Qiagen
Potassium chloride	Sigma
Potassium phosphate monobasic	Sigma
Potassium perruthanate	Sigma
Phenol:Chloroform:Isoamyl alcohol	Thermo Fisher Scientific
Pierce ECL western blotting substrate	Thermo Fisher Scientific
PMSF	Thermo Fisher Scientific
COmplete, Protease inhibitor cocktail	Roche
Proteinase K	Roth
Q solution	Qiagen
QIAzol	Invitrogen
RNase-free DNase	Qiagen
Sodium acetate	Sigma
Sodium chloride	Fisher Bioreagents
Sodium citrate	Merck
Sodium dodecyl sulphate (SDS)	Roth
Sodium phosphate monobasic	Sigma
Sodium phosphate dibasic	Sigma
Sodium hydroxide	Roth
SYBR green	Qiagen
SYBR safe DNA gel stain	Thermo Fisher Scientific
Tamoxifen	Sigma
Taq DNA Polymerase	Qiagen
TEMED	Sigma
Tissue Tek	Hartenstein Labor.
Tris Base	Sigma

Tris-HCl	Sigma
Trizma acetate	Sigma
Triton-X-100	Roth
Tween-20	Sigma

6.1.2 Tissue Culture Reagents

Chemical	Company
B-27 Serum-Free Supplement	Thermo Fisher Scientific
Cre recombinant protein	Synthesized by Arie Geerdof at the Helmholtz Zentrum
DMEM:F12 (Dulbecco's Modified Eagle Medium:Nutrient Mixture F12)+ GlutaMAX	Thermo Fisher Scientific
DMSO	Sigma
EGF (Epidermal Growth Factor)	Roche
FGF2 (Fibroblast Growth Factor-2)	Roche
HBSS 1X (Hank's balanced salt solution)	Thermo Fisher Scientific
HBSS 10X	Thermo Fisher Scientific
HEPES (1M)	Thermo Fisher Scientific
N2 supplement	Thermo Fisher Scientific
Penicillin/Streptomycin (Pen/Strep)	Thermo Fisher Scientific
Poly-D-Lysine (PDL)	Sigma
Poly L-Ornithine	Sigma

Trypan Blue	Thermo Fisher Scientific
Trypsin (EDTA), 0.05%	Thermo Fisher Scientific

6.1.3 Standard Solutions and Buffers

Phosphate Buffer Saline (PBS) (0.15M)

137 mM NaCl

27 mM KCl

83 mM Na₂HPO₄

15 mM KH₂PO₄

pH 7.4

Paraformaldehyde (PFA) 4%

To prepare 4% PFA, 40 g of PFA was dissolved in 800ml MilliQ water with gentle heating whilst stirring. 3 NaOH pellets were added to aid the PFA to go into solution and dissolve. The solution was cooled down to room temperature and HCl was added slowly till the pH dropped dramatically between pH 1-3. The pH was then adjusted to 7.2 -7.3 with 100 ml of 10X PBS and the solution was made upto 1 litre with MilliQ water. The solution was then filtered through a paper filter and stored at 4°C.

Lysis Buffer for tail DNA extraction

100mM Tris, pH8.0-8.5

200mM NaCl

5mM EDTA, pH8.0

2% SDS

50X TAE Buffer

2 M Tris Acetate

50 mM EDTA

Adjust pH 8.0 with Acetic Acid

Western blotting 1X Running Buffer

25 mM Tris-base

192 mM Glycine

0.1 % SDS

Western blotting 1X transfer buffer

192 mM Glycine

25 mM Tris-Base,

20 % Methanol

Nuclear/cytoplasmic protein extraction - Tween lysis buffer

25 mM Tris or Hepes,pH 8.0

20m mM NaCl

2 mM EDTA

1 mM phenylmethylsulfonyl fluoride (PMSF)

0.5% Tween 20

Add Roche protease inhibitor cocktail just before use

5hmeDIP - DNA Lysis buffer:

50mM tris pH 8.0

0.5% SDS

0.5mM EDTA pH 8.0

5hmeDIP - IP buffer

100mM sodium phosphate pH 7

1.4M NaCl

0.5% Triton X

5hmeDIP - 1M Sodium phosphate buffer

2M monobasic sodium phosphate

2M dibasic sodium phosphate

pH 7

5hmeDIP - TE (Tris-EDTA) buffer

10mM Tris-HCl pH 8.0

1mM EDTA pH 8.0

6.1.4 Cell Culture media

Dissection medium

Add 5 ml of HEPES 1 M (final concentration 10 mM) to 500 ml of HBSS 1X

NS cell proliferation medium

To DMEM F-12 media with Glutamax add 1% Penicillin/Streptomycin, B27 and N2 supplement.
Before use, add EGF and FGF.

6.1.5 Kits

Name	Company
RNeasy Mini Kit	Qiagen
Qiagen plasmid Maxi kit	Qiagen
Gel Extraction Kit	Qiagen
NEBNext Ultra Directional RNA library prep kit for Illumina	NEB
NEBNext Ultra DNA library prep kit for Illumina	NEB
NEBNext Multiplex oligos for Illumina	NEB
EZ DNA methylation-gold kit	Zymo research
DNeasy blood and tissue extraction kit	Qiagen
Picopure RNA isolation kit	Thermo Fisher scientific
EpiJET DNA methylation analysis kit	Thermo Fisher Scientific
Ribozero gold rRNA removal kit (Human/mouse/rat)	Illumina
SMARTer Stranded Total RNA Sample Prep Kit - Low Input Mammalian	Clontech
Ribogone – Mammalian kit	Clontech
Apoptag Red In Situ Apoptosis detection kit	Millipore

6.1.6 Antibodies**6.1.6.1 Primary Antibodies**

Antigen (species)	Working Dilution	Company
Anti-5mC (mIgG1)	1:1000	Millipore
Anti-5hmC (rabbit)	1:1000	Active motif
Anti- β - tubulin-III (mouse, IgG2b)	1:500	Sigma Aldrich
Anti-Ctip2 (rat)	1:200	Abcam
Anti-Gfap (rabbit)	1:200	DAKO
Anti-Gfap (mouse, IgG1)	1:200	Sigma
Anti-GFP (chicken)	1:800	Aves Labs
Anti-Histone H3 (rabbit)	1:1000	Abcam
Anti-IAP (rabbit)	1:1000	Kind gift from Dr. Cullen
Anti-Iba1 (rabbit)	1:500	Wako
Anti-Ki67 (rat)	1:200	Thermo Scientific
Anti-Ki67 (rabbit)	1:200	eBioscience
Anti-NeuN (mouse, IgG1)	1:100	Millipore
Anti-Olig2 (rabbit)	1:500	Millipore
Anti-Pax6 (rabbit)	1:200	Millipore
Anti-pH3 (rabbit)	1:500	Millipore
Anti –Tbr1 (rabbit)	1:200	Abcam
Anti –Tbr2 (rabbit)	1:200	Abcam

Anti Uhrf1 (rabbit)	1:1000	Kind gift from I.M. Bonapace
-----------------------	--------	---------------------------------

6.1.6.2 Secondary Antibodies

Antigen (species)	Working Dilution	Company
Anti rabbit Alexa488 ,546 ,633	1:1000	Invitrogen
Anti chick Alexa 488	1:1000	Invitrogen
Anti rat 488, 546	1:1000	Invitrogen
Anti-mouse IgG1 Alexa 488,546,633	1:1000	Invitrogen
Anti-mouse IgG2b Alexa546 , 633	1:1000	Invitrogen
Anti-guinea pig 633	1:1000	Thermo Fisher Scientific
Anti-rabbit, HRP	1:25,000	Thermo Fisher Scientific
Anti-mouse IgG, HRP	1:20,000	Thermo Fisher Scientific

6.1.7 Primers

6.1.7.1 Genotyping Primers

Name	Sequence 5'-3'
Glast for	GAGGCACTTGG TAGGCTCTG AGGA
Glast rev	GAGGAGATCCTGACCGATCAGTTGG
CER1(CreERT2 specific)	GGTGTACGGTCAGTAAATTGGACAT

Emx1 for	GTGAGTGCATGTGCCAGGCTTG
Emx1 rev	TGGGGTGAGGATAGTTGAGCGC
Cre	GCGGCATAACCAGTGAAACAGC
Uhrf1 for	ACCACATCACTCTTGATCTGTGCC
Uhrf1 rev	GGATGTTAGGTGTGAGCCACCATG
CAG for	CTG CTA ACC ATG TTC ATG CC
CAG rev	GGT ACA TTG AGC AAC TGA CTG

6.1.7.2 RT-qPCR Primers

Primer name	Sequence	Reference
IAP-5'UTR-F	CGGGTCGCGGTAATAAAGGT	(Rowe et al. 2010)
IAP-5'UTR-R	ACTCTCGTTCCCCAGCTGAA	
LINE-1-ORF1-F	GAACCAAGACCACTCACCATCA	(Vitullo et al. 2012)
LINE-1-ORF1-R	CCCTGGACTGGGCGAAGT	
SINE-B1-F	TGGCGCACGCCTTTAATC	(Gualtieri et al. 2013)
SINE-B1-R	TGGCCTCGAACTCAGAATCC	
Uhrf1-F	AAACGCCCTGAGTTTTTCGC	Designed in this work
Uhrf1-R	GCCGATGTA CTCTCTCACG	
Gapdh - F	ATTCAACGGCACAGTCAAGG	Designed in our lab
Gapdh - R	TGGATGCAGGGATGATGTTC	

6.1.7.3 Bisulfite sequencing primers

Primer name	Sequence	Reference
IAP-Gag-F	AGGTTAGTTTGTGATTGGTTTTAG	(Sadic et al. 2015)
IAP-Gag-R	AATCAACAAAATAAACTCCCTAACC	
LINE-1-F	GTTAGAGGATTTGATAGTTTTTGG AATAGG	(Tommasi et al. 2012)
LINE-1-R	CCAAAACAAAACCTTTCTCAAACACTATAT	

6.1.7.4 CHIP primers

Primer name	Sequence	Reference
Polrmt-F	TCAGCAAACCTCCAATAGCGCAC	(Bilodeau et al. 2009)
Polrmt-R	TTGCCGCACAACATGGACTT	
Gapdh-F	CTCTGCTCCTCCCTGTTCC	(Jörg Tost 2009)
Gapdh-R	TCCCTAGACCCGTACAGTGC	
LINE - 1 ORF2-F	TTTGGGACACAATGAAAGCA	Designed in Schotta lab
LINE - 1 ORF2-R	CTGCCGTCTACTCCTCTTGG	
SINE-B1-F	GTGGCGCACGCCTTTAATC	Designed in Schotta lab
SINE-B1-R	GACAGGGTTTCTCTGTGTAG	
IAP-5'UTR-F	CGGGTCGCGGTAATAAAGGT	(Rowe et al. 2010)
IAP-5'UTR-R	ACTCTCGTTCCCCAGCTGAA	

6.1.8 Constructs

The Tet2, Tet3 and Scrambled shRNA constructs were kindly provided by Dr. Qiang Lu at the Beckmann Research Institute (USA) (Hahn et al. 2013)

6.2 Methods

6.2.1 In vivo Methods

6.2.1.1 Mouse lines

All the animals used for the experiments were kept at the in the animal facility of the Helmholtz Zentrum München on a 12h light-dark cycle. All the animal procedures were performed in accordance with German and European Union guidelines. Adult animals were used at the age of 2-3 months and embryonic animals were used at the indicated embryonic day where day of vaginal plug was considered to be embryonic day 0 (E0)

Strain	Characteristics	Producer
Emx1Cre	This line expresses Cre recombinase from the endogenous <i>Emx1</i> locus.	Iwasato et al.2000
CAG CAT eGFP	The CAG CAT GFP reporter line contained CMV- β actin promoter and loxP flanked CAT gene upstream of the enhanced green fluorescent protein (eGFP) cassette. With Cre excision, the GFP is expressed.	Nakamura et al 2006
GlastCreERT2	The GLAST::CreERT2 mouse line contains the inducible form of Cre (CreERT2) in the astrocyte specific glutamate transporter (GLAST) locus. In this line, Cre is fused to the ligand binding domain of the modified estrogen receptor (ERT2), thus it is restricted to the cytoplasm. Upon Tamoxifen induction,	Mori et al 2006

	the Cre can translocate to the nucleus and carry out excision and recombination.	
Uhrf1 ^{tm1a(EUCOMM)Wtsi}	The Uhrf1 ^{tm1a(EUCOMM)Wtsi} mouse line was generated by EUCOMM by using promoterless targeting cassettes for the generation of knockout-first alleles (Skarnes et al., 2011). A critical exon is identified such that when it is deleted, a frame shift mutation is created which in turn causes nonsense mediated decay of the corresponding transcript. The exon chosen is common to all transcript variants of that gene.	EUCOMM

6.2.1.2 Anesthesia and Perfusion

For perfusion, animals were anesthetized by intraperitoneal injection of Ketamin (Ketaminhydrochlorid, 100mg per kg of body weight) and Rompun (Xylazinhydrochlorid, 20mg per kg of body weight) prepared in 0,9 % NaCl solution (Braun). Then they were transcardially perfused first with a preflush of PBS followed by 4 % PFA in PBS. The brains were then removed and post fixed in 4 % PFA overnight.

6.2.1.3 In utero electroporation

Animals were operated as approved by the Government of Upper Bavaria. E13.5 timed pregnant mice were anaesthetized by intra-peritoneal (i.p.) injection of Fentanyl (0.05mg/kg), Midazolam (5mg/kg) and Medetomidine (0.5mg/kg). Plasmids used were Scrambled, Tet2 and Tet3 shRNA kindly provided by Professor Qiang Lu at the Beckmann research institute, USA (Hahn et al. 2013). In utero electroporation was done as described earlier (Saito, 2006). Briefly, pregnant mice were anesthetized placed on heated pads to keep warm. The shaved abdomen was opened to expose the uterine horns, which were kept moist by pre-warmed saline. Plasmids were mixed with Fast Green (2.5mg/μl, Sigma) and injected at a concentration of 1 μg/μl into the ventricles of the embryos, using glass capillaries. An electrical pulse was applied to direct the DNA towards the dorsal telencephalon, 4 pulses of 33mV and 100ms. The embryos were replaced into the

uterus which is then sewn together using surgical sutures. Anesthesia was terminated by subcutaneous injection of Buprenorphine (0.1mg/kg), Atipamezol (2.5mg/kg), Flumazenil (0.5mg/kg) and the animals were monitored as they woke up. At E16, the pregnant mother was sacrificed and the embryos were obtained for further analysis.

6.2.1.4 Tamoxifen Treatment

Tamoxifen was dissolved in pre-warmed corn oil at a concentration of 20mg/ml by sonicating it for 15 min. 50µl of tamoxifen was injected intraperitoneally twice a day for 5 consecutive days to achieve efficient recombination in mice carrying the *Glast*^{CreERT2} allele. Tamoxifen was stored at 4°C for a maximum time of 1 month to avoid precipitation.

6.2.2 Methods in Cell Biology

6.2.2.1 Dissection

Embryos harvested from pregnant mothers or postnatal pups which had been perfused were dissected for the brain. The embryonic brains were fixed either for 2 hours (E12), 3 hours (E14), 4 hours (E16) or overnight (E18 or postnatal) in 4% PFA. Brains dissected from perfused pups were post-fixed for 1 hour in 4% PFA. Following fixation, the brains were washed 2 times in PBS.

For RNA and DNA extraction, cerebral cortices were dissected from embryonic and postnatal brains. For the E16 germinal zones RNAseq, the cerebral cortex was further dissected for the germinal zones by first sectioning with the tissue chopper at 300µm thickness. These slices were then cut into half with the lower part being considered as the germinal zones. For RNA, the tissue was dissolved in QIAzol and for DNA the tissue was snap frozen in liquid nitrogen.

6.2.2.2 Tissue Preparation

For embryonic and postnatal stages, the brains were sliced using a cryostat. First the brains were cryoprotected in 30% sucrose/PBS solution overnight and then embedded in Tissue-Tek and snap-frozen in dry ice. The frozen brains were then sectioned at a thickness of 14µm using a cryostat and collected on Superfrost glass slides. The slides were kept at -20°C until immunohistochemical analyses.

For postnatal and adult stages, the brains were sectioned with a vibratome. The brains were embedded in 4% agarose prepared in PBS and cut at a thickness of 70µm. The sections were stored in PBS.

6.2.2.3 Immunostaining

Cryosection and free-floating sections were immunostained using the same protocol as follows. Sections were first incubated in a solution of 0.1% Triton-X-100, 10% NGS in 0.1M PBS for 30 minutes as a blocking step. Following this, they were incubated overnight at 4°C with primary antibodies diluted in the blocking solution. Primary antibodies used are listed below in the table. The next day, sections were washed 3 times in PBS and incubated with secondary antibodies (conjugated to a fluorophore and DAPI (4', 6' Diamidino-2-phenylindole) to visualize the nucleus, for 1.5 hours. The secondary antibodies and DAPI were also diluted in the blocking solution. The sections were again washed 3 times with PBS and mounted with Aqua Polymount.

For certain antigen, additional steps were required to retrieve and unmask it prior to antibody incubation. To retrieve the Ctip2 and Ki67 antigens, the sections were boiled for 2-5 min in a microwave in 0.01M sodium citrate buffer and then rinsed in PBS a few times before incubation with the primary antibody. In the case of floating section, the sections were first mounted on slides prior to antigen retrieval. In the case of 5mC and 5hmC staining, the section needed to first be denatured with HCl. Thus, sections were first incubated with 2N HCl for 30 minutes followed by 2 washes of 15 minutes with 100mM Tris-HCl buffer with pH 8.0.

6.2.2.4 Fluorescence Activated Cell Sorting (FACS)

Cortices from the electroporated E16 embryos were isolated and the midline and meninges were removed. The tissue was then enzymatically dissociated using 0.05% Trypsin for 15 minutes at 37°C and resuspended in DMEM containing 10% fetal calf serum (FCS). The dissociated cells were then washed with PBS twice and filtered prior to analysis on the FACSAriaIII (BD bioscience). Gating parameters were determined by side and forward scatter to eliminate debris (P1 gate) and any aggregated cells (P2 gate). For isolation of GFP+ cells, the positive gate was set using non-electroporated tissue and set to include a maximum 0.1% of non-fluorescent cells. GFP+ve and GFP-ve cells were isolated using the purity mode and directly sorted into PBS.

For isolation of subpopulations (neural stem cells and neurons) at E14, the samples were first incubated with APC-conjugated Prominin-1 antibody (CD133, eBioscience) and PE-conjugated PSA-NCAM antibody (Miltenyi Biotec). Additionally, a PE- and APC conjugated isotype control (eBioscience, Miltenyi Biotec) was used to set the positive gate for the stained populations. The cells were also isolated using the purity mode and into PBS and RLT buffer from the Qiagen micro RNeasy kit.

6.2.3 Methods in Molecular Biology

6.2.3.1 DNA Extraction from tail or ear

To identify the genotype of animals, mice were genotyped by using DNA extracted from the tail or ear. The biopsies were incubated in 0.5ml DNA lysis buffer at 55 °C overnight or for 2 hours with shaking. After lysis, the debris was removed by centrifugation in at maximum speed for 10 min. The supernatant containing DNA was precipitated using 0.5ml and centrifuged for 20min. The pellet was finally washed with 70% ethanol for 5 min and completely dried at room temperature. Finally, the DNA was eluted in 250µl double distilled H₂O.

6.2.3.2 Transformation of the competent bacteria

Competent E.coli cells were used for the transformation of plasmid DNA. The cells were first thawed on ice and then about 100-500ng of DNA was added to the cells and incubated for 15 min on ice. The mixture was heat shocked for 30 sec at 42°C and immediately placed on ice for 5 min. 250µl of pre-warmed LB medium was added to the transformation reaction mixture and the cells were then allowed to recover for 1 hour at 37°C with shaking. Finally, the cells were plated on LB-ampicillin plates and incubated overnight at 37°C.

6.2.3.3 Bacterial liquid cultures

For small-scale plasmid DNA preparation, transformed colonies of bacteria were inoculated in 5ml of LB-ampicillin and incubated overnight at 37°C. For large scale preparations, 1ml of the 5ml media was inoculated into 100ml of LB medium supplemented with ampicillin and incubated at 37 °C with shaking.

6.2.3.4 DNA extraction from plasmids

Plasmid DNA from 5ml bacterial cultures was extracted using the Qiagen miniprep kit and plasmid DNA from 100ml cultures was extracted using the Qiagen Maxiprep kit according to manufacturer's protocols.

6.2.3.5 Determination of the concentration and quality of nucleic acids

The concentrations of nucleic acids were determined using the Nanodrop, which is a spectrophotometer that can measure the concentration of nucleic acids. Samples which had a 260/280 ratio of between 1.8-2 were considered of good quality.

The quality of RNA for RNAseq was further analyzed using the Agilent Bioanalyzer. Agilent Bioanalyzer can accurately measure ribosomal 18S, and 28S RNAs. It can then assign a RNA Integrity Number (RIN) that ranges from 1 (reflecting totally degraded RNA) to 10 (reflecting completely intact RNA). For RNAseq only high quality RNA (RIN > 8) samples were used. The bioanalyzer was also used to check the RNAseq and hmeDIPseq DNA library sizes.

6.2.3.6 RNA extraction, cDNA synthesis and qPCR

Total RNA was isolated using the Qiagen RNeasy kit for all qRT-PCR experiments using the manufacturer's protocol, except the FACS sorted cells. In the case of FACS sorted cells, PicoPure RNA isolation kit from Thermo Scientific was used to extract RNA per the manufacturer's protocol. cDNA synthesis was performed using random primers with the Maxima first strand synthesis kit (Thermo Scientific). Real-time qPCR was conducted using SYBR green and the Thermo Fisher Quant Studio 6 machine. qRT-PCR primers are listed in the primer's section. Gapdh was used as a housekeeping gene.

6.2.3.7 RNAseq - E16 ventricular zone

Total RNA was extracted using QIAzol and the RNA clean and concentrator - 25 kit (Zymo Research) per the manufacturer's protocol. Ribosomal RNA was depleted using the Ribogone mammalian kit from Clontech and the corresponding protocol. RNAseq libraries were prepared using SMARTer Stranded RNA-Seq Kit from Clontech for RNA concentrations between 10-100ng

per the kit protocol. Finally, quality control was carried out with a Bioanalyzer (Agilent) and 100bp paired end sequencing with a HiSeq sequencer (Illumina) at LAFUGA (Gene Center, Munich). 3 biological replicates were used per genotype.

6.2.3.8 RNAseq for E16 full cortex and P5

Cerebral cortices were dissected from E16 embryos and postnatal day 5 pups. Total RNA was extracted using QIAzol and the RNA clean and concentrator – 25 kit (Zymo Research). Ribosomal RNA was depleted using the Ribozero gold kit for human/mouse/rat (Illumina) and the RNA clean and concentrator – 5 kit. Libraries were prepared using the NEBNext Ultra Directional RNA Library Prep Kit and the manufacturer's protocol. Quality control was assessed with a Bioanalyzer (Agilent) and 100bp paired end sequencing was performed on a HiSeq sequencer (Illumina) at LAFUGA (Gene center, Munich, Germany). For P5 datasets, 3 biological replicates were used per genotype. For E16 full cortex, 2 biological replicates were used for cKO and 3 for controls.

6.2.3.9 Oxidative Reduced Representation Bisulfite Sequencing

Genomic DNA was extracted from the cerebral cortices of E16 controls and cKO using the DNeasy blood and tissue kit (Qiagen). 1 µg of mouse from each sample was first digested with MspI enzyme (NEB) at 37°C overnight. MspI enzyme digestion is enriched at CpG sites in the genome. The digested DNA was cleaned up with the MinElute Reaction Cleanup Kit (Qiagen) per the manufacturer's instructions. Following this step, 500 ng of digested and purified DNA was used for preparing libraries with the NEXTflex™ Bisulfite Library Prep Kit (BIOO Scientific), per the manufacturer's instructions with some modifications. To obtain an accurate analysis of 5mC and avoid false positives, we included a DNA oxidation step to account for the 5hmC. This oxidation step converts 5hmC to 5fmC but does not affect 5mC. Oxidation was performed with KRuO₄ (Sigma-Aldrich) according to published data (Booth et al. 2012). The bisulfite conversion of DNA was performed using the EZ Methylation Gold Kit (Zymo Research), following the manufacturer's protocol. The libraries were purified using AMPure XP beads (Beckmann Coulter) and PCR amplification of the libraries was performed to assess positive and negative controls, with PfuC_x Hot Start (Agilent). Finally, quality control with a Bioanalyzer (Agilent) was carried out and next-generation sequencing with a HiSeq 1000 sequencer (Illumina Inc.) at a genomics core facility: Center of Excellence for Fluorescent Bioanalytics (KFB, University of Regensburg, Germany).

6.2.3.10 Oxidative Bisulfite sequencing

Genomic DNA was extracted from E16 cortical tissue from controls and Uhrf1 cKO and Uhrf1 floxed NS cells uninduced and induced with Cre protein, using the DNeasy blood and tissue kit (Qiagen). Oxidation and bisulfite conversion was performed as described in the above Ox-RRBS method. Loci specific PCR was performed on a 500bp region of IAP Gag and a 200bp region of LINE-1 (list of primers in the primers section of materials). The amplicons were adapter tagged using NEBNext Multiplex Oligos for Illumina (New England Biolabs). Briefly, 100-200 ng of amplicon and 62.5 pmol each of universal PCR primer and index primer were amplified in a total volume of 50 μ L with NEBNext High-Fidelity PCR Master Mix (New England Biolabs) and the cycling conditions were 98°C/30"-[98°C/10"-65°C/30"-72°C/30"]x4-72°C/5'. PCR reactions were purified by using 80% (v/v) CleanPCR magnetic beads (GC biotech) and finally eluted using 25 μ L of water. In order to make all the fragments double stranded, a single round of amplification with P5 and P7 primers (Illumina) was added. To this end, 20 μ L of the purified tagged amplicons and 25 pmol each of P5 and P7 primers were set up in a total reaction volume of 50 μ L with Phusion Polymerase (New England Biolabs) according to the manufacturer's instructions. The PCR program used was 98°C/2'-60°C/1'-72°C/10'. Purification was the same as mentioned earlier with magnetic beads. Libraries were checked for quality control and correct fragment length on a Bioanalyzer 2100 (Agilent) and concentrations were determined with Qubit dsDNA HS Assay Kit (Life Technologies). Final sequencing was carried out on a MiSeq sequencer (2x300 bp paired end) with v3 chemistry (Illumina) at the Genomics Service Unit at LMU Biocenter. Primary sequencing reads were merged using CLC Genomics Workbench 9.0.1 (Qiagen) according to the following parameters: mismatch cost = 2; minimum score = 8; gap cost = 3; maximum unaligned end mismatches = 0.

6.2.3.11 Hydroxy methylated DNA immunoprecipitation (hmeDIP)

The germinal zones of cerebral cortices of E16 controls and cKO were dissected according the E16 GZ RNAseq workflow. Genomic DNA was then extracted as follows. The tissue was lysed using the gDNA lysis buffer (Tris, 0.5% SDS, EDTA). Following this, proteinase K was added to the samples and incubated for 2 hours. The gDNA was extracted using 2 rounds of phenol:chloroform: isoamyl alcohol extraction and 2 rounds of chloroform extraction to obtain the

aqueous phase everytime. This phase was precipitated with glycogen, 3M Sodium acetate and 100% ethanol. The pellet was purified with 70% ethanol and eluted in DNAase free water.

The protocol for hmeDIP was adapted from chapter 5 of book 'DNA methylation:Methods and Protocols, second edition volume 507, 2009 – Fabio Mohn, Micheal Weber, Dirk Schubeler and Tim-Christoph Roloff (Tost. 2009) and from (Maunakea et al. 2010). Chromatin was sheared using the Covaris machine and assessed using the Bioanalyzer (Agilent). For the immunoprecipitation, 1ug of gDNA was used per sample. Briefly, the gDNA was denatured at 95°C and incubated overnight with the primary antibody, rotating at 4°C. The antibody bound sample was incubated with prewashed dynabeads for 2 hours at 4°C, rotating. The supernatant was washed 5 times with IP buffer, and eluted in the TE buffer. The sample was then de-crosslinked overnight at 55°C with proteinase K and finally purified with Qiagen PCR purification kit. The antibodies used for immunoprecipitation were 5mC (Millipore) and 5hmC (Active motif). DNA libraries were generated using the NEBNext Ultra DNA library preparation kit for Illumina. Quality control was carried out with a Bioanalyzer (Agilent) and 50bp single end sequencing with a HiSeq sequencer (Illumina) at LAFUGA. N= 3-4 embryos for each genotype. The samples were pooled to obtain one sample per genotyped which was immunoprecipitated and sequenced.

6.2.3.12 Genotyping by Polymearse Chain Reaction (PCR)

Reaction mix	2.5 µl 10x buffer
	5µl Q-Solution (Qiagen)
	0.5µl dNTPs,
	1µl each Primer
	0.2µl Taq Polymerase
	1 µl DNA
	upto 25µl with H ₂ O

Emx1-Cre mice

The genotyping protocol of the Emx1::Cre mice was adapted from (Iwasato et al. 2000).

	<u>94°C</u>	<u>2 min</u>	
	94°C	30 sec	Band size : WT 200bp ; transgenic 500bp
35X	65°C	1 min	
	<u>72°C</u>	<u>30 sec</u>	
	72°C	10 min	

CAG CAT eGFP mice

The genotyping protocol of the CAG CAT eGFP mice was adapted from (Nakamura et al. 2006).

	<u>94°C</u>	<u>5 min</u>	
	94°C	30 sec	Band size : 350bp
29X	55°C	30 sec	
	<u>72°C</u>	<u>1 min</u>	
	72°C	10 min	

GlastCreERT2 mice

The genotyping protocol of the Glast::CreERT2 mice was adapted from (Mori et al. 2006)

	<u>94°C</u>	<u>2 min</u>	
	94°C	20 sec	Band size: WT 700 bp; Recombinant 400 bp
35X	55°C	20 sec	
	<u>72°C</u>	<u>30 sec</u>	
	72°C	5 min	

6.2.3.12.4 Uhf flox / flox mice

The genotyping protocol was established according to the protocol received from EUCOMM

	<u>95C</u>	<u>5min</u>	
	94°C	30 sec	Band size: WT = 331bp ; Recombinant = 523 bp
39 X	65°C	45 sec	
	<u>72°C</u>	<u>45sec</u>	
	72°C	10 min	

6.2.3.13 Gel Electrophoresis

The percentage of the agarose gel depends on the size of the nucleic acid of interest. The appropriate amount of agarose was dissolved in 1X TAE buffer by boiling in a microwave to obtain a 1% or 0.5% gel. After slight cooling, SYBR safe DNA stain was added in the concentration of 1:25,000 and the gel was poured into a prepared gel chamber. Once the gel solidified, DNA or RNA samples mixed with 6X loading dye and loaded into the wells, alongwith a 1kb DNA ladder. Electrophoresis was performed between 70-100V.

For the Ox-BS experiments the DNA fragments with the right size were excised using UV light (254 nm) and purified using the QIAquick gel extraction kit (Qiagen), according to the manufacturer's protocol.

6.2.3.14 Western blotting and mass spectrometry

Protein was extracted from E16 cerebral cortices of controls and cKO as follows. The tissue pellet was resuspended in 200-300 microlitres of Tween 20 lysis buffer, placed on ice for 30 minutes and pelleted at 2500 rpm. The supernatant was collected as the cytoplasmic fraction. The pellet was washed with Tween 20 lysis buffer with 500mM NaCl twice and resuspended in 100 microlitres of this solution. The sample was sonicated for a few seconds at low intensity. The sample was incubated on ice for 15 minutes and another 100 microlitres of tween 20 lysis buffer

without NaCl was added. The sample was centrifuged at 10,000g for 15 minutes at 4°C and the supernatant was recovered as the nuclear fraction.

Protein was quantified using the Pierce BCA protein assay kit. Western blot was performed by first running the proteins on a 10% Bis-acrylamide gel (30 % (w/v) Acrylamide/Bis Solution, 20 % (w/v) SDS, 10 % (w/v) APS and TEMED) with a separation gel buffer (1.5 M Tris/HCl, pH 8.8) and stacking gel buffer (0.5 M Tris/HCl, pH 6.8) on a Mini Protean Tetra System and transferred into nitrocellulose membranes using the 1X transfer buffer. The blotted membranes were washed with 0.5% Tween 20/PBS (TBST) and blocked for 30 minutes with 5% milk/TBST. The primary antibodies were incubated overnight at 4°C and washed 3 times with TBST. Following secondary antibody incubation, the membranes were visualized using the ECL substrate. The protein samples for mass spectrometry were analysed at the Proteomics Unit at the Helmholtz Zentrum Munich. Further analysis was performed using the Scaffold software.

6.2.3.15 Methylation digests

Genomic DNA was extracted from E16 cerebral cortices using the extraction method for 5hmeDIP. 500ng of DNA was digested with HpaII and MspI using the EpiJET DNA methylation kit according to the manufacturer's protocol. The digested DNA was run on a 0.5% agarose gel.

6.2.4 Data Analysis

6.2.4.1 Bioinformatic analyses

RNA-seq

RNA-seq reads (100bp paired-end) were mapped to the mouse genome (mm10) using tophat2 (Kim et al. 2013), resulting in alignments with minimal mismatches. The resulting BAM files were filtered to allow only reads in a proper pair and to remove reads with multiple mapping in the genome as well as duplicated reads and low quality alignments using samtools (-F 2 -f 1280). Expression of genes in FPKM was calculated with cuffdiff and cummerbund (Trapnell et al. 2013). Regulated genes were selected based on the cufflinks p-value ($p < 0.05$) and change in expression (> 2 fold). Genes indicated as derepressed were selected based on very low expression in control (FPKM < 0.1) and higher expression in cKO (FPKM > 0.1). Dot plots were generated with ggplot2. Gene set enrichment analysis of differentially expressed genes was performed as described (Mootha et al. 2003; Subramanian et al. 2005).

For expression analysis of individual repeat elements, filtered BAM files were converted to homer tag directories using makeTagDirectory. For individual IAP elements, the genomic positions were extracted from the rmsk dataset (UCSC). The coverage across repeat families and individual repeats was analyzed using analyzeRepeats (Heinz et al. 2010).

Genes which might be regulated by activated IAP elements were identified by (1) selecting the upregulated genes (fold change > 2); and (2) testing for activated IAP elements within a certain distance of upregulated genes (+/- 50.000 bp).

Hydroxy-meDIP

Hydroxy-MeDIP reads (50bp single end) were mapped to the mouse genome (mm10) using bowtie with options -q -n 2 --best. These resulting SAM files were converted to homer tag directories using makeTagDirectory (Heinz et al. 2010). The cumulative IAP coverage plots depicted were generated as in (Sadic et al. 2015).

Oxidative Reduced Representation Bisulfite Sequencing

All reads generated were mapped to the mouse genome version GRCm38 with the commercially available Genomatix software (version 2.2.2 Genomatix) allowing no mismatch in sequence. For analysis of the control sequences and the cKO status, a custom mapping library with the methylated and unmethylated DNA sequences of the PCR products and vector was generated. The methylation status per CpG or CpH was extracted, positions with a coverage = < 5 were excluded. Data analysis was then performed with custom scripts using the free software R ver. 3.1.1 and the package methylkit (Akalin et al. 2012). For the analysis of differentially methylated regions, the region length was set to 100 bp in length.

Genomatix was used to predict promoter regions that were used for the differential methylation analysis.

Oxidative Bisulfite sequencing

All reads generated were filtered for size (490bp to 510bp for IAP and 250-270bp for LINE-1) using Perl. 300 independent PCR products were subsampled for each genotype and analysed with QUMA software for their methylation status per CpG. % of 5hmC was inferred from the difference between oxidized and unoxidised samples, within each genotype.

6.2.4.2 Data analysis of immunostainings and qRT-PCR

In vivo stainings were analyzed at an Olympus FV1000 laser-scanning confocal microscope. In vitro stainings were analyzed on a Zeiss epifluorescence microscope.

All error bars are presented as standard errors of the mean (\pm SEM). Statistical significance was tested using the Mann-Whitney test for immunostainings and Annexin assay.

For immunostaining experiments without quantifications, a minimum of 3 embryos/animals per genotype was analyzed.

For all qRT-PCR experiments, data was analysed with a unpaired t-test, except in the Tet knockdown experiments wherein a paired t-test was used. All 'n' refers to individual embryos or animals.

7. Abbreviations

%	Percent
°C	Degree Celsius
µg	Microgram(s)
µl	Microlitre(s)
µM	Micromolar
5mC	5-methyl cytosine
5hmC	5-hydroxy methyl cytosine
5CaC	5-carboxyl methyl cytosine
5fC	5-formyl methyl cytosine
aNSCs	Adult neural stem cells
AP	Apical Progenitor
bHLH	Basic helix-loop-helix
BP	Basal Progenitor
Bp	Base pairs
CC	Corpus callosum
cDNA	Complementary Deoxyribonucleic Acid
cKO	Conditional knock out
CNS	Central Nervous System
Ctx	Cortex
CP	Cortical plate
Cux1	Cut-Like homeobox 1
DAPI	4',6-diamidino-2-phenylindole

dATP	DeoxyAdenosine TriPhosphate
dCTP	DeoxyCytidine TriPhosphate
Dcx	Doublecortin
DG	Dentate Gyrus
dGTP	DeoxyGuanosine TriPhosphate
Dnmt	DNA methyltransferase
DMEM	Dulbecco's Modified Eagle Medium
DNA	Deoxyribonucleic Acid
dNTP	DeoxyNucleoside TriPhosphate
dTTP	DeoxyThymidine TriPhosphate
dpi	days post-induction
E	Embryonic Day
e.g.	For example (Latin 'exempli gratia')
EDTA	Ethylene-Diamine-tetra-Acetic-Acid
EGF	Epidermal Growth Factor
Emx1/2	Empty spiracles homeobox 1/2
ERV	Endogeneous retroviral elements
FCS	Fetal Calf Serum
FDR	False discovery rate
FPKM	Fragment Per Kilobase of transcript per Million mapped reads
FGF	Fibroblast growth factor
FSC-A	Forward scatter-area
FSC-W	Forward scatter- width
G	Gram

GAPDH	GlycerAldehyde 3-Phosphate DeHydrogenase
GE	Ganglionic Eminence
GFAP	Glial Fibrillary Acidic Protein
GFP	Green Fluorescent Protein
GLAST	Glutamate Aspartate Transporter
H	Hour(s)
HBSS	Hank's balanced salt solution
HCl	Hydrochloric acid
HDAC1	Histone deactylase 1
HEPES	4-(2-Hydroxyethyl)-1-piperazineethanesulfonic acid
het	heterozygous
IAP	Intracisternal A-Particle
Kb	Kilobase
kDa	Kilodalton
Kg	Kilogram(s)
L	Litre
LB	Luria-Bertani medium
LGE	Lateral Ganglionic Eminence
MGE	Medial Ganglionic Eminence
Min	Minute
mM	Millimolar
mRNA	Messenger Ribonucleic Acid
NaCl	Sodium Chloride
Ng	Nanogram(s)

OB	Olfactory Bulb
Olig2	Oligodendrocyte transcription factor2
OPCs	Oligodendrocyte progenitor cells
P	Postnatal day
Pax6	Paired box 6
PBS	Phosphate Buffered Saline
PCR	Polymerase Chain Reaction
P/S	Penicillin/Streptomycin
PFA	Paraformaldehyde
PH3	Phospho-Histone 3
PHD	Plant Homeodomain
qPCR	Quantitative Polymerase Chain Reaction
RG	Radial Glia
RIN	RNA integrity number
RING	Really Interesting New Gene
RMS	Rostral Migratory Stream
RNA	Ribonucleic Acid
rpm	Revolutions per minute
RPKM	Reads Per Kilobase of transcript per Million mapped reads
RT	Room Temperature
Sec	Seconds
SDS	Sodium dodecyl sulphate
SEM	Standard Error of the Mean
SEZ	Subependymal Zone

Abbreviations

SP	Subapical Progenitor
SVZ	Subventricular Zone
TAE	Tris Acetate EDTA
Taq	DNA polymerase of bacterium <i>Thermus aquaticus</i>
Tbr	T-box brain
Tet	Ten-eleven-translocase
TF	Transcription factor
TTD	Tandem Tudor Domain
TUNEL	Terminal deoxynucleotidyl transferase (TdT) dUTP Nick-End Labeling
U	Enzyme unit
Uhrf1	Ubiquitin-like, containing PHD and RING finger domains, 1
VZ	Ventricular Zone
w/v	Weight/Volume
WT	Wild Type

8. References

- Achour M, Fuhrmann G, Alhosin M, Ronde P, Chataigneau T, Mousli M, Schini-Kerth VB, Bronner C. 2009. UHRF1 recruits the histone acetyltransferase Tip60 and controls its expression and activity. *Biochem Biophys Res Commun* 390: 523-528.
- Aguirre A, Dupree JL, Mangin JM, Gallo V. 2007. A functional role for EGFR signaling in myelination and remyelination. *Nat Neurosci* 10: 990-1002.
- Akalin A, Kormaksson M, Li S, Garrett-Bakelman FE, Figueroa ME, Melnick A, Mason CE. 2012. methylKit: a comprehensive R package for the analysis of genome-wide DNA methylation profiles. *Genome Biol* 13: R87.
- Alhosin M, Sharif T, Mousli M, Etienne-Selloum N, Fuhrmann G, Schini-Kerth VB, Bronner C. 2011. Down-regulation of UHRF1, associated with re-expression of tumor suppressor genes, is a common feature of natural compounds exhibiting anti-cancer properties. *J Exp Clin Cancer Res* 30: 41.
- Arima Y, Hirota T, Bronner C, Mousli M, Fujiwara T, Niwa S, Ishikawa H, Saya H. 2004. Down-regulation of nuclear protein ICBP90 by p53/p21Cip1/WAF1-dependent DNA-damage checkpoint signals contributes to cell cycle arrest at G1/S transition. *Genes Cells* 9: 131-142.
- Arita K, Ariyoshi M, Tochio H, Nakamura Y, Shirakawa M. 2008. Recognition of hemimethylated DNA by the SRA protein UHRF1 by a base-flipping mechanism. *Nature* 455: 818-821.
- Babbio F, Pistore C, Curti L, Castiglioni I, Kunderfranco P, Brino L, Oudet P, Seiler R, Thalman GN, Roggero E et al. 2012. The SRA protein UHRF1 promotes epigenetic crosstalks and is involved in prostate cancer progression. *Oncogene* 31: 4878-4887.
- Barau J, Teissandier A, Zamudio N, Roy S, Nalesso V, Herault Y, Guillou F, Bourc'his D. 2016. The DNA methyltransferase Dnmt3C protects male germ cells from transposon activity. *Science* 354: 909-912.
- Barbot W, Dupressoir A, Lazar V, Heidmann T. 2002. Epigenetic regulation of an IAP retrotransposon in the aging mouse: progressive demethylation and de-silencing of the element by its repetitive induction. *Nucleic Acids Res* 30: 2365-2373.
- Barry DS, Pakan JM, McDermott KW. 2014. Radial glial cells: key organisers in CNS development. *Int J Biochem Cell Biol* 46: 76-79.

- Barski A, Cuddapah S, Cui K, Roh TY, Schones DE, Wang Z, Wei G, Chepelev I, Zhao K. 2007. High-resolution profiling of histone methylations in the human genome. *Cell* 129: 823-837.
- Bayam, Efil. Transcriptome analysis of adult neural stem cells and functional analysis of novel candidate genes TSP-4 and Uhrf1 (2014) (Doctoral dissertation)
- Beckervordersandforth R, Tripathi P, Ninkovic J, Bayam E, Lepier A, Stempfhuber B, Kirchhoff F, Hirrlinger J, Haslinger A, Lie DC et al. 2010. In vivo fate mapping and expression analysis reveals molecular hallmarks of prospectively isolated adult neural stem cells. *Cell Stem Cell* 7: 744-758.
- Belgnaoui SM, Gosden RG, Semmes OJ, Haoudi A. 2006. Human LINE-1 retrotransposon induces DNA damage and apoptosis in cancer cells. *Cancer Cell Int* 6: 13.
- Belluzzi O, Benedusi M, Ackman J, LoTurco JJ. 2003. Electrophysiological differentiation of new neurons in the olfactory bulb. *J Neurosci* 23: 10411-10418.
- Benevolenskaya EV. 2007. Histone H3K4 demethylases are essential in development and differentiation. *Biochem Cell Biol* 85: 435-443.
- Berkyurek AC, Suetake I, Arita K, Takeshita K, Nakagawa A, Shirakawa M, Tajima S. 2014. The DNA methyltransferase Dnmt1 directly interacts with the SET and RING finger-associated (SRA) domain of the multifunctional protein Uhrf1 to facilitate accession of the catalytic center to hemi-methylated DNA. *J Biol Chem* 289: 379-386.
- Bilodeau S, Kagey MH, Frampton GM, Rahl PB, Young RA. 2009. SetDB1 contributes to repression of genes encoding developmental regulators and maintenance of ES cell state. *Genes Dev* 23: 2484-2489.
- Bird A. 1992. The essentials of DNA methylation. *Cell* 70: 5-8.-. 1999. DNA methylation de novo. *Science* 286: 2287-2288.
- Bonapace IM, Latella L, Papait R, Nicassio F, Sacco A, Muto M, Crescenzi M, Di Fiore PP. 2002. Np95 is regulated by E1A during mitotic reactivation of terminally differentiated cells and is essential for S phase entry. *J Cell Biol* 157: 909-914.
- Booth MJ, Branco MR, Ficz G, Oxley D, Krueger F, Reik W, Balasubramanian S. 2012. Quantitative sequencing of 5-methylcytosine and 5-hydroxymethylcytosine at single-base resolution. *Science* 336: 934-937.
- Bostick M, Kim JK, Esteve PO, Clark A, Pradhan S, Jacobsen SE. 2007. UHRF1 plays a role in maintaining DNA methylation in mammalian cells. *Science* 317: 1760-1764.

- Bouloy M, Janzen C, Vialat P, Khun H, Pavlovic J, Huerre M, Haller O. 2001. Genetic evidence for an interferon-antagonistic function of rift valley fever virus nonstructural protein NSs. *J Virol* **75**: 1371-1377.
- Bourc'his D, Bestor TH. 2004. Meiotic catastrophe and retrotransposon reactivation in male germ cells lacking Dnmt3L. *Nature* **431**: 96-99.
- Bourc'his D, Xu GL, Lin CS, Bollman B, Bestor TH. 2001. Dnmt3L and the establishment of maternal genomic imprints. *Science* **294**: 2536-2539.
- Bray M. 2001. The role of the Type I interferon response in the resistance of mice to filovirus infection. *J Gen Virol* **82**: 1365-1373.
- Bronner C, Achour M, Arima Y, Chataigneau T, Saya H, Schini-Kerth VB. 2007. The UHRF family: oncogenes that are drugable targets for cancer therapy in the near future? *Pharmacol Ther* **115**: 419-434.
- Cao R, Wang L, Wang H, Xia L, Erdjument-Bromage H, Tempst P, Jones RS, Zhang Y. 2002. Role of histone H3 lysine 27 methylation in Polycomb-group silencing. *Science* **298**: 1039-1043.
- Cao R, Zhang Y. 2004. The functions of E(Z)/EZH2-mediated methylation of lysine 27 in histone H3. *Curr Opin Genet Dev* **14**: 155-164.
- Cappello S, Attardo A, Wu X, Iwasato T, Itohara S, Wilsch-Brauninger M, Eilken HM, Rieger MA, Schroeder TT, Huttner WB et al. 2006. The Rho-GTPase cdc42 regulates neural progenitor fate at the apical surface. *Nat Neurosci* **9**: 1099-1107.
- Carleton A, Petreanu LT, Lansford R, Alvarez-Buylla A, Lledo PM. 2003. Becoming a new neuron in the adult olfactory bulb. *Nat Neurosci* **6**: 507-518.
- Chawla-Sarkar M, Lindner DJ, Liu YF, Williams BR, Sen GC, Silverman RH, Borden EC. 2003. Apoptosis and interferons: role of interferon-stimulated genes as mediators of apoptosis. *Apoptosis* **8**: 237-249.
- Chen HZ, Guo S, Li ZZ, Lu Y, Jiang DS, Zhang R, Lei H, Gao L, Zhang X, Zhang Y et al. 2014. A critical role for interferon regulatory factor 9 in cerebral ischemic stroke. *J Neurosci* **34**: 11897-11912.
- Chiappinelli KB, Strissel PL, Desrichard A, Li H, Henke C, Akman B, Hein A, Rote NS, Cope LM, Snyder A et al. 2015. Inhibiting DNA Methylation Causes an Interferon Response in Cancer via dsRNA Including Endogenous Retroviruses. *Cell* **162**: 974-986.
- Cicero S, Herrup K. 2005. Cyclin-dependent kinase 5 is essential for neuronal cell cycle arrest and differentiation. *J Neurosci* **25**: 9658-9668.

- Citterio E, Papait R, Nicassio F, Vecchi M, Gomiero P, Mantovani R, Di Fiore PP, Bonapace IM. 2004. Np95 is a histone-binding protein endowed with ubiquitin ligase activity. *Mol Cell Biol* **24**: 2526-2535.
- Corbin JG, Gaiano N, Machold RP, Langston A, Fishell G. 2000. The Gsh2 homeodomain gene controls multiple aspects of telencephalic development. *Development* **127**: 5007-5020.
- Cordaux R, Batzer MA. 2009. The impact of retrotransposons on human genome evolution. *Nat Rev Genet* **10**: 691-703.
- Creyghton MP, Cheng AW, Welstead GG, Kooistra T, Carey BW, Steine EJ, Hanna J, Lodato MA, Frampton GM, Sharp PA et al. 2010. Histone H3K27ac separates active from poised enhancers and predicts developmental state. *Proc Natl Acad Sci U S A* **107**: 21931-21936.
- Cui Y, Chen X, Zhang J, Sun X, Liu H, Bai L, Xu C, Liu X. 2016. Uhrf1 Controls iNKT Cell Survival and Differentiation through the Akt-mTOR Axis. *Cell Rep* **15**: 256-263.
- Dai C, Shi D, Gu W. 2013. Negative regulation of the acetyltransferase TIP60-p53 interplay by UHRF1 (ubiquitin-like with PHD and RING finger domains 1). *J Biol Chem* **288**: 19581-19592.
- Dawlaty MM, Breiling A, Le T, Barrasa MI, Raddatz G, Gao Q, Powell BE, Cheng AW, Faull KF, Lyko F et al. 2014. Loss of Tet enzymes compromises proper differentiation of embryonic stem cells. *Dev Cell* **29**: 102-111.
- Dawlaty MM, Breiling A, Le T, Raddatz G, Barrasa MI, Cheng AW, Gao Q, Powell BE, Li Z, Xu M et al. 2013. Combined deficiency of Tet1 and Tet2 causes epigenetic abnormalities but is compatible with postnatal development. *Dev Cell* **24**: 310-323.
- Dawlaty MM, Ganz K, Powell BE, Hu YC, Markoulaki S, Cheng AW, Gao Q, Kim J, Choi SW, Page DC et al. 2011. Tet1 is dispensable for maintaining pluripotency and its loss is compatible with embryonic and postnatal development. *Cell Stem Cell* **9**: 166-175.
- De Vos M, El Ramy R, Quenet D, Wolf P, Spada F, Magroun N, Babbio F, Schreiber V, Leonhardt H, Bonapace IM et al. 2014. Poly(ADP-ribose) polymerase 1 (PARP1) associates with E3 ubiquitin-protein ligase UHRF1 and modulates UHRF1 biological functions. *J Biol Chem* **289**: 16223-16238.
- Deaton AM, Bird A. 2011. CpG islands and the regulation of transcription. *Genes Dev* **25**: 1010-1022.
- Dewannieux M, Heidmann T. 2013. Endogenous retroviruses: acquisition, amplification and taming of genome invaders. *Curr Opin Virol* **3**: 646-656.

- Diaz-Castro B, Pardal R, Garcia-Flores P, Sobrino V, Duran R, Piruat JI, Lopez-Barneo J. 2015. Resistance of glia-like central and peripheral neural stem cells to genetically induced mitochondrial dysfunction--differential effects on neurogenesis. *EMBO Rep* **16**: 1511-1519.
- Doetsch F, Caille I, Lim DA, Garcia-Verdugo JM, Alvarez-Buylla A. 1999. Subventricular zone astrocytes are neural stem cells in the adult mammalian brain. *Cell* **97**: 703-716.
- Fan G, Beard C, Chen RZ, Csankovszki G, Sun Y, Siniiaia M, Biniszkiewicz D, Bates B, Lee PP, Kuhn R et al. 2001. DNA hypomethylation perturbs the function and survival of CNS neurons in postnatal animals. *J Neurosci* **21**: 788-797.
- Fan G, Martinowich K, Chin MH, He F, Fouse SD, Hutnick L, Hattori D, Ge W, Shen Y, Wu H et al. 2005. DNA methylation controls the timing of astrogliogenesis through regulation of JAK-STAT signaling. *Development* **132**: 3345-3356.
- Fasano CA, Dimos JT, Ivanova NB, Lowry N, Lemischka IR, Temple S. 2007. shRNA knockdown of Bmi-1 reveals a critical role for p21-Rb pathway in NSC self-renewal during development. *Cell Stem Cell* **1**: 87-99.
- Fasching L, Kapopoulou A, Sachdeva R, Petri R, Jonsson ME, Manne C, Turelli P, Jern P, Cammas F, Trono D et al. 2015. TRIM28 represses transcription of endogenous retroviruses in neural progenitor cells. *Cell Rep* **10**: 20-28.
- Feng J, Chang H, Li E, Fan G. 2005. Dynamic expression of de novo DNA methyltransferases Dnmt3a and Dnmt3b in the central nervous system. *J Neurosci Res* **79**: 734-746.
- Feng J, Zhou Y, Campbell SL, Le T, Li E, Sweatt JD, Silva AJ, Fan G. 2010. Dnmt1 and Dnmt3a maintain DNA methylation and regulate synaptic function in adult forebrain neurons. *Nat Neurosci* **13**: 423-430.
- Fischer J, Beckervordersandforth R, Tripathi P, Steiner-Mezzadri A, Ninkovic J, Gotz M. 2011. Prospective isolation of adult neural stem cells from the mouse subependymal zone. *Nat Protoc* **6**: 1981-1989.
- Florio M, Huttner WB. 2014. Neural progenitors, neurogenesis and the evolution of the neocortex. *Development* **141**: 2182-2194.
- Foti SB, Chou A, Moll AD, Roskams AJ. 2013. HDAC inhibitors dysregulate neural stem cell activity in the postnatal mouse brain. *Int J Dev Neurosci* **31**: 434-447.
- Frade JM, Ovejero-Benito MC. 2015. Neuronal cell cycle: the neuron itself and its circumstances. *Cell Cycle* **14**: 712-720.

- Fraga MF, Ballestar E, Montoya G, Taysavang P, Wade PA, Esteller M. 2003. The affinity of different MBD proteins for a specific methylated locus depends on their intrinsic binding properties. *Nucleic Acids Res* **31**: 1765-1774.
- Frauer C, Hoffmann T, Bultmann S, Casa V, Cardoso MC, Antes I, Leonhardt H. 2011. Recognition of 5-hydroxymethylcytosine by the Uhrf1 SRA domain. *PLoS One* **6**: e21306.
- Fukuda S, Kato F, Tozuka Y, Yamaguchi M, Miyamoto Y, Hisatsune T. 2003. Two distinct subpopulations of nestin-positive cells in adult mouse dentate gyrus. *J Neurosci* **23**: 9357-9366.
- Furutachi S, Matsumoto A, Nakayama KI, Gotoh Y. 2013. p57 controls adult neural stem cell quiescence and modulates the pace of lifelong neurogenesis. *EMBO J* **32**: 970-981.
- Gandhi S, Abramov AY. 2012. Mechanism of oxidative stress in neurodegeneration. *Oxid Med Cell Longev* **2012**: 428010.
- Garcia AD, Doan NB, Imura T, Bush TG, Sofroniew MV. 2004. GFAP-expressing progenitors are the principal source of constitutive neurogenesis in adult mouse forebrain. *Nat Neurosci* **7**: 1233-1241.
- Ge TT, Yang M, Chen Z, Lou G, Gu T. 2016. UHRF1 gene silencing inhibits cell proliferation and promotes cell apoptosis in human cervical squamous cell carcinoma CaSki cells. *J Ovarian Res* **9**: 42.
- Gomez-Lopez S, Lerner RG, Petritsch C. 2014. Asymmetric cell division of stem and progenitor cells during homeostasis and cancer. *Cell Mol Life Sci* **71**: 575-597.
- Gotz M, Huttner WB. 2005. The cell biology of neurogenesis. *Nat Rev Mol Cell Biol* **6**: 777-788.
- Greig LC, Woodworth MB, Galazo MJ, Padmanabhan H, Macklis JD. 2013. Molecular logic of neocortical projection neuron specification, development and diversity. *Nat Rev Neurosci* **14**: 755-769.
- Grieder FB, Vogel SN. 1999. Role of interferon and interferon regulatory factors in early protection against Venezuelan equine encephalitis virus infection. *Virology* **257**: 106-118.
- Gualtieri A, Andreola F, Sciamanna I, Sinibaldi-Vallebona P, Serafino A, Spadafora C. 2013. Increased expression and copy number amplification of LINE-1 and SINE B1 retrotransposable elements in murine mammary carcinoma progression. *Oncotarget* **4**: 1882-1893.

- Guan D, Factor D, Liu Y, Wang Z, Kao HY. 2013. The epigenetic regulator UHRF1 promotes ubiquitination-mediated degradation of the tumor-suppressor protein promyelocytic leukemia protein. *Oncogene* **32**: 3819-3828.
- Guibert S, Forne T, Weber M. 2012. Global profiling of DNA methylation erasure in mouse primordial germ cells. *Genome Res* **22**: 633-641.
- Hackett JA, Surani MA. 2013. DNA methylation dynamics during the mammalian life cycle. *Philos Trans R Soc Lond B Biol Sci* **368**: 20110328.
- Hahn MA, Qiu R, Wu X, Li AX, Zhang H, Wang J, Jui J, Jin SG, Jiang Y, Pfeifer GP et al. 2013. Dynamics of 5-hydroxymethylcytosine and chromatin marks in Mammalian neurogenesis. *Cell Rep* **3**: 291-300.
- Haller O, Kochs G, Weber F. 2006. The interferon response circuit: induction and suppression by pathogenic viruses. *Virology* **344**: 119-130.
- Hasegawa K, Yoshikawa K. 2008. Necdin regulates p53 acetylation via Sirtuin1 to modulate DNA damage response in cortical neurons. *J Neurosci* **28**: 8772-8784.
- Hashimoto H, Horton JR, Zhang X, Bostick M, Jacobsen SE, Cheng X. 2008. The SRA domain of UHRF1 flips 5-methylcytosine out of the DNA helix. *Nature* **455**: 826-829.
- Haubensak W, Attardo A, Denk W, Huttner WB. 2004. Neurons arise in the basal neuroepithelium of the early mammalian telencephalon: a major site of neurogenesis. *Proc Natl Acad Sci U S A* **101**: 3196-3201.
- He YF, Li BZ, Li Z, Liu P, Wang Y, Tang Q, Ding J, Jia Y, Chen Z, Li L et al. 2011. Tet-mediated formation of 5-carboxylcytosine and its excision by TDG in mammalian DNA. *Science* **333**: 1303-1307.
- Heinz S, Benner C, Spann N, Bertolino E, Lin YC, Laslo P, Cheng JX, Murre C, Singh H, Glass CK. 2010. Simple combinations of lineage-determining transcription factors prime cis-regulatory elements required for macrophage and B cell identities. *Mol Cell* **38**: 576-589.
- Herrera DG, Garcia-Verdugo JM, Alvarez-Buylla A. 1999. Adult-derived neural precursors transplanted into multiple regions in the adult brain. *Ann Neurol* **46**: 867-877.
- Herrup K, Yang Y. 2007. Cell cycle regulation in the postmitotic neuron: oxymoron or new biology? *Nat Rev Neurosci* **8**: 368-378.
- Hervouet E, Lalier L, Debien E, Cheray M, Geairon A, Rogniaux H, Loussouarn D, Martin SA, Vallette FM, Cartron PF. 2010. Disruption of Dnmt1/PCNA/UHRF1 interactions promotes tumorigenesis from human and mice glial cells. *PLoS One* **5**: e11333.

- Hirabayashi Y, Suzuki N, Tsuboi M, Endo TA, Toyoda T, Shinga J, Koseki H, Vidal M, Gotoh Y. 2009. Polycomb limits the neurogenic competence of neural precursor cells to promote astrogenic fate transition. *Neuron* **63**: 600-613.
- Hutnick LK, Golshani P, Namihira M, Xue Z, Matynia A, Yang XW, Silva AJ, Schweizer FE, Fan G. 2009. DNA hypomethylation restricted to the murine forebrain induces cortical degeneration and impairs postnatal neuronal maturation. *Hum Mol Genet* **18**: 2875-2888.
- Hwang SY, Hertzog PJ, Holland KA, Sumarsono SH, Tymms MJ, Hamilton JA, Whitty G, Bertoncello I, Kola I. 1995. A null mutation in the gene encoding a type I interferon receptor component eliminates antiproliferative and antiviral responses to interferons alpha and beta and alters macrophage responses. *Proc Natl Acad Sci U S A* **92**: 11284-11288.
- Ito S, D'Alessio AC, Taranova OV, Hong K, Sowers LC, Zhang Y. 2010. Role of Tet proteins in 5mC to 5hmC conversion, ES-cell self-renewal and inner cell mass specification. *Nature* **466**: 1129-1133.
- Ito S, Shen L, Dai Q, Wu SC, Collins LB, Swenberg JA, He C, Zhang Y. 2011. Tet proteins can convert 5-methylcytosine to 5-formylcytosine and 5-carboxylcytosine. *Science* **333**: 1300-1303.
- Iwasato T, Datwani A, Wolf AM, Nishiyama H, Taguchi Y, Tonegawa S, Knopfel T, Erzurumlu RS, Itohara S. 2000. Cortex-restricted disruption of NMDAR1 impairs neuronal patterns in the barrel cortex. *Nature* **406**: 726-731.
- Iyengar BR, Choudhary A, Sarangdhar MA, Venkatesh KV, Gadgil CJ, Pillai B. 2014. Non-coding RNA interact to regulate neuronal development and function. *Front Cell Neurosci* **8**: 47.
- Johri A, Beal MF. 2012. Mitochondrial dysfunction in neurodegenerative diseases. *J Pharmacol Exp Ther* **342**: 619-630.
- Kaneda M, Okano M, Hata K, Sado T, Tsujimoto N, Li E, Sasaki H. 2004. Essential role for de novo DNA methyltransferase Dnmt3a in paternal and maternal imprinting. *Nature* **429**: 900-903.
- Karagianni P, Amazit L, Qin J, Wong J. 2008. ICBP90, a novel methyl K9 H3 binding protein linking protein ubiquitination with heterochromatin formation. *Mol Cell Biol* **28**: 705-717.
- Kassiotis G. 2014. Endogenous retroviruses and the development of cancer. *J Immunol* **192**: 1343-1349.

-
- Kato Y, Kaneda M, Hata K, Kumaki K, Hisano M, Kohara Y, Okano M, Li E, Nozaki M, Sasaki H. 2007. Role of the Dnmt3 family in de novo methylation of imprinted and repetitive sequences during male germ cell development in the mouse. *Hum Mol Genet* **16**: 2272-2280.
- Kessarlis N, Fogarty M, Iannarelli P, Grist M, Wegner M, Richardson WD. 2006. Competing waves of oligodendrocytes in the forebrain and postnatal elimination of an embryonic lineage. *Nat Neurosci* **9**: 173-179.
- Kim D, Pertea G, Trapnell C, Pimentel H, Kelley R, Salzberg SL. 2013. TopHat2: accurate alignment of transcriptomes in the presence of insertions, deletions and gene fusions. *Genome Biol* **14**: R36.
- Kim JK, Esteve PO, Jacobsen SE, Pradhan S. 2009. UHRF1 binds G9a and participates in p21 transcriptional regulation in mammalian cells. *Nucleic Acids Res* **37**: 493-505.
- Koch CM, Andrews RM, Flicek P, Dillon SC, Karaoz U, Clelland GK, Wilcox S, Beare DM, Fowler JC, Couttet P et al. 2007. The landscape of histone modifications across 1% of the human genome in five human cell lines. *Genome Res* **17**: 691-707.
- Kriegstein A, Alvarez-Buylla A. 2009. The glial nature of embryonic and adult neural stem cells. *Annu Rev Neurosci* **32**: 149-184.
- Santhosh Kumar, Saranya. G9a is required for cerebral cortical development (2014) Master's thesis. 652
- Kurita M, Kuwajima T, Nishimura I, Yoshikawa K. 2006. Necdin downregulates CDC2 expression to attenuate neuronal apoptosis. *J Neurosci* **26**: 12003-12013.
- Lane N, Dean W, Erhardt S, Hajkova P, Surani A, Walter J, Reik W. 2003. Resistance of IAPs to methylation reprogramming may provide a mechanism for epigenetic inheritance in the mouse. *Genesis* **35**: 88-93.
- Leeb M, Pasini D, Novatchkova M, Jaritz M, Helin K, Wutz A. 2010. Polycomb complexes act redundantly to repress genomic repeats and genes. *Genes Dev* **24**: 265-276.
- Levison SW, Goldman JE. 1993. Both oligodendrocytes and astrocytes develop from progenitors in the subventricular zone of postnatal rat forebrain. *Neuron* **10**: 201-212.
- Lewis TL, Jr., Courchet J, Polleux F. 2013. Cell biology in neuroscience: Cellular and molecular mechanisms underlying axon formation, growth, and branching. *J Cell Biol* **202**: 837-848.
- Li E, Bestor TH, Jaenisch R. 1992. Targeted mutation of the DNA methyltransferase gene results in embryonic lethality. *Cell* **69**: 915-926.

- Li W, Lee MH, Henderson L, Tyagi R, Bachani M, Steiner J, Campanac E, Hoffman DA, von Geldern G, Johnson K et al. 2015. Human endogenous retrovirus-K contributes to motor neuron disease. *Sci Transl Med* **7**: 307ra153.
- Li X, Barkho BZ, Luo Y, Smrt RD, Santistevan NJ, Liu C, Kuwabara T, Gage FH, Zhao X. 2008. Epigenetic regulation of the stem cell mitogen Fgf-2 by Mbd1 in adult neural stem/progenitor cells. *J Biol Chem* **283**: 27644-27652.
- Liu DX, Nath N, Chellappan SP, Greene LA. 2005. Regulation of neuron survival and death by p130 and associated chromatin modifiers. *Genes Dev* **19**: 719-732.
- Liu S, Brind'Amour J, Karimi MM, Shirane K, Bogutz A, Lefebvre L, Sasaki H, Shinkai Y, Lorincz MC. 2014. Setdb1 is required for germline development and silencing of H3K9me3-marked endogenous retroviruses in primordial germ cells. *Genes Dev* **28**: 2041-2055.
- Liu X, Gao Q, Li P, Zhao Q, Zhang J, Li J, Koseki H, Wong J. 2013. UHRF1 targets DNMT1 for DNA methylation through cooperative binding of hemi-methylated DNA and methylated H3K9. *Nat Commun* **4**: 1563.
- Lois C, Alvarez-Buylla A. 1994. Long-distance neuronal migration in the adult mammalian brain. *Science* **264**: 1145-1148.
- MacDonald JL, Roskams AJ. 2008. Histone deacetylases 1 and 2 are expressed at distinct stages of neuro-glial development. *Dev Dyn* **237**: 2256-2267.
- Maiti A, Drohat AC. 2011. Thymine DNA glycosylase can rapidly excise 5-formylcytosine and 5-carboxylcytosine: potential implications for active demethylation of CpG sites. *J Biol Chem* **286**: 35334-35338.
- Manuel MN, Mi D, Mason JO, Price DJ. 2015. Regulation of cerebral cortical neurogenesis by the Pax6 transcription factor. *Front Cell Neurosci* **9**: 70.
- Maragakis NJ, Rothstein JD. 2006. Mechanisms of Disease: astrocytes in neurodegenerative disease. *Nat Clin Pract Neurol* **2**: 679-689.
- Marin O, Rubenstein JL. 2001. A long, remarkable journey: tangential migration in the telencephalon. *Nat Rev Neurosci* **2**: 780-790.
- Martins-Taylor K, Schroeder DI, LaSalle JM, Lalande M, Xu RH. 2012. Role of DNMT3B in the regulation of early neural and neural crest specifiers. *Epigenetics* **7**: 71-82.
- Martynoga B, Drechsel D, Guillemot F. 2012. Molecular control of neurogenesis: a view from the mammalian cerebral cortex. *Cold Spring Harb Perspect Biol* **4**.
- Marx V. 2012. Epigenetics: Reading the second genomic code. *Nature* **491**: 143-147.

- Matsumoto S, Banine F, Struve J, Xing R, Adams C, Liu Y, Metzger D, Chambon P, Rao MS, Sherman LS. 2006. Brg1 is required for murine neural stem cell maintenance and gliogenesis. *Dev Biol* **289**: 372-383.
- Matsushita R, Yoshino H, Enokida H, Goto Y, Miyamoto K, Yonemori M, Inoguchi S, Nakagawa M, Seki N. 2016. Regulation of UHRF1 by dual-strand tumor-suppressor microRNA-145 (miR-145-5p and miR-145-3p): Inhibition of bladder cancer cell aggressiveness. *Oncotarget* **7**: 28460-28487.
- Maunakea AK, Nagarajan RP, Bilenky M, Ballinger TJ, D'Souza C, Fouse SD, Johnson BE, Hong C, Nielsen C, Zhao Y et al. 2010. Conserved role of intragenic DNA methylation in regulating alternative promoters. *Nature* **466**: 253-257.
- Meilinger D, Fellingner K, Bultmann S, Rothbauer U, Bonapace IM, Klinkert WE, Spada F, Leonhardt H. 2009. Np95 interacts with de novo DNA methyltransferases, Dnmt3a and Dnmt3b, and mediates epigenetic silencing of the viral CMV promoter in embryonic stem cells. *EMBO Rep* **10**: 1259-1264.
- Menn B, Garcia-Verdugo JM, Yaschine C, Gonzalez-Perez O, Rowitch D, Alvarez-Buylla A. 2006. Origin of oligodendrocytes in the subventricular zone of the adult brain. *J Neurosci* **26**: 7907-7918.
- Merkle FT, Tramontin AD, Garcia-Verdugo JM, Alvarez-Buylla A. 2004. Radial glia give rise to adult neural stem cells in the subventricular zone. *Proc Natl Acad Sci U S A* **101**: 17528-17532.
- Messerschmidt DM, Knowles BB, Solter D. 2014. DNA methylation dynamics during epigenetic reprogramming in the germline and preimplantation embryos. *Genes Dev* **28**: 812-828.
- Miyata T, Kawaguchi A, Saito K, Kawano M, Muto T, Ogawa M. 2004. Asymmetric production of surface-dividing and non-surface-dividing cortical progenitor cells. *Development* **131**: 3133-3145.
- Molofsky AV, Pardal R, Iwashita T, Park IK, Clarke MF, Morrison SJ. 2003. Bmi-1 dependence distinguishes neural stem cell self-renewal from progenitor proliferation. *Nature* **425**: 962-967.
- Molyneaux BJ, Arlotta P, Menezes JR, Macklis JD. 2007. Neuronal subtype specification in the cerebral cortex. *Nat Rev Neurosci* **8**: 427-437.
- Montgomery RL, Hsieh J, Barbosa AC, Richardson JA, Olson EN. 2009. Histone deacetylases 1 and 2 control the progression of neural precursors to neurons during brain development. *Proc Natl Acad Sci U S A* **106**: 7876-7881.

- Mootha VK, Lindgren CM, Eriksson KF, Subramanian A, Sihag S, Lehar J, Puigserver P, Carlsson E, Ridderstrale M, Laurila E et al. 2003. PGC-1alpha-responsive genes involved in oxidative phosphorylation are coordinately downregulated in human diabetes. *Nat Genet* **34**: 267-273.
- Mori T, Tanaka K, Buffo A, Wurst W, Kuhn R, Gotz M. 2006. Inducible gene deletion in astroglia and radial glia--a valuable tool for functional and lineage analysis. *Glia* **54**: 21-34.
- Morrish TA, Gilbert N, Myers JS, Vincent BJ, Stamato TD, Taccioli GE, Batzer MA, Moran JV. 2002. DNA repair mediated by endonuclease-independent LINE-1 retrotransposition. *Nat Genet* **31**: 159-165.
- Mouret A, Gheusi G, Gabellec MM, de Chaumont F, Olivo-Marin JC, Lledo PM. 2008. Learning and survival of newly generated neurons: when time matters. *J Neurosci* **28**: 11511-11516.
- Mouret A, Lepousez G, Gras J, Gabellec MM, Lledo PM. 2009. Turnover of newborn olfactory bulb neurons optimizes olfaction. *J Neurosci* **29**: 12302-12314.
- Muller M, Ibelgaufts H, Kerr IM. 1994. Interferon response pathways--a paradigm for cytokine signalling? *J Viral Hepat* **1**: 87-103.
- Muotri AR, Chu VT, Marchetto MC, Deng W, Moran JV, Gage FH. 2005. Somatic mosaicism in neuronal precursor cells mediated by L1 retrotransposition. *Nature* **435**: 903-910.
- Muto M, Kanari Y, Kubo E, Takabe T, Kurihara T, Fujimori A, Tatsumi K. 2002. Targeted disruption of Np95 gene renders murine embryonic stem cells hypersensitive to DNA damaging agents and DNA replication blocks. *J Biol Chem* **277**: 34549-34555.
- Nait-Oumesmar B, Decker L, Lachapelle F, Avellana-Adalid V, Bachelin C, Baron-Van Evercooren A. 1999. Progenitor cells of the adult mouse subventricular zone proliferate, migrate and differentiate into oligodendrocytes after demyelination. *Eur J Neurosci* **11**: 4357-4366.
- Nakamura T, Colbert MC, Robbins J. 2006. Neural crest cells retain multipotential characteristics in the developing valves and label the cardiac conduction system. *Circ Res* **98**: 1547-1554.
- Roxana Nat, Galina Apostolova and Georg Dechant (2013). Telencephalic Neurogenesis Versus Telencephalic Differentiation of Pluripotent Stem Cells, Trends in Cell Signaling Pathways in Neuronal Fate Decision, Dr Sabine Wislet-Gendebien (Ed.), InTech, DOI: 10.5772/54251. Available from: <http://www.intechopen.com/books/trends-in-cell-signaling-pathways-in-neuronal-fate-decision/telencephalic-neurogenesis-versus-telencephalic-differentiation-of-pluripotent-stem-cells>

- Nguyen L, Besson A, Heng JI, Schuurmans C, Teboul L, Parras C, Philpott A, Roberts JM, Guillemot F. 2006. p27kip1 independently promotes neuronal differentiation and migration in the cerebral cortex. *Genes Dev* **20**: 1511-1524.
- Ninkovic J, Gotz M. 2013. Fate specification in the adult brain--lessons for eliciting neurogenesis from glial cells. *Bioessays* **35**: 242-252.
- Ninkovic J, Steiner-Mezzadri A, Jawerka M, Akinci U, Masserdotti G, Petricca S, Fischer J, von Holst A, Beckers J, Lie CD et al. 2013. The BAF complex interacts with Pax6 in adult neural progenitors to establish a neurogenic cross-regulatory transcriptional network. *Cell Stem Cell* **13**: 403-418.
- Nishiyama A, Yamaguchi L, Sharif J, Johmura Y, Kawamura T, Nakanishi K, Shimamura S, Arita K, Kodama T, Ishikawa F et al. 2013. Uhrf1-dependent H3K23 ubiquitylation couples maintenance DNA methylation and replication. *Nature* **502**: 249-253.
- Noctor SC, Martinez-Cerdeno V, Ivic L, Kriegstein AR. 2004. Cortical neurons arise in symmetric and asymmetric division zones and migrate through specific phases. *Nat Neurosci* **7**: 136-144.
- Noctor SC, Martinez-Cerdeno V, Kriegstein AR. 2007. Contribution of intermediate progenitor cells to cortical histogenesis. *Arch Neurol* **64**: 639-642.
- . 2008. Distinct behaviors of neural stem and progenitor cells underlie cortical neurogenesis. *J Comp Neurol* **508**: 28-44.
- Noguchi H, Kimura A, Murao N, Matsuda T, Namihira M, Nakashima K. 2015. Expression of DNMT1 in neural stem/precursor cells is critical for survival of newly generated neurons in the adult hippocampus. *Neurosci Res* **95**: 1-11.
- Obata Y, Furusawa Y, Endo TA, Sharif J, Takahashi D, Atarashi K, Nakayama M, Onawa S, Fujimura Y, Takahashi M et al. 2014. The epigenetic regulator Uhrf1 facilitates the proliferation and maturation of colonic regulatory T cells. *Nat Immunol* **15**: 571-579.
- Okano M, Bell DW, Haber DA, Li E. 1999. DNA methyltransferases Dnmt3a and Dnmt3b are essential for de novo methylation and mammalian development. *Cell* **99**: 247-257.
- Pacaud R, Brocard E, Lalier L, Hervouet E, Vallette FM, Cartron PF. 2014. The DNMT1/PCNA/UHRF1 disruption induces tumorigenesis characterized by similar genetic and epigenetic signatures. *Sci Rep* **4**: 4230.
- Papait R, Pistore C, Grazini U, Babbio F, Cogliati S, Pecoraro D, Brino L, Morand AL, Dechampsme AM, Spada F et al. 2008. The PHD domain of Np95 (mUHRF1) is involved in large-scale reorganization of pericentromeric heterochromatin. *Mol Biol Cell* **19**: 3554-3563.

- Pasquarella A, Ebert A, de Almeida GP, Hinterberger M, Kazerani M, Nuber A, Ellwart J, Klein L, Busslinger M, Schotta G. 2016. Retrotransposon derepression leads to activation of the unfolded protein response and apoptosis in pro-B cells. *Development*.
- Pereira JD, Sansom SN, Smith J, Dobenecker MW, Tarakhovsky A, Livesey FJ. 2010. Ezh2, the histone methyltransferase of PRC2, regulates the balance between self-renewal and differentiation in the cerebral cortex. *Proc Natl Acad Sci U S A* **107**: 15957-15962.
- Petreau L, Alvarez-Buylla A. 2002. Maturation and death of adult-born olfactory bulb granule neurons: role of olfaction. *J Neurosci* **22**: 6106-6113.
- Pichler G, Wolf P, Schmidt CS, Meilinger D, Schneider K, Frauer C, Fellingner K, Rottach A, Leonhardt H. 2011. Cooperative DNA and histone binding by Uhrf2 links the two major repressive epigenetic pathways. *J Cell Biochem* **112**: 2585-2593.
- Pilz GA, Shitamukai A, Reillo I, Pacary E, Schwausch J, Stahl R, Ninkovic J, Snippert HJ, Clevers H, Godinho L et al. 2013. Amplification of progenitors in the mammalian telencephalon includes a new radial glial cell type. *Nat Commun* **4**: 2125.
- Pinto L, Mader MT, Irmeler M, Gentilini M, Santoni F, Drechsel D, Blum R, Stahl R, Bulfone A, Malatesta P et al. 2008. Prospective isolation of functionally distinct radial glial subtypes-lineage and transcriptome analysis. *Mol Cell Neurosci* **38**: 15-42.
- Pringle NP, Richardson WD. 1993. A singularity of PDGF alpha-receptor expression in the dorsoventral axis of the neural tube may define the origin of the oligodendrocyte lineage. *Development* **117**: 525-533.
- Qin W, Wolf P, Liu N, Link S, Smets M, La Mastra F, Forne I, Pichler G, Horl D, Fellingner K et al. 2015. DNA methylation requires a DNMT1 ubiquitin interacting motif (UIM) and histone ubiquitination. *Cell Res* **25**: 911-929.
- Ramesh V, Bayam E, Cernilogar FM, Bonapace IM, Schulze M, Riemenschneider MJ, Schotta G, Gotz M. 2016. Loss of Uhrf1 in neural stem cells leads to activation of retroviral elements and delayed neurodegeneration. *Genes Dev* **30**: 2199-2212.
- Reillo I, de Juan Romero C, Garcia-Cabezas MA, Borrell V. 2011. A role for intermediate radial glia in the tangential expansion of the mammalian cerebral cortex. *Cereb Cortex* **21**: 1674-1694.
- Reynolds BA, Weiss S. 1992. Generation of neurons and astrocytes from isolated cells of the adult mammalian central nervous system. *Science* **255**: 1707-1710.
- Richardson WD, Kessaris N, Pringle N. 2006. Oligodendrocyte wars. *Nat Rev Neurosci* **7**: 11-18.

- Ross SE, Greenberg ME, Stiles CD. 2003. Basic helix-loop-helix factors in cortical development. *Neuron* **39**: 13-25.
- Rowe HM, Jakobsson J, Mesnard D, Rougemont J, Reynard S, Aktas T, Maillard PV, Layard-Liesching H, Verp S, Marquis J et al. 2010. KAP1 controls endogenous retroviruses in embryonic stem cells. *Nature* **463**: 237-240.
- Ryman KD, Klimstra WB, Nguyen KB, Biron CA, Johnston RE. 2000. Alpha/beta interferon protects adult mice from fatal Sindbis virus infection and is an important determinant of cell and tissue tropism. *J Virol* **74**: 3366-3378.
- Sadic D, Schmidt K, Groh S, Kondofersky I, Ellwart J, Fuchs C, Theis FJ, Schotta G. 2015. Atrp promotes heterochromatin formation at retrotransposons. *EMBO Rep* **16**: 836-850.
- Sadler KC, Krahn KN, Gaur NA, Ukomadu C. 2007. Liver growth in the embryo and during liver regeneration in zebrafish requires the cell cycle regulator, uhrf1. *Proc Natl Acad Sci U S A* **104**: 1570-1575.
- Sano R, Reed JC. 2013. ER stress-induced cell death mechanisms. *Biochim Biophys Acta* **1833**: 3460-3470.
- Santos F, Hendrich B, Reik W, Dean W. 2002. Dynamic reprogramming of DNA methylation in the early mouse embryo. *Dev Biol* **241**: 172-182.
- Sayre LM, Smith MA, Perry G. 2001. Chemistry and biochemistry of oxidative stress in neurodegenerative disease. *Curr Med Chem* **8**: 721-738.
- Schultz DC, Ayyanathan K, Negorev D, Maul GG, Rauscher FJ, 3rd. 2002. SETDB1: a novel KAP-1-associated histone H3, lysine 9-specific methyltransferase that contributes to HP1-mediated silencing of euchromatic genes by KRAB zinc-finger proteins. *Genes Dev* **16**: 919-932.
- Schuermans C, Guillemot F. 2002. Molecular mechanisms underlying cell fate specification in the developing telencephalon. *Curr Opin Neurobiol* **12**: 26-34.
- Sen GL, Reuter JA, Webster DE, Zhu L, Khavari PA. 2010. DNMT1 maintains progenitor function in self-renewing somatic tissue. *Nature* **463**: 563-567.
- Seri B, Garcia-Verdugo JM, Collado-Morente L, McEwen BS, Alvarez-Buylla A. 2004. Cell types, lineage, and architecture of the germinal zone in the adult dentate gyrus. *J Comp Neurol* **478**: 359-378.
- Seri B, Garcia-Verdugo JM, McEwen BS, Alvarez-Buylla A. 2001. Astrocytes give rise to new neurons in the adult mammalian hippocampus. *J Neurosci* **21**: 7153-7160.
- Sharif J, Endo TA, Nakayama M, Karimi MM, Shimada M, Katsuyama K, Goyal P, Brind'Amour J, Sun MA, Sun Z et al. 2016. Activation of Endogenous Retroviruses in Dnmt1 ESCs

- Involves Disruption of SETDB1-Mediated Repression by NP95 Binding to Hemimethylated DNA. *Cell Stem Cell*.
- Sharif J, Muto M, Takebayashi S, Suetake I, Iwamatsu A, Endo TA, Shinga J, Mizutani-Koseki Y, Toyoda T, Okamura K et al. 2007. The SRA protein Np95 mediates epigenetic inheritance by recruiting Dnmt1 to methylated DNA. *Nature* **450**: 908-912.
- Sharif J, Shinkai Y, Koseki H. 2013. Is there a role for endogenous retroviruses to mediate long-term adaptive phenotypic response upon environmental inputs? *Philos Trans R Soc Lond B Biol Sci* **368**: 20110340.
- Shimamura K, Rubenstein JL. 1997. Inductive interactions direct early regionalization of the mouse forebrain. *Development* **124**: 2709-2718.
- Simon JA, Kingston RE. 2013. Occupying chromatin: Polycomb mechanisms for getting to genomic targets, stopping transcriptional traffic, and staying put. *Mol Cell* **49**: 808-824.
- Singer T, McConnell MJ, Marchetto MC, Coufal NG, Gage FH. 2010. LINE-1 retrotransposons: mediators of somatic variation in neuronal genomes? *Trends Neurosci* **33**: 345-354.
- Sinibaldi-Vallebona P, Lavia P, Garaci E, Spadafora C. 2006. A role for endogenous reverse transcriptase in tumorigenesis and as a target in differentiating cancer therapy. *Genes Chromosomes Cancer* **45**: 1-10.
- Smith ZD, Meissner A. 2013. DNA methylation: roles in mammalian development. *Nat Rev Genet* **14**: 204-220.
- Smrt RD, Eaves-Egenes J, Barkho BZ, Santistevan NJ, Zhao C, Aimone JB, Gage FH, Zhao X. 2007. Mecp2 deficiency leads to delayed maturation and altered gene expression in hippocampal neurons. *Neurobiol Dis* **27**: 77-89.
- Song CX, Yi C, He C. 2012. Mapping recently identified nucleotide variants in the genome and transcriptome. *Nat Biotechnol* **30**: 1107-1116.
- Spassky N, Goujet-Zalc C, Parmantier E, Olivier C, Martinez S, Ivanova A, Ikenaka K, Macklin W, Cerruti I, Zalc B et al. 1998. Multiple restricted origin of oligodendrocytes. *J Neurosci* **18**: 8331-8343.
- Spruijt CG, Gnerlich F, Smits AH, Pfaffeneder T, Jansen PW, Bauer C, Munzel M, Wagner M, Muller M, Khan F et al. 2013. Dynamic readers for 5-(hydroxy)methylcytosine and its oxidized derivatives. *Cell* **152**: 1146-1159.
- Stoykova A, Treichel D, Hallonet M, Gruss P. 2000. Pax6 modulates the dorsoventral patterning of the mammalian telencephalon. *J Neurosci* **20**: 8042-8050.
- Subramanian A, Tamayo P, Mootha VK, Mukherjee S, Ebert BL, Gillette MA, Paulovich A, Pomeroy SL, Golub TR, Lander ES et al. 2005. Gene set enrichment analysis: a

- knowledge-based approach for interpreting genome-wide expression profiles. *Proc Natl Acad Sci U S A* **102**: 15545-15550.
- Tahiliani M, Koh KP, Shen Y, Pastor WA, Bandukwala H, Brudno Y, Agarwal S, Iyer LM, Liu DR, Aravind L et al. 2009. Conversion of 5-methylcytosine to 5-hydroxymethylcytosine in mammalian DNA by MLL partner TET1. *Science* **324**: 930-935.
- Tan SL, Nishi M, Ohtsuka T, Matsui T, Takemoto K, Kamio-Miura A, Aburatani H, Shinkai Y, Kageyama R. 2012. Essential roles of the histone methyltransferase ESET in the epigenetic control of neural progenitor cells during development. *Development* **139**: 3806-3816.
- Tao W, Lai E. 1992. Telencephalon-restricted expression of BF-1, a new member of the HNF-3/fork head gene family, in the developing rat brain. *Neuron* **8**: 957-966.
- Tekki-Kessarlis N, Woodruff R, Hall AC, Gaffield W, Kimura S, Stiles CD, Rowitch DH, Richardson WD. 2001. Hedgehog-dependent oligodendrocyte lineage specification in the telencephalon. *Development* **128**: 2545-2554.
- Tien AL, Senbanerjee S, Kulkarni A, Mudbhary R, Goudreau B, Ganesan S, Sadler KC, Ukomadu C. 2011. UHRF1 depletion causes a G2/M arrest, activation of DNA damage response and apoptosis. *Biochem J* **435**: 175-185.
- Tittle RK, Sze R, Ng A, Nuckels RJ, Swartz ME, Anderson RM, Bosch J, Stainier DY, Eberhart JK, Gross JM. 2011. Uhrf1 and Dnmt1 are required for development and maintenance of the zebrafish lens. *Dev Biol* **350**: 50-63.
- Tommasi S, Zheng A, Yoon JI, Li AX, Wu X, Besaratinia A. 2012. Whole DNA methylome profiling in mice exposed to secondhand smoke. *Epigenetics* **7**: 1302-1314.
- Toresson H, Potter SS, Campbell K. 2000. Genetic control of dorsal-ventral identity in the telencephalon: opposing roles for Pax6 and Gsh2. *Development* **127**: 4361-4371.
- Tost, Jörg. DNA methylation : Methods and Protocols. Second edition volume 507. 2009 Humana Press, a part of Springer Science and Business media.
- Trapnell C, Hendrickson DG, Sauvageau M, Goff L, Rinn JL, Pachter L. 2013. Differential analysis of gene regulation at transcript resolution with RNA-seq. *Nat Biotechnol* **31**: 46-53.
- Unoki M, Nishidate T, Nakamura Y. 2004. ICBP90, an E2F-1 target, recruits HDAC1 and binds to methyl-CpG through its SRA domain. *Oncogene* **23**: 7601-7610.
- van den Broek MF, Muller U, Huang S, Aguet M, Zinkernagel RM. 1995. Antiviral defense in mice lacking both alpha/beta and gamma interferon receptors. *J Virol* **69**: 4792-4796.

- Vitullo P, Sciamanna I, Baiocchi M, Sinibaldi-Vallebona P, Spadafora C. 2012. LINE-1 retrotransposon copies are amplified during murine early embryo development. *Mol Reprod Dev* **79**: 118-127.
- Volpe TA, Kidner C, Hall IM, Teng G, Grewal SI, Martienssen RA. 2002. Regulation of heterochromatic silencing and histone H3 lysine-9 methylation by RNAi. *Science* **297**: 1833-1837.
- Wang X, Tsai JW, LaMonica B, Kriegstein AR. 2011. A new subtype of progenitor cell in the mouse embryonic neocortex. *Nat Neurosci* **14**: 555-561.
- Watanabe D, Suetake I, Tada T, Tajima S. 2002. Stage- and cell-specific expression of Dnmt3a and Dnmt3b during embryogenesis. *Mech Dev* **118**: 187-190.
- Wilkinson G, Dennis D, Schuurmans C. 2013. Proneural genes in neocortical development. *Neuroscience* **253**: 256-273.
- Wu H, Coskun V, Tao J, Xie W, Ge W, Yoshikawa K, Li E, Zhang Y, Sun YE. 2010. Dnmt3a-dependent nonpromoter DNA methylation facilitates transcription of neurogenic genes. *Science* **329**: 444-448.
- Wu H, D'Alessio AC, Ito S, Wang Z, Cui K, Zhao K, Sun YE, Zhang Y. 2011. Genome-wide analysis of 5-hydroxymethylcytosine distribution reveals its dual function in transcriptional regulation in mouse embryonic stem cells. *Genes Dev* **25**: 679-684.
- Yao B, Christian KM, He C, Jin P, Ming GL, Song H. 2016. Epigenetic mechanisms in neurogenesis. *Nat Rev Neurosci* **17**: 537-549.
- Yoshikawa K. 2000. Cell cycle regulators in neural stem cells and postmitotic neurons. *Neurosci Res* **37**: 1-14.
- Yu H, Guo P, Xie X, Wang Y, Chen G. 2016. Ferroptosis, a new form of cell death, and its relationships with tumourous diseases. *J Cell Mol Med*.
- Yu M, Hon GC, Szulwach KE, Song CX, Zhang L, Kim A, Li X, Dai Q, Shen Y, Park B et al. 2012. Base-resolution analysis of 5-hydroxymethylcytosine in the mammalian genome. *Cell* **149**: 1368-1380.
- Yun K, Potter S, Rubenstein JL. 2001. Gsh2 and Pax6 play complementary roles in dorsoventral patterning of the mammalian telencephalon. *Development* **128**: 193-205.
- Zhao J, Chen X, Song G, Zhang J, Liu H, Liu X. 2016. Uhrf1 controls the self-renewal versus differentiation of hematopoietic stem cells by epigenetically regulating the cell-division modes. *Proc Natl Acad Sci U S A*.
- Zhao X, Ueba T, Christie BR, Barkho B, McConnell MJ, Nakashima K, Lein ES, Eadie BD, Willhoite AR, Muotri AR et al. 2003. Mice lacking methyl-CpG binding protein 1 have

- deficits in adult neurogenesis and hippocampal function. *Proc Natl Acad Sci U S A* **100**: 6777-6782.
- Zhou Q, Dalgard CL, Wynder C, Doughty ML. 2011. Histone deacetylase inhibitors SAHA and sodium butyrate block G1-to-S cell cycle progression in neurosphere formation by adult subventricular cells. *BMC Neurosci* **12**: 50.
- Zoghbi HY, Bear MF. 2012. Synaptic dysfunction in neurodevelopmental disorders associated with autism and intellectual disabilities. *Cold Spring Harb Perspect Biol* **4**.

9. Curriculum vitae

Vidya Ramesh

Education

- P.hD** – Institute for Stem Cell Research, **October 2011 – present**
Helmholtz Zentrum Munich, Germany
- M.Sc** - University of Leicester, UK **September 2007 – September 2008**
Course – Cancer Cell and Molecular biology
- B.Sc** – Bangalore University, India **June 2004 – May 2007**

Research Experience

- P.hD** – Helmholtz Zentrum, Munich, Germany **October 2011 - present**
Project – Investigating the function of Uhrf1 in neurogenesis and reprogramming.
Supervised by Prof. Magdalena Götz.
- Research Technician** – National Institute for Medical Research **June 2009 – October 2011**
London, UK. Project – Function of Ascl1 in the developing ventral forebrain.
Supervised by Dr.Francois Guillemot and Dr.Diogo Castro
- Research Assistant** – University of Sheffield, UK **October 2008 – April 2009**
Project – Screening chemical compounds in an in vitro model of ALS

Supervised by Professor Pamela Shaw and Dr.Sian Barber

Conference presentations

- From stem cells to behaviour in the normal and diseased nervous system. 21st Biennial Meeting of the International Society for Developmental Neuroscience (**ISDN**). Nice, France 2016. **Poster**.
- The Mobile Genome: Genetic and Physiological Impacts of Transposable Elements. EMBL Symposium. **EMBO**. Heidelberg, Germany 2015. **Talk**.
- Molecular mechanisms of Telencephalic development, workshop with Dr.Victor Borrell's group. Instituto de Neurociencias, Alicante, Spain 2015. **Talk**.
- Neuroepigenetics. **Keystone** Symposia. Santa Fe, USA 2015. **Talk**.
- Neural stem cells to neural circuits. **Cortical Development**. Crete, Greece 2014. **Poster**.
- 3rd German-Japanese Bilateral event on Neural stem cells and Mammalian Neurogenesis. Organised by Dr. Yoichi Kosodo, Dr.Elena Taverna and Dr.Frederico Calegari. Miyagi-Ken, Japan 2013. **Talk**.
- Chromatin mechanisms and Cell Physiology. **Keystone symposia**. Oberstdorf, Germany 2013. **Poster**.

10. List of Publications

Ramesh V*, Bayam E*, Cernilogar FM, Bonapace IM, Schulze M, Riemenschneider MJ, Schotta G and Götz M. (2016) Loss of Uhrf1 in neural stem cells leads to activation of retroviral elements and delayed neurodegeneration. *Genes and Dev* 30: 2199-2212. *co-first authors

Seibt J, Armant O, Le Digarcher A, Castro D, **Ramesh V**, Journot L, Guillemot F, Vanderhaeghen P and Bouchet T. (2012) Expression at the imprinted dlk1-gtl2 locus is regulated by proneural genes in the developing telencephalon. *PLoS One* 7(11):e48675.

Castro D, Martynoga B, Parras C, **Ramesh V**, Pacary E, Johnston C, Drechsel D, Lebel M, Hunt C, Doll D, Bithell A, Etwiller L, Buckley N and Guillemot F. (2011) *Ascl1* promotes neural progenitor proliferation through activation of multiple cell cycle regulators. *Genes and Dev* 25: 930-945.

11. Affidavit

Eidesstattliche Versicherung/Affidavit Hiermit versichere ich an Eides statt, dass ich die vorliegende Dissertation **Cellular and molecular function of Uhrf1 in neural stem cells** selbstständig angefertigt habe, mich außer der angegebenen keiner weiteren Hilfsmittel bedient und alle Erkenntnisse, die aus dem Schrifttum ganz oder annähernd übernommen sind, als solche kenntlich gemacht und nach ihrer Herkunft unter Bezeichnung der Fundstelle einzeln nachgewiesen habe.

I hereby confirm that the dissertation **Cellular and molecular function of Uhrf1 in neural stem cells** is the result of my own work and that I have only used sources or materials listed and specified in the dissertation.

München, 2.3.2017

Vidya Ramesh

12. List of contributions

The following people contributed materials, provided help with an experiment or helped with analysis of data –

Dr. Ian Bonapace (University of Insubria, Italy) and **Dr. Fabio Spada** (LMU, Munich) kindly provided us with the Uhrf1 antibody. Dr. Spada also provided us with the Uhrf1 KO NSCs. **Dr. Bryan Cullen** (Duke university, USA) kindly gave us the IAP-Gag antibody. **Dr. Qiang Lu** (Beckmann Research Institute, USA) kindly gave us the Tet and Scrambled shRNA constructs. **Dr. Pia Johansson** gave us cDNA for the E14 FACS sorted cells. **Dr. Efil Bayam** (Strasbourg, France) gave us some sections of the adult controls and cKO and some sections of embryonic controls and cKO. **Dr. Filippo Cernilogar** (BMC, Munich) performed the H3K9me3 ChIP. **Dr. Gunnar Schotta** (BMC, Munich) analysed the RNAseq and 5hmeDIP data in this study. **Dr. Markus Schulze** and **Dr. Markus Riemenschneider** (both from Regensburg University Hospital) collaborated with us on the Ox-RRBS and Ox-BS experiments and the sequencing was performed there. Dr. Markus Schulze performed a part of the Ox-RRBS and Ox-BS work-flow. The mass spectrometry analysis was performed by **Dr. Stefanie Hauck** and **Dr. Juliane Merl-Pham** at the Research Unit Protein Science at the Helmholtz Zentrum, Munich. **Dr. Arie Geerdorf** from the Helmholtz Zentrum, Munich and **German Camargo-Ortega** (BMC, Munich) provided us with the Cre recombinant protein.

Vidya Ramesh

Dr. Magdalena Götz